REPORT DOCUMENTATION PAGE

Form Approved
OMB No. 0704-0188

PLEASE DO NOT RETURN YOUR FORM TO THE ABOVE ORGANIZATION.

1. REPORT DATE *(DD-MM-YYYY)*	2. REPORT TYPE	3. DATES COVERED *(From - To)*
06/15/2012	Final Report	05/15/2009 to 06/30/2012

4. TITLE AND SUBTITLE
DEVELOPMENT AND IMPLEMENTATION OF HIGH-BANDWIDTH PULSED MICROACTUATORS FOR SUB- AND SUPERSONIC APPLICATIONS

5a. CONTRACT NUMBER

5b. GRANT NUMBER
FA9550-09-1-0353

5c. PROGRAM ELEMENT NUMBER

6. AUTHOR(S)
FARRUKH S ALVI

5d. PROJECT NUMBER
002070

5e. TASK NUMBER

5f. WORK UNIT NUMBER

7. PERFORMING ORGANIZATION NAME(S) AND ADDRESS(ES)
FLORIDA A &M UNIVERSITY
410 FOOTE-HILYER ADMINISTRATION CENTER TALLAHASSEE, FL 32303

8. PERFORMING ORGANIZATION REPORT NUMBER

9. SPONSORING/MONITORING AGENCY NAME(S) AND ADDRESS(ES)
Program Manager - Douglas Smith
Air Force Office of Scientific Research
875 North Randolph Street
Suite 325, Rm 3112
Arlington, VA 22203

10. SPONSOR/MONITOR'S ACRONYM(S)
US AFOSR

11. SPONSOR/MONITOR'S REPORT NUMBER(S)
AFRL-OSR-VA-TR-2012-0899

12. DISTRIBUTION/AVAILABILITY STATEMENT
Public
Distribution A: Approved for Public Release

13. SUPPLEMENTARY NOTES

14. ABSTRACT

Unsteady actuators with a high amplitude output and tunable frequency are needed for the effective control of many sub and supersonic flows. The development, design, characterization, modeling and implementation of a novel high-bandwidth micro fluidic actuator were the main focus of this project and are described in this report. This micro fluidic actuator system essentially consists of an underexpanded primary source jet impinging upon (and exiting) a short cylindrical cavity where the array of unsteady supersonic microjets emanate through multiple micro orifices in the lower cavity surface. The frequency and amplitude response of pulsed microjets are examined in detail over a range of geometric and flow parameters, such as the source jet nozzle to cavity distance h; the nozzle pressure ratio NPR; cavity length L; actuator volume V and the inflow to outflow area ratio nSc/Sm. The results clearly show that the pulsed microjets produced by this actuator possess very high mean momentum (they are supersonic for most cases, >300 m/s) as well as a very significant unsteady component (more than 30% of the mean velocity). By proper selection of the geometric and fluid parameters, the actuator frequency can be 'fine tuned' to any value in between 100 Hz-60 kHz.

15. SUBJECT TERMS
Microactuators, High speed flow control, Pulsed microjets

16. SECURITY CLASSIFICATION OF:			17. LIMITATION OF ABSTRACT	18. NUMBER OF PAGES	19a. NAME OF RESPONSIBLE PERSON
a. REPORT	b. ABSTRACT	c. THIS PAGE			Farrukh S Alvi
U	U	U	SAR	20	19b. TELEPHONE NUMBER *(Include area code)* 850 644 0053

DEVELOPMENT AND IMPLEMENTATION OF HIGH BANDWIDTH PULSED MICROACTUATORS FOR SUB AND SUPERSONIC APPLICATIONS
AFOSR GRANT FA9550-09-1-0353
FINAL REPORT- 2009-2012

F. S. Alvi
Department of Mechanical Engineering
Florida A&M University and Florida State University (FAMU-FSU)
Tallahassee, FL 32310

Abstract

Unsteady actuators with a high amplitude output and tunable frequency are needed for the effective control of many sub and supersonic flows. The development, design, characterization, modeling and implementation of a novel high-bandwidth micro fluidic actuator were the main focus of this project and are described in this report. This micro fluidic actuator system essentially consists of an underexpanded primary source jet impinging upon (and exiting) a short cylindrical cavity where the array of unsteady supersonic microjets emanate through multiple micro orifices in the lower cavity surface. The frequency and amplitude response of pulsed microjets are examined in detail over a range of geometric and flow parameters, such as the source jet nozzle to cavity distance h; the nozzle pressure ratio NPR; cavity length L; actuator volume V and the inflow to outflow area ratio nS_c/S_m. The results clearly show that the pulsed microjets produced by this actuator possess very high mean momentum (they are supersonic for most cases, >300 m/s) as well as a very significant unsteady component (more than 30% of the mean velocity). By proper selection of the geometric and fluid parameters, the actuator frequency can be 'fine tuned' to any value in between 100 Hz-60 kHz. To better understand the flow dynamics of this micro fluidic actuator, a high resolution microschlieren system that uses plasma –derived from the laser-induced break down of air –as light source, has been developed for the study. Actuator flowfield images with high spatial and temporal resolution were acquired using this specialized flow visualization technique. Two actuator modules that can generate 12 pulsed microjets at a design frequency range of 4 to 6 kHz were designed and integrated to the leading edge of a Mach 1.5 cavity to study its effectiveness. Unsteady actuators were also implemented in a supersonic impinging jet to evaluate their control authority. In both cavity and supersonic jet applications, unsteady actuation had a beneficial impact on the flowfield where the noise and/or flow unsteadiness was significantly reduced. To further improve the control authority in terms of fast time response and phase control, we are in the process of integrating smart materials into these actuators for a next generation design which will be implemented and tested in canonical high-speed flows.

A. Introduction

Active control of shear and boundary layer flows by means of unsteady momentum addition has drawn the attention of flow control researchers in recent years. The natural flow characteristics such as transition, turbulence, flow separation, mixing etc. can potentially be controlled: suppressed, attenuated or enhanced, more efficiently through

schemes that use such actuators. As an example, flow separation over an airfoil is an important practical problem where unsteady actuation techniques have been extensively studied for its control. Seifert et al. [22] have shown that periodic excitation by momentum addition, with a frequency higher than the natural vortex shedding frequency, may achieve similar gains in performance in comparison with steady blowing, with 99% less momentum. McManus and Magill [23] used pulsed angular injection to create co-rotating vortices to attach separated flow. This actuation technique reportedly worked well for high angles of attack and is referred to as pulsed vortex generators. Bryant et al. [24], Wiltse et al. [25] and Smith et al. [26] used piezoelectric actuators for imparting unsteady momentum for flow separation control. These actuators, also called synthetic jets, produce zero net mass flux jets with velocities in the range of 10-80 m/sec at a frequency range up to 1 kHz. This technology has been developed further with input from many others on the modeling, design and fabrication of compact ZNMF actuator systems (Cattafesta et al. [27] and Joslin et al. [28]). Some of the actuators mentioned above were found promising for a number of subsonic flow control applications but were ineffective when the flow velocities are very high. The highly unsteady flowfield of an impinging supersonic jet or the flowfield inside a cavity, such as a weapon/cargo bay of a fighter aircraft subjected to cruise conditions from high subsonic to supersonic, are examples of flows that demand unsteady, high-amplitude actuation techniques. Such high speed flows require actuators that can provide high mean and unsteady momentum. Moreover, in most applications, the unsteady properties of the base flows largely depend on operating conditions that vary over a wide range of frequencies. An actuator with high unsteady momentum whose frequency can be tuned over a large bandwidth will be useful for such applications.

Plasma actuators were reported to have the capability for boundary layer separation control by imparting near wall flow momentum (List et al. [29], Jacob et al. [30], and Corke et al. [31]). Ganiev et al. [32] used plasma jet injection for reducing the drag over a cone-cylinder model by a factor of two. Kelley et al. [33] used an AC dielectric barrier discharge plasma actuator for the leading edge flow separation control of a high subsonic flow. The high voltage requirement, EMI, complexities associated with plasma systems and limited bandwidth are some issues that may restrict the implementation of these devices into practical systems. Sparkjet actuators use an electric discharge to generate high pressure within a chamber and produce an air discharge through the orifice (Grossman et al [34]). Similar to plasma actuators these devices also require a very high voltage to operate. Another variant, described as pulsed detonation actuator, has been recently developed and characterized by Cutler and Drummon [35]; it can generate a perturbation up to 1.5 kHz. A mixture of reactants (hydrogen and air) burns inside a resonating tube equipped with a high speed valve resulting in pulsed flow of hot combustion gases through the orifices. LAFPAs, localized arc filament plasma actuators, are another recently introduced design that is being examined for controlling high-speed flows (Samimy et al., 2011 [36]). Even though high control authority actuation may be achieved using some of these designs and as such hold promise for the future, other alternatives that are perhaps less complex, robust with a high dynamic range are still desirable.

Yeung et al. [37] proposed that in turbulent flows there exist a bi-directional coupling between the large scale and fine structures and this coupling can be excited by coherent

high frequency forcing either at large or at fine scales. Exciting the shear layer at a frequency higher than its dominant natural frequency may provoke an accelerated transfer of energy from large to small scales, in subsonic flows (Wiltse and Glezer) [38]. This argument has led to studies on the 'high frequency forcing control' concept in recent years. Stanek et al. [39] employed 'high frequency forcing' to suppress supersonic cavity oscillations using powered resonance tubes as actuators. Interestingly, they reported that high frequency excitation caused deceleration of the turbulent energy cascade contrary to the findings of previous researchers. The design and development of robust and tunable actuators that can deliver sufficient unsteady momentum at higher frequencies over a large range remain as a challenge.

The original concepts of powered resonance tubes were introduced by Hartmann in 1927 [40] who described the device as a novel acoustic generator. Though it was not originally intended for the active flow control, subsequently many researchers (Raman et al. [41], Stanek et al. [39], Kaster and Samimy [42], Dziuba and Rossmann [43]) used the resonance tube concept as a source for high energy and high frequency acoustic perturbations for active flow control. A detailed study of this device can be found in Brocher et al. [44]. Kastner and Samimy [42] studied the effect of forcing frequency on the control of an impinging high speed jet by using a Hartmann tube fluidic actuator. They noticed that by forcing the base jet with a frequency 7.5 kHz or above, or using a steady mass injection, the dominant tone and its harmonics were suppressed. They also reported that at a lower mass flow rate, the high frequency actuators were found to be more effective than the comparable steady mass injection. A major drawback associated with this actuator is the very large mass flow requirement.

B. High-bandwidth resonance enhanced microactuator (REM) development

From the above discussion, it is clear that actuators with high amplitude unsteadiness and tunable frequency are needed for the effective and efficient control of high speed flows. The present studies focus on the design and characterization of a high-bandwidth micro fluidic actuator, and its implementation to control the unsteady flowfield encountered in a number of high speed applications, such as supersonic cavity flows and high speed jet flows. This micro fluidic actuator has three major components, i) a primary under-expanded source jet incident upon ii) a cylindrical cavity with micro orifices at the bottom surfaces, through which the iii) pulsed microjets flows out as shown in Fig. 1. In this basic configuration, the main parameters of the actuator are the length of cavity L, the distance of nozzle to the cavity h and the source jet nozzle pressure ratio NPR. Detailed characterization of actuators with a geometric configuration as shown in Fig. 1 is reported in reference [2].

An example spectra of the actuator for L/d=3 is shown in Fig. 2. As seen in the figure, for a fixed L/d and h/d, the actuator frequency can be varied from 17 kHz to 24 kHz by varying the source jet nozzle pressure ratio from 4.4 to 5.5. The striking feature of this micro-actuator is its ability to produce supersonic, high frequency, tunable pulsed microjets over a large bandwidth that could be adapted to the various operating conditions of the base flow. During our earlier studies the actuator frequency and amplitude were characterized over a large range of geometric and flow parameters such as h/d, L/d, and source nozzle pressure ratio NPR, based on which an empirical design

correlation was derived as an elementary tool for the actuator design. This correlation is as shown in Fig.3. In the empirical correlation $St_{ideal}=0.4(H/d)^{-1.45}$, H is the length of the jet column, d is the diameter of source jet nozzle and St_{ideal} is the actuator frequency non-dimensionalized using the ideally expanded jet velocity of source jet.

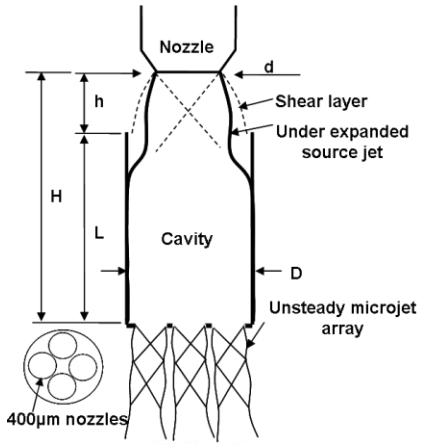

Fig. 1 Schematic of Microactuator

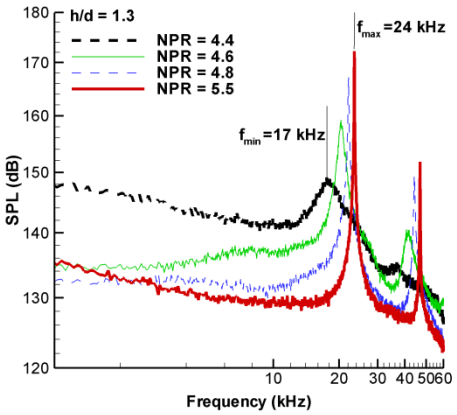

Fig. 2 Actuator spectra at L/d=3

C. Detailed parametric studies on REM actuator

(a) Effect of volume on REM properties

The effect of actuator volume on its frequency was also investigated. In the earlier studies described in reference 2 in the publication list, the actuator geometry was a simple cylindrical cavity (Fig. 1) where actuator volume is proportional to the cavity length L, as the cavity diameter D was kept constant. Hence any inference regarding the actuator frequency dependence on cavity length L can also be extended to its volume. The correlation suggested for this cylindrical design indicates that the actuator frequency has a strong dependence on jet column length H. This parameter essentially captures the effect of cavity length L, which is directly related to the volume V of the actuator, and the nozzle to actuator distance h. As discussed in [2], the actuator frequency f can be varied by the parameter h and/or L. Since a change in cavity length changes the volume of the actuator as well as the parameter H, it is important to delineate the dependence of frequency on actuator volume from the effect of cavity length L or jet column length H. Such an experiment should keep the parameters L and h constant while the actuator volume will be varied. One such geometry is shown in Fig. 4. In this configuration, the actuator has a

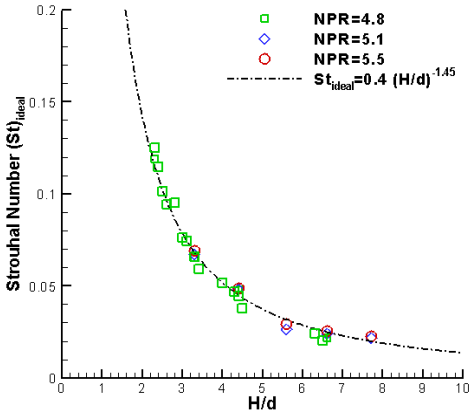

Fig. 3 Design correlation derived for a geometry shown in Fig. 1

square cross section cavity that opens to a rectangular spreader. Four micro nozzles (orifices) are located at the bottom of the spreader in a linear array pattern as shown in Fig. 4*c*.

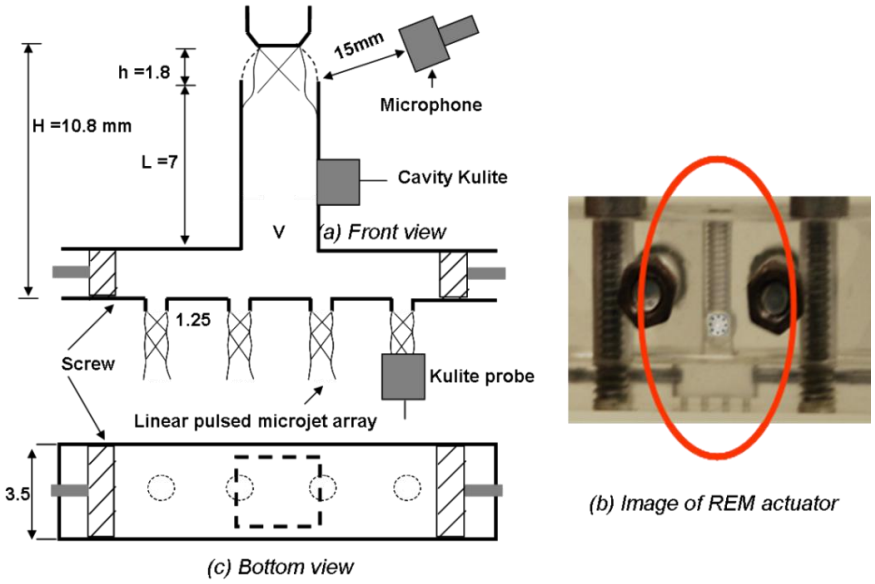

Fig. 4 Schematic of variable volume actuator used for parametric studies

In this way the pulsed microjets can be distributed in different configurations for various flow control applications. The square cross section is chosen to provide optical access inside the cavity as well to flush mount a Kulite sensor in the cavity wall inside the actuator for unsteady pressure measurements. The volume of the actuator can be varied by adjusting the two screws attached on either end of the spreader (Fig. 4*a*). In this way the cavity length (*L*) and the jet column length (*H*) can be kept constant while the volume of the actuator (*V*) is varied. In the present study, the actuator volume is varied from 34 mm^3 to 73 mm^3 while all other parameters are kept constant.

Fig. 5 presents the pressure spectra of the actuator for different actuator volumes as measured by a Kulite probe located 2mm from the exhaust orifice of one of the unsteady/pulsed microjets as shown in Fig. 4*a*. As seen in Fig. 5*a*, for a fixed *H/d*=10.8 and constant volume of 34 mm^3, an *NPR* variation from 5.1 to 5.5 changes the actuator frequency from 5 to 6 kHz. At a higher volume (73 mm^3) the frequency shifts to the 1.9 to 2.3 kHz range as shown in Fig. 5*b*. In summary, changes in actuator volume from 34 to 73mm^3 have shifted the frequency from 1.9 to 6 kHz. This experiment clearly confirms the importance of actuator volume as a critical parameter that determines the resonance frequency of the microactuator.

(b) Effect of inflow-out flow area ratio, $n(S_m/S_c)$, on properties

The influence of another parameter on actuator frequency was also investigated. An area ratio parameter, $n(S_m/S_c)$ is introduced for this purpose, where S_c is the area of cross section of the cavity where source jet flows into, S_m is the cross sectional area of each micro nozzle/orifice (see Fig. 6*a*), and n is the number of microjets. This parameter mainly determines the exhaust mass flow rate from the REM actuator and is useful for

the output optimization of the actuator system from a mass flow perspective. The area ratio parameter also represents the blockage of flow inside the actuator. In this section, the experimental study on an actuator with a single microjet nozzle (with variable diameter) is presented.

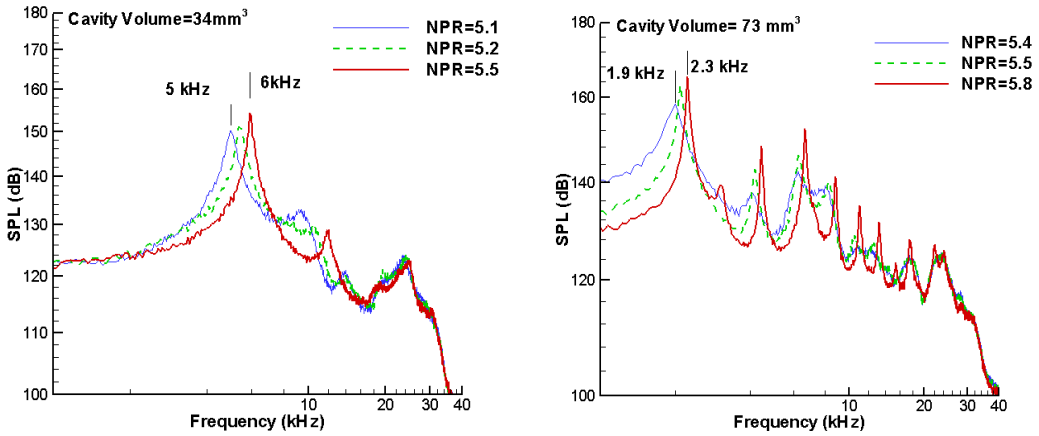

a) Cavity Volume=34 mm^3 b) Cavity Volume=73 mm^3

Fig. 5 Pressure spectra showing the influence of cavity volume in actuator frequency

In such a case if S_m is zero the flow entering the cavity will be completely blocked. On the other hand if S_m/S_c =1 the geometric blockage is zero, i.e. the flow entering the cavity can leave through the other end without flow accumulation inside the actuator. The two limiting cases are shown on either side (Fig.6*b*&*c*) of REM actuator.

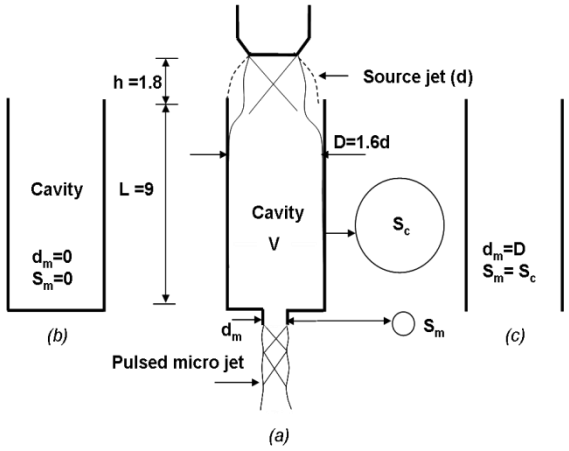

Fig. 6 Actuator configuration used to study the dependence of parameter $n(S_m/S_c)$ on frequency, n=1

The goal of this experiment is to understand the dependence of area ratio (S_m/S_c) on the actuator frequency and to explore the limits of resonance. The jet column length H and the actuator volume V are kept constant respectively at 10.8 mm and 18 mm^3 for the present experiments while the area ratio (S_m/S_c) is varied from 0.01-1. The cavity and the

source jet diameter are 1.6 and 1 mm respectively, similar to the dimensions used in previous experiments. Further details are provided in Table 1 along with a summary of results.

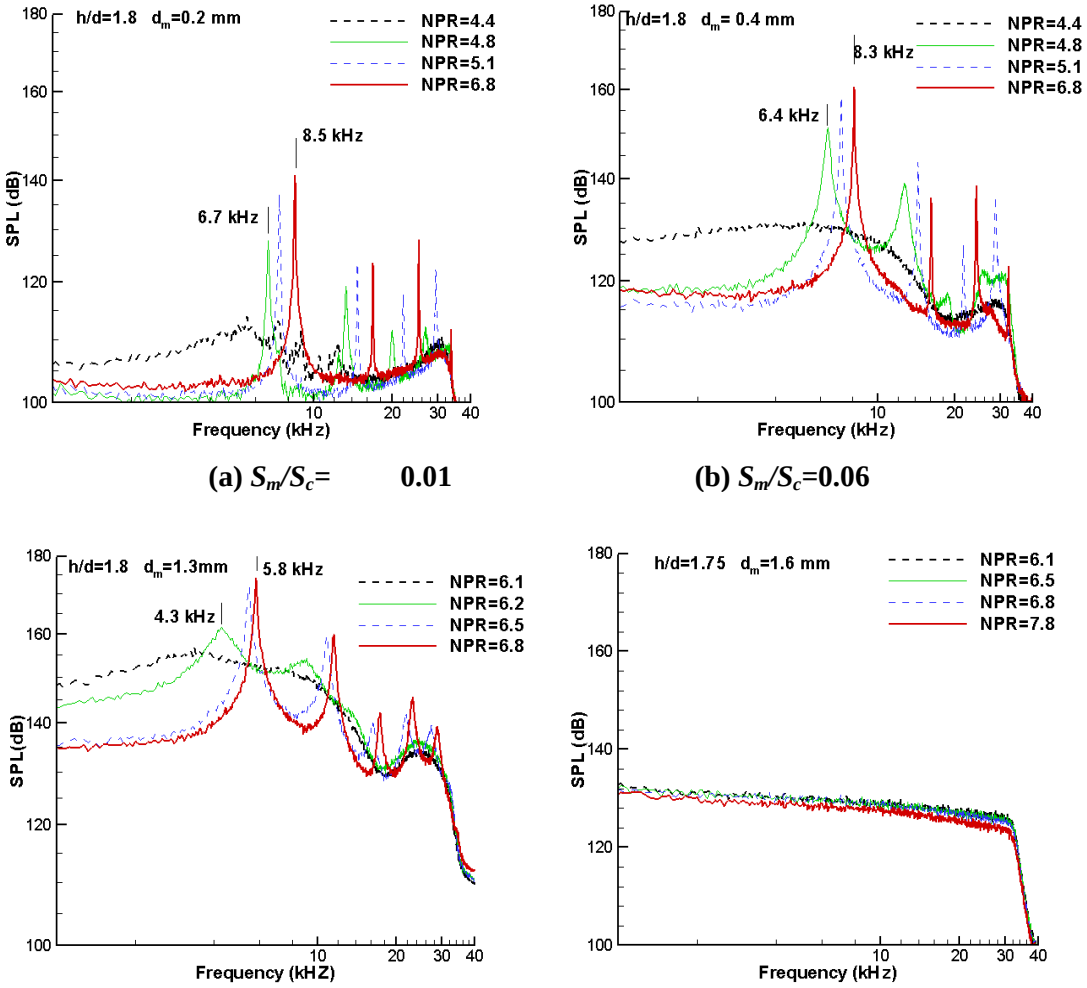

(a) S_m/S_c= 0.01 **(b) S_m/S_c=0.06**

(c) S_m/S_c=0.66 **(d) S_m/S_c=1**

Fig. 7 Pressure spectra of actuator with single orifice at different $n(S_m/S_c)$ ratios

The pressure spectra measured at the actuator exit for this single orifice actuator at different S_m/S_c values are shown in Figure 7*a-d.* As shown in Fig. 7*a*, for the actuator with area ratio S_m/S_c=0.01, the amplified frequency varies from 6.7 to 8.5 kHz, for an *NPR* variation of 4.4 to 6.8. The frequency range remains nearly same (6.4 to 8.3 kHz) for the next case i.e. for S_m/S_c=0.06 as seen in Fig. 7*b*. This shows that for relatively low area ratios, the frequency of the actuator mainly depends on other parameters such as volume *V* and the jet column length *H*, which were discussed above. For a higher area ratio S_m/S_c=0.66, the amplified frequency was reduced to a range of 4.3 to 5.8 kHz. Resonance was not observed for the last case where the area ratio is equal to 1 i.e. $S_m=S_c$ (Fig.7*d*).This is the case where the inflow area and the out flow area are equal so that

there is no flow accumulation inside the actuator. To better understand the effect of the area ratio parameter $n(S_m/S_c)$ on actuator frequency, the resonance frequencies of this actuator at h/d=1.8 and NPR=6.8 are plotted in Fig. 8. In the case of lower area ratios, $n(S_m/S_c) < 0.4$, the frequency remains nominally constant while for a higher area ratio it shifts and is reduced significantly. In the limiting case (S_m/S_c =1) no resonance is observed. This experiment highlights the importance of the parameter $n(S_m/S_c)$ on the REM actuator properties.

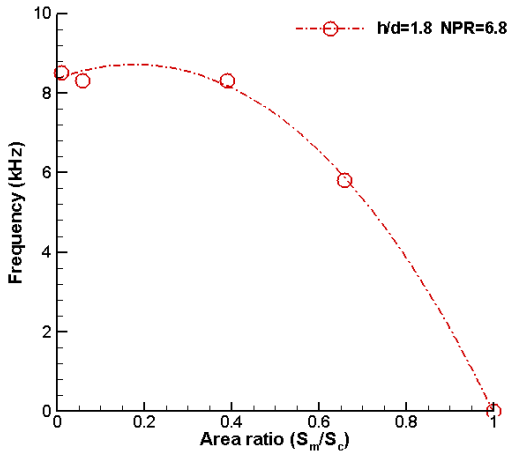

Fig. 8 Frequency variation with area ratio parameter $n(S_m/S_c)$ for actuators with single microjet output at h/d=1.8 and NPR=6.8

Table1: Geometrical details of actuators used to study the effect of inflow-outflow area ratio (S_m/S_c) on REM properties and their frequency responses

d_m (mm)	S_m (mm²)	S_c (mm²)	S_m/S_c	V (mm³)	f_{max} (kHz)
0.18	0.025	2.01	0.01	18.1	8.5
0.4	0.126	2.01	0.06	18.1	8.3
1.0	0.785	2.01	0.39	18.1	8.3
1.3	1.33	2.01	0.66	18.1	5.8
1.6	2.01	2.01	1.0	18.1	No resonance

(c) REM actuator design- An improved model for complex actuator configuration

In general, the results presented so far indicate that the actuator volume V and the area ratio parameter nS_m/S_c are important variables that need to be taken into account while designing actuators with complex geometries. The studies reported earlier [2] can now be seen as a particular case of such a generalized configuration. Table 2 summarizes the details of various parameters of actuators used in the present study. In order to better understand and utilize the larger parametric space tested for the REM actuator (Table 2) and to develop more general design tools for its design, the resonance frequencies with maximum amplitude of various actuators studied were plotted (Fig. 10) against the actuator *Volume.* These results are compared with a semi empirical relation (Equation 4)

derived for the maximum resonance frequency of REM actuator based on a lumped element modeling approach used by Solomon [14]. This comparison is shown in Fig.10 where the parameters used in Equation 4 are indicated in Fig. 9.

$$f_{\max} = \frac{c_0}{2\pi}\left\{\left(\frac{nS_m\ell'_c + S_c\ell'_m}{\ell'_m\,\ell'_c\,V}\right)\left(1-\frac{nS_m}{S_c}\right)\right\}^{1/2} \tag{4}$$

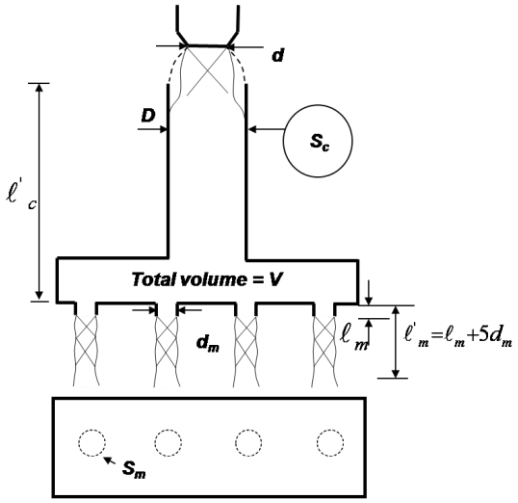

Fig. 9 Parameters used in Equation 4 to determine the actuator resonance frequency with maximum amplitude [8].

Table 2: Geometric details of REM actuators used for the current studies

Actuator	ℓ'_c mm	ℓ_m mm	n	V mm³	S_c mm²	S_m mm²	$n(S_m/S_c)$
A	1	0.5	4	2	2	0.13	0.26
B	2	0.5	4	4	2	0.13	0.26
C	3	0.5	4	6	2	0.13	0.26
D	5	0.5	4	10	2	0.13	0.26
E	9	1.0	1	18	2	0.03 0.13 0.79 1.33 2.01	0.02 0.06 0.39 0.66 1.00
F	9	0.5	6	27	2	0.13	0.39
G	9	0.5	4	34	2.6	0.13	0.2
H	9	0.5	4	54	2.6	0.13	0.2
I	9	0.5	4	73	2.6	0.13	0.2

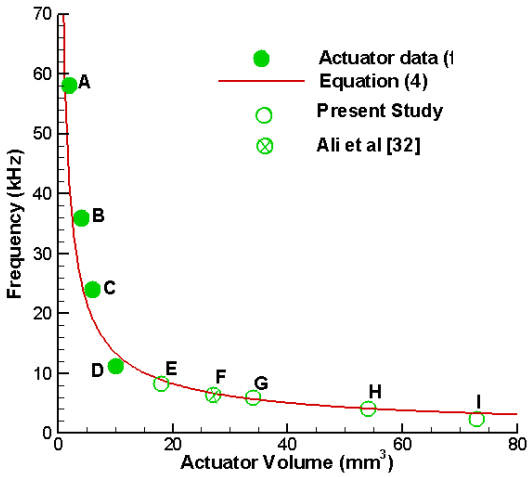

Fig. 10 Resonance frequencies with maximum amplitude of various actuators are compared with the semi empirical equation given in Equation 4

Actuators A-D have a simple cylindrical geometry with 4 microjet output, as shown in Fig. 1. Actuator E is cylindrical with circular cross-section having a single microjet output (Fig. 6). Geometry F is a cylindrical cavity with rectangular spreader at the bottom, similar to Fig. 4, but it has six microjet output. This actuator design was used by Ali et al. [15] to control the resonant flow inside a cavity subjected to supersonic flow. The geometric details of actuators G-I were discussed earlier in section B (a). From the above discussions it is evident that the semi empirical correlation based on actuator volume and the area-ratio parameter, i.e., equation (4), is more general and comprehensive for predicting the most amplified resonance frequency of actuators with complex geometry. Using this improved model, REM actuators may be designed for practical applications that require more complex actuator configurations.

D. Phase conditioned flow visualizations of actuator flowfield

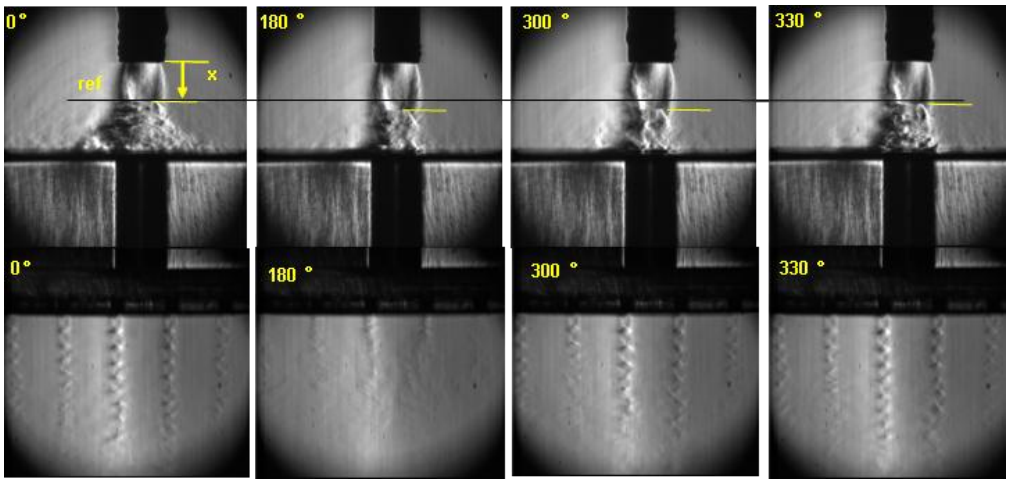

Fig. 11 Phase conditioned images of actuator flowfield (Foster et al. 13)

Fig.11 shows phase locked instantaneous images of the actuator flowfield using a laser based microschlieren system developed for this study [13]. These instantaneous images clearly show the pulsing behavior of source jet, seen as 'filling' and 'spilling' processes. It is evident that the pulsed microjets goes from very low subsonic (close to zero) to supersonic (>300m/sec) velocity at a design frequency of 4 kHz. Fig 12*a* shows a phase averaged image of source jet where Mach disc is seen at a non dimensional distance *x/d* from the source nozzle, where *d* is the source jet nozzle diameter. Fig. 12*b* shows the variation of Mach disc location with the phase angle. A periodic movement of the Mach disc is clearly visible during the unsteady operation of the actuator. Mach disc oscillate from *x/d*=1.3 to *x/d*=1.55 with an amplitude of approximately 300 micrometers. Detailed analysis of these phase locked images indicates that the filling process begins approximately at 180^o while spilling at 330^o as indicated in the Figure 12b. More details of the flow visualization study are available in Foster et al. [13]

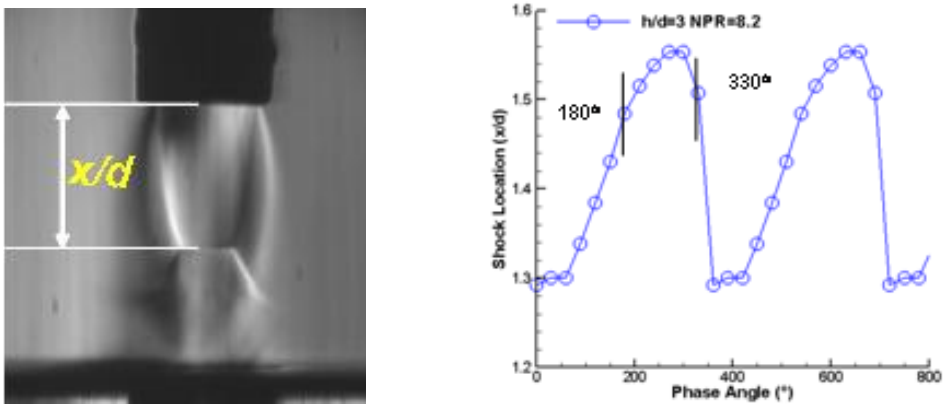

(a) **(b)**

Fig. 12 Phase averaged image of source jet (b) Oscillatory nature of Mach disc

In summary, using high resolution images of actuator flowfield captured using a highly sensitive lens based laser-schlieren system, a better understanding on the actuator dynamics is achieved from this study.

E. Actuator Dynamics: Synchronous unsteady pressure measurements

The flow features of various REM actuator designs discussed so far indicate that the physical mechanisms are very similar, irrespective of the actuator geometry. To better understand the resonance mechanism and the unsteady properties of REM actuator, synchronous measurements were carried out using multiple ultra-miniature unsteady pressure sensors and microphones. Using two Kulite probes and a microphone, the unsteady pressures inside the actuator cavity, of microjets and in the near field were measured simultaneously. The configuration was shown earlier in Fig. 4 and the pressure spectra are shown in Fig. 13. As seen in Fig. 13, the measurements show same spectral peaks with a discrete frequency of 6.1 kHz for a given condition, confirming the global nature of the flow unsteadiness. However, as expected, a phase lag is noticed between

these frequencies measured at 3 different locations. More details of the synchronized unsteady pressure measurements are available in Solomon et al. [1].

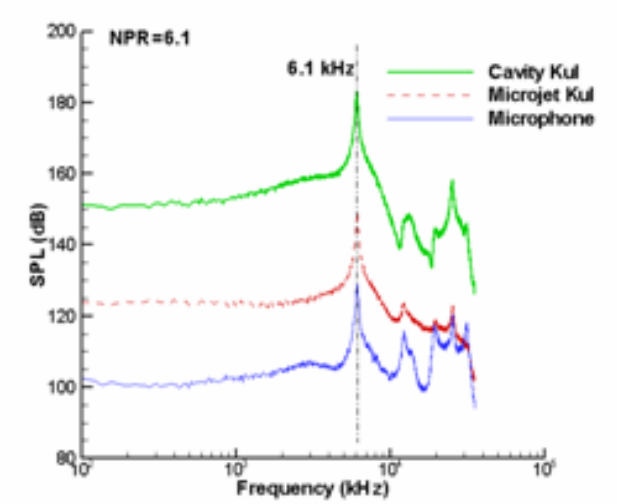

Fig. 13 Pressure spectra measured by two Kulite probes, one kept inside the cavity and other exposed to the pulsing microjets, and a microphone positioned in the near field as shown in Fig.6

F. Design and implementation of pulsed microactuators for cavity flow control

A cavity subjected to supersonic flow, such as a weapon or cargo bay (Fig 14), generates highly unsteady flow and cause significant pressure fluctuations inside that affect the dynamics of the released load. Zhuang et al. [45] have studied this problem experimentally using a miniature cavity model. A rectangular cavity subjected to Mach 1.5 flow experienced flow unsteadiness in a range of 4-6 kHz, as reported in reference [45]. Zhuang et al. used a flow control scheme based on microjet injection at the leading edge of the cavity to suppress the flow unsteadiness inside. With a motivation to develop a better control scheme based on pulsed microjet injection, REM actuators were designed and integrated to a scaled model of a generic rectangular cavity subjected to Mach 1.5 flow as shown in Fig. 15 that has a dominant frequency in a range of 4-6 kHz. In Fig. 15 CF1, CF2, CF3 are locations of Kulite probes inside the cavity. The design details and the frequency response of the integrated actuator are shown in Fig.16 and 17 respectively.

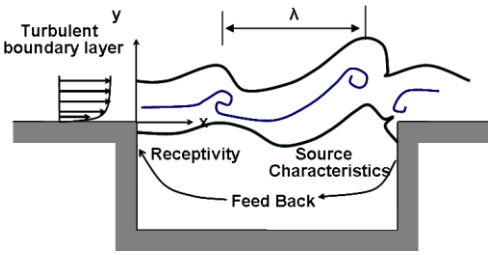

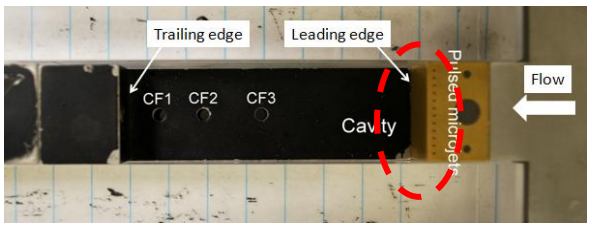

Fig.14 Unsteady flow inside a cavity

Fig.15 Cavity model with integrated actuators

At *NPR*= 5.9 the microactuators were pulsing nearly at 6 kHz as indicated in Fig. 17. Fig. 18*a* and *b* shows unsteady spectra of the cavity measured by Kulites located at the cavity floor at distance *x/L*=.74 (CF1) and *x/L*=0.53 (CF2) respectively from the leading edge with and without control. It is evident that pulsed actuation has reduced the peak cavity tone over 7 dB while an OASPL reduction of 4-5 dB is achieved using this control approach. More details of the actuator design and experiment are available in Ali et al. [15].

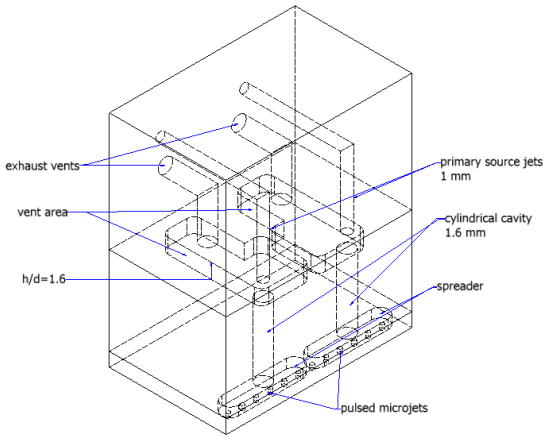

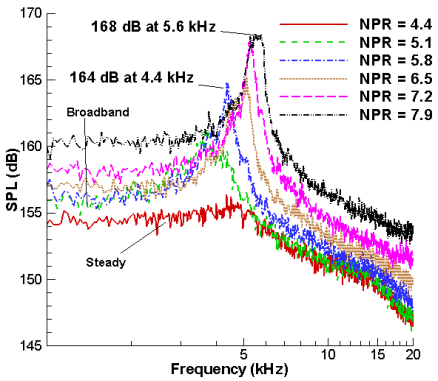

Fig. 16 Design details of actuator module **Fig. 17 Actuator spectra integrated inside cavity**

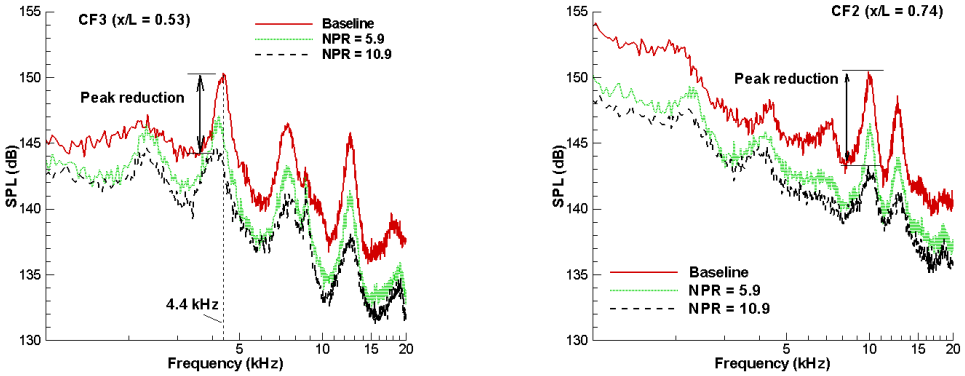

a) **b)**

Fig. 18 Pulsed actuation control: Cavity spectra with and without control @ a) x/L=0.53 b) x/L=0.74

We also explored another high-speed flow control application to study the potential capabilities of this control approach based on resonating supersonic pulsed microjets. For this study REM actuators were designed and used for the control of a resonating impinging jet, which is discussed next.

G. Design and implementation of pulsed microactuators for impinging jet control

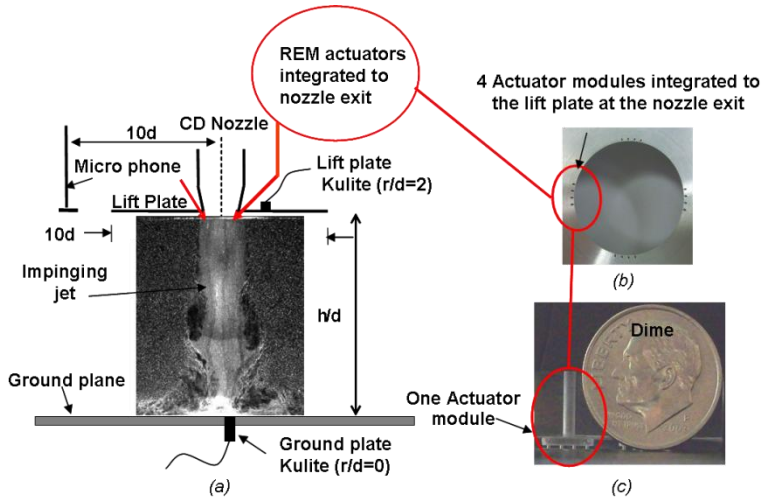

Fig. 19 Schematic of Impinging jet test facility *a*) locations of unsteady sensors *b*) 4 REM actuator modules integrated to the lift plate; *c*) Picture of an actuator module that generate 4 pulsed microjets

An impinging supersonic jet can generate highly unsteady flowfield with discrete high energy noise at certain operating conditions. Previous research [46, 47] shows such a flowfield produces high amplitude discrete tones in a range of 4–6 kHz. The main goal of present study is to design and implement REM actuators, close to this frequency range of baseline flow unsteadiness, and study the effect of pulsed actuation in an impinging jet flow.

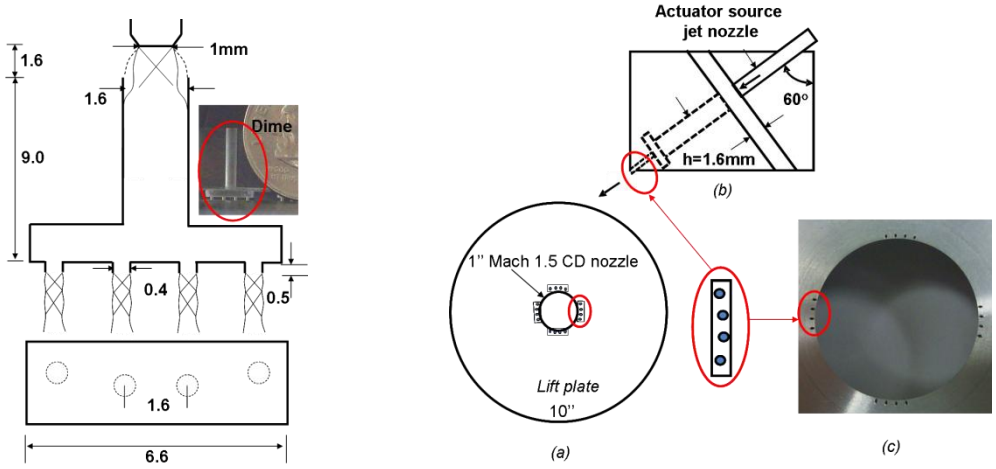

i) ***ii)***

Fig. 20 Design details of a REM actuator module integrated on to the lift plate *i*) Geometric details of one module *ii*) (*a*) Configuration of 4 actuator modules integrated the lift plate (*b*) Resonant microjets are inclined at an angle of 60° to the axis of the Mach 1.5 CD nozzle (*c*) Image of REM actuator distribution along the circumference of CD nozzle exit

In order to meet such a requirement the present actuator was designed and fabricated with certain parameter values as shown in Fig. 20, which is chosen based on detailed parametric studies conducted on REM actuator by Solomon [1], where actuator volume is observed strongly correlated to its frequency. Four of these REM actuator modules, that produce 16 resonant microjets, are integrated to the lift plate in a configuration as shown in Figure 20. The microjets will interact with the main jet from the Mach 1.5 CD nozzle at an inclination angle of 60º.

Characterization of Integrated REM actuator

Fig. 21 shows the pressure spectra of the REM actuator integrated to the lift plate of impinging test facility close to the CD nozzle exit. As seen in Fig. 21, by varying the nozzle pressure ratio of actuator source jet from 5.4 to 6.7, the actuator frequency can be tuned from 4.4 to 6 kHz. The actuator is designed for maximum resonance frequency of 5.5 kHz, predicted by the design correlation given in Equation 4 for this geometry. Actuator response is nearly broadband, close to the resonance threshold at NPR_m =5.4 and the resonance behavior starts approximately at NPR_m =5.6, showing a low amplitude peak at 4.4 kHz. At higher NPR_m=5.9, the amplitude of this tone increases indicating high energy concentration at this frequency. Further increase in NPR_m has changed the pulsing frequency from 4.4 to 6 kHz as seen in Fig. 21.

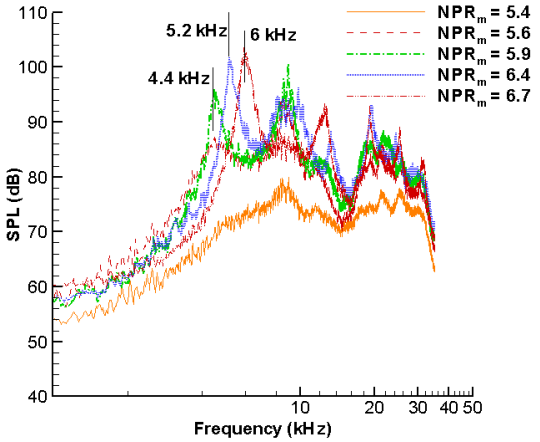

Fig. 21 In-situ characterization of the actuator integrated into the 'lift plate' using a near-field microphone

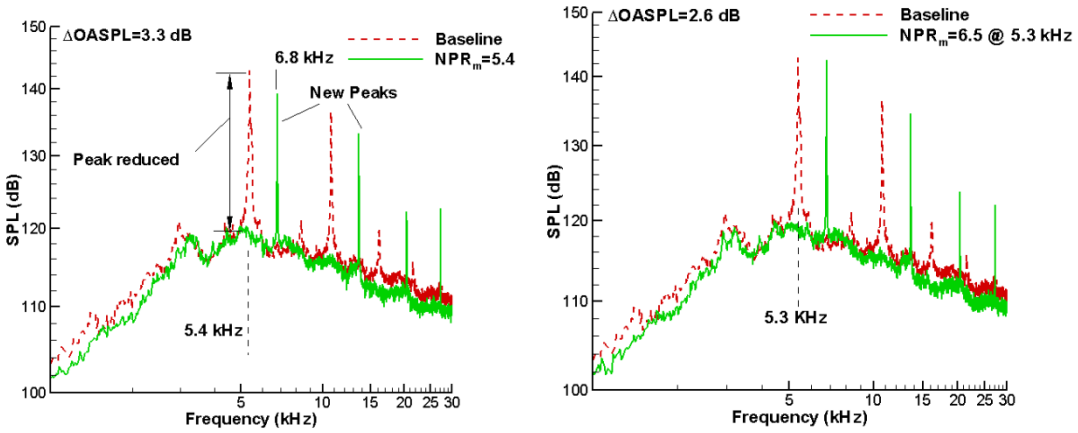

a) Actuator source jet NPR_m =5.4 b) Actuator source jet NPR_m=6.4 @ 5.4 kHz

Fig. 22 Impinging jet spectra with and without control at h/d=4.5

The effect of REM actuation, at two different actuator source jet NPR values, on the impinging jet flowfield are shown in Fig. 22, for a nozzle-impinging surface distance h/d = 4.5. The baseline unsteady spectra of the impinging jet are shown as red dotted legends that show a discrete impinging tone at 5.4 kHz. Green spectra indicate the effect of REM actuation.

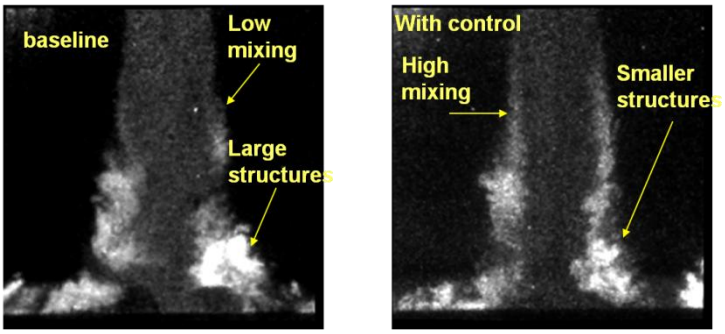

Fig. 23 Effect of high frequency excitation on shear layer of a supersonic impinging jet

The interesting observation is that REM actuation has completely removed the impinging tone from the spectra. However, new tones with less energy appeared in the spectra that resulted in a reduction in the OASPL of the flowfield up to 3-5 dB for a range of test conditions. More details of this experiment are reported in [17]. Fig. 23 shows the impinging flowfield with and without actuation using a planar laser scattering (PLS) method. As indicated in the figure, pulsed actuation has reduced the size of vortex structures in the shear layer as well as increased its mixing characteristics. These results indicate potential capabilities of REM actuators to manipulate unsteady properties of a supersonic flow.

Though we have successfully designed and implemented high bandwidth REM actuators and achieved remarkable control over two supersonic flows, an optimized design is expected to improve the efficiency of this control approach. Currently we are in the process of redesigning the actuator while keeping in mind the lessons learned from this study. Furthermore, to improve the control authority of resonance enhanced microactuator in terms of phase control and fast time response, active smart materials are also being integrated to these devices, which are discussed next.

H. Future studies on resonance enhance microactuator: Integrating smart materials for faster time response and phase control

The next generation design of REM actuators aims at a faster time response and phase control on their unsteady output. Fig. 24 shows such a design where smart PZT materials were integrated to the actuator cavity walls. The actuator geometry can be changed using PZT stacks controlled by an external forcing signal. This design –integrating fluidic and smart materials –called SMART REM, was studied recently by Kreth et al. [12] and the

initial results were very promising. These studies will be continued further to develop a comprehensive active control scheme for high speed flows.

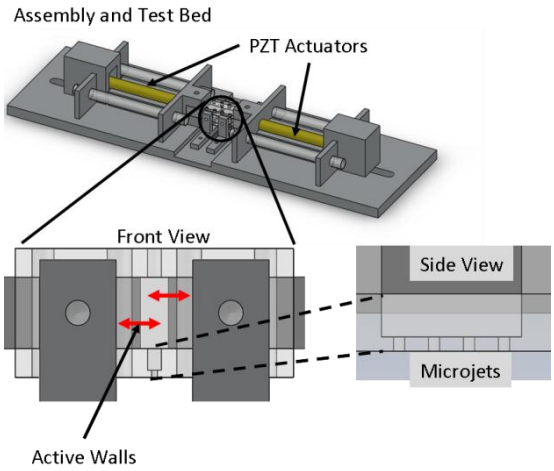

Fig. 24 REM actuators with integrated smart materials for precise frequency and phase control

Related Publications (2008-2012)

Archival Journal Publications

1. Solomon, J.T., Foster, C., Alvi F.S., "Design and characterization of High-Bandwidth, Resonance Enhanced, Pulsed Microactuators: A parametric Study", submitted to *AIAA Journal*, 2012-Accepted.
2. Solomon, J.T., Kumar R., Alvi F.S., "High Bandwidth Pulsed Microjets for High Speed Flow Control", *AIAA Journal*, 2010, Vol. 48, No.10, pp.2386-2396.
3. Kumar, V., Hays, M.., Fernandez E., Oates, W. and Alvi, F. S., "Flow Sensory Actuators for Micro Air Vehicles," *Smart Mater. Structures*, Vol. 20, September 2011, HYPERLINK "http://dx.doi.org/10.1088/0964-1726/20/10/105033" doi:10.1088/0964-1726/20/10/105033
4. Kumar, R., Ali, Y., Alvi, F. S. and Venkatkrishnan, L., "Generation and Control of Oblique Shocks Using Microjets," *AIAA Journal*, 2011, Vol. 49, No. 12, pp. 2751-2759.
5. Alvi, F. S. and Cattafesta, L. N., "The Art and Science of Flow Control – Case Studies Using Visual and Optical Methods," in "Revealing the Invisible- A Review of Flow Visualization Techniques," *European Physical Journal*, Special Topics, Vol. 182, pp. 97–112 (2010). DOI: 10.1140/epjst/e2010-01227.
6. Kumar, V. and Alvi, F. S., "Towards Understanding and Optimizing Separation Control Using Microjets," *AIAA Journal*, 2009, Vol. 47, No. 11, pp. 2544-2557.
7. Arunajatesan, S., Kannepali, C., Sinha, N., Sheehan, M., Alvi, F. S., Shumway, G. and Ukeiley, L., "Suppression of Cavity Loads Using Leading Edge Blowing," *AIAA Journal*, 2009, DOI: 10.2514/1.38211, 2009.

8. Alvi, F. S., H. Lou, C., Shih, C and R. Kumar., "Experimental study of physical mechanisms in the control of supersonic impinging jets using microjets," *Journal of Fluid Mechanics*, vol. 613, 2008, pp. 55-83, 2008.

Conference Proceedings

9. Topolski, N., Arora, N., Ali, M.Y., Solomon, J.T., Alvi, F.S., "Study on Resonance Enhanced Microactuators in Supersonic Crossflow", To be presented in 42nd AIAA Fluid dynamics Conference and Exhibit 25-28 June 2012.
10. Garret, S., Solomon, J.T., Gustavson, G., Alvi, F.S., "Implementing Resonance Enhanced Microactuators for the control supersonic microjets'', AIAA-0065, 2012.
11. Uzun, A., Foster, C.H., Solomon, J.T., Oates, W.S., Hussaini, M.Y., Alvi, F.S., "Silumations of Pulsed Microactuators of High –Speed Flow Control", AIAA-2938, 2011.
12. Kreth, P., Solomon, J.T., Alvi, F.S., "Resonance-Enhanced High Frequency Micro-actuators with Active Structures", AIAA-2939, 2011.
13. Foster, C., Solomon, J.T., Alvi, F.S., "Visual Study of Resonance dominated Microjet flows using laser based micro- Schlieren", AIAA-2011-766, 2011.
14. Solomon, J.T., PhD dissertation, Florida State University, 2010.
15. Ali, M.Y., Solomon, J.T., Gustavsson, J., Alvi, F.S., "Control of Supersonic Cavity Flows Using High Bandwidth Micro actuators", AIAA-197194-564, 2010.
16. Solomon, J.T., Alvi, F.S., Kumar, R., Gustavsson, J., "Principles of a High Bandwidth Micro-actuator Producing Supersonic Pulsed Microjets", AIAA-197237-476, 2010.
17. Solomon, J.T., Wiley, A., Kumar, R., Alvi, F.S., "Active and Adaptive Control of Supersonic flow using High Bandwidth Pulsed Micro-actuators", FCAAP meeting Aug 13-14 2009.
18. Solomon, J.T., Wiley, A., Kumar, R., Alvi, F.S., "Development and Implementation of High Frequency Pulsed Microactuators for Active Control of Supersonic Impinging Jet", SAROD meeting, National Aerospace Lab, India, 2009.
19. Solomon, J.T., Hong, S., Wiley, A., Kumar, R., Annswamy, A.M., Alvi, F.S., "Control of Supersonic Resonant flows Using High bandwidth Micro- Actuators", AIAA -3247, 2009.
20. Solomon, J.T., Kumar, R., Alvi, F.S., "Development and characterization of High bandwidth micro actuator", ASME FEDSM 55032, 2008.
21. Solomon, J.T., Kumar. R, Alvi, F.S., "High band width pulsed micro actuators for active flow control', AIAA-3042, 2008.

Honors and Awards (2009-2012)

F.S. Alvi: Elected Fellow of American Society of Mechanical Engineers (ASME)
F.S. Alvi: Invited Professor at Université d'Orléans, France, 2009-2010.
F.S. Alvi: *Engineering Invention Award* – "In Recognition of Exceptional Achievement," (with Profs. C. Shih & A. Krothapalli) 2009

Patents

High Frequency Pulsed Microjet Actuation (with Oates & Clarke), utility patent filed, March 2011.

High Bandwidth & Control Authority Micro-Actuators for Active Flow & Noise Control (with Kumar & Solomon) – utility patent application filed, May 2010

Acknowledgement/Disclaimer

This work is supported by the Air Force Office of Scientific Research, USAF, under AFOSR Grant number FA9550-09-1-0353. The views and conclusions contained herein are those of the authors and should not be interpreted as necessarily representing the official policies and endorsements, either expressed or implied, of the Air Force Office of Scientific Research or the U. S. Government.

References

22. Seifert, A., Darabi, A., and Wygnanski, I., "Delay of Airfoil Stall by Periodic Excitation," *Journal of Aircraft*, Vol. 33, No. 4, 1996, pp. 691-698.
23. McManus, K., and Magill, J., "Separation Control in Incompressible and Compressible Flows using Pulsed Jets," AIAA Paper 1948, 1996.
24. Bryant, R. G., Fox, R. L., Lachowicz, J. T., and Cheri, F.J., "Piezoelectric Synthetic Jets for Aircraft Control Surfaces," SPIE Paper 3674, 1999.
25. Wiltse, J. M., and Glezer, A., "Manipulation of Free Shear Flows Using Piezoelectric Actuators," *Journal of Fluid Mechanics*, Vol. 249, 1993, pp. 261-285.
26. Smith, B, L., and Glezer, A., "The Formation and Evolution of Synthetic Jets," *Physics of Fluids*, Vol. 10, No. 9, 1998, pp. 2281-2297.
27. Cattafesta, L., Mathew, J., Wang, W., and Kurdila.A., "Modeling of Piezoelectric Actuators for Fluid Flow Control," SAE Paper 01-5534, 2000.
28. Joslin, R. D., Horta, L. G., and Chen, F.J., "Transitioning Active Flow Control to Applications," AIAA Paper 3575, 1999.
29. List, J., Byerley, A., McLaughlin, T., and Dyken, R. V., "Using a Plasma Actuator to Control Laminar Separation on a Linear Cascade Turbine Blade," AIAA Paper 1026, 2003.
30. Jacob, J. D., Rivir, R., Carter, C., and Estevadeordal, J., "Boundary Layer Flow Control using AC Discharge Plasma Actuators," AIAA Paper 2128, 2004.
31. Corke, T. C., Enloe, C. L., and Wilkinson, S. P., "Dielectric Barrier Discharge Plasma Actuators for Flow Control," *Annual Review of Fluid Mechanics*, Vol. 42, 2010, pp 505-529.
32. Ganiev, Y. C., Gordeev, V. P., Krasilnikov, A. V., Lagutin, V. I., Otmennikov, V. N., Panasenko, A. V., "Theoretical and Experimental Study of The Possibility of Reducing Aerodynamic Drag by Employing Plasma Injection," AIAA paper1999-0603.
33. Kelley, C., Bowles, P., Cooney, J., He, C., Corke, T., "High Mach number Leading-Edge Flow Separation Control Using AC DBD Plasma Actuators," AIAA paper 0906, 2012.

34. Grossman, K. R., Cybyk, B. Z., and Van Wie, D. M., “Spark Jet Actuators for Flow Control,” AIAA Paper 57, 2003.
35. Cutler, A., Drummon, J. P., “Toward a High-Frequency Pulsed-Detonation Actuator,” AIAA paper 555, 2006.
36. Samimy, M., Kearney-Fisher, M., Kim, J., and Sinha, A., "High speed and High Reynolds Number Jet Control Using Arc Filament Plasma Actuators for Noise Mitigation and for Flow and Noise Diagnostics," AIAA paper 2011-22.
37. Yeung, P. K., Brasseur, J. G., and Wang, Q., “Dynamics of Direct Large-Scale Couplings in Coherently- Forced Turbulence: Concurrent Physical-Space and Fourier-Space Views,” *Journal of. Fluid Mechanics*, Vol. 283, 1995, pp 43-95.
38. Wiltse, J. M., and Glezer, A., “Direct Excitation of Small Scale Motions in Free Shear Flows,” *Physics of Fluids*, Vol. 10, No. 8, 1998, pp 2026-2036.
39. Stanek, M. J., Raman, G., Kibens, V., Ross, J. A., Odedra, J., and Peto, J. W., “Control of Cavity Resonance Through Very High Frequency Forcing,” AIAA paper 1905, 2000.
40. Hartmann, J., and Trolle, B., “A new acoustic generator,” *Journal of Scientific Instruments*, Vol. 4, No. 4 ,1927, pp 101-111.
41. Raman, G., and Kibens, V., “Active Flow Control using Integrated Powered Resonance tube Actuators,” AIAA Paper 3024, 2001.
42. Kastner, J., and Samimy, M., “Development and Characterization of Hartmann tube fluidic actuators for high-speed flow control,” *AIAA Journal*, Vol. 40, No.10, 2002, pp. 1926-1934.
43. Dziuba, M., and Rossmann, T., “Active control of a Sonic Transverse Jet in a Supersonic Cross Flow using a powered Resonance tube,” AIAA Paper 897, 2005.
44. Brocher, E., Maresca, C., and Bournay, M. H., “Fluid Dynamics of the Resonance Tube,” *Journal of Fluid Mechanics*, Vol. 43, Part 2, 1970, pp 369-384.
45. Zhuang, N., Alvi, F.S., Alkislar, M.B., and Shih, C., “Supersonic Cavity Flows and their Control,” *AIAA Journal*, Vol. 44, No. 9, 2006, pp. 2118-2128.
46. Alvi, F.S., Shih, C., Elavarasan, R., Garg, G., and Krothapalli, Al., “Control of Supersonic Impinging Jet Flows Using Supersonic Microjets,” *AIAA Journal,* Vol. 41, No. 7, 2003, pp. 1347-1355.
47. Kumar, R., Lazic, S. and Alvi, F. S., “Control Of High Temperature Supersonic Impinging Jets Using Microjets,” *AIAA Journal*, 2009, Vol. 47, No. 12, pp. 2800-2811.

Appendix: Copies of Papers Published.

1. Solomon, J.T., Foster, C., Alvi F.S., “Design and characterization of High-Bandwidth, Resonance Enhanced, Pulsed Microactuators: A parametric Study”, submitted to *AIAA Journal*, 2012-Accepted.
2. Solomon, J.T., Kumar R., Alvi F.S., “High Bandwidth Pulsed Microjets for High Speed Flow Control”, *AIAA Journal,* 2010, Vol. 48, No.10, pp.2386-2396.
3. Garret, S., Solomon, J.T., Gustavson, G., Alvi, F.S., “Implementing Resonance Enhanced Microactuators for the control supersonic microjets’’, AIAA-0065, 2012.

4. Solomon, J.T., Hong, S., Wiley, A., Kumar, R., Annswamy, A.M., Alvi, F.S., “Control of Supersonic Resonant flows Using High bandwidth Micro- Actuators”, AIAA -3247, 2009.
5. Ali, M.Y., Solomon, J.T., Gustavsson, J., Alvi, F.S., “Control of Supersonic Cavity Flows Using High Bandwidth Micro actuators”, AIAA-197194-564, 2010.

AIAA JOURNAL
Vol. 48, No. 10, October 2010

High-Bandwidth Pulsed Microactuators for High-Speed Flow Control

John T. Solomon,* Rajan Kumar,† and Farrukh S. Alvi‡
Florida A&M and Florida State University, Tallahassee, Florida 32310

DOI: 10.2514/1.J050405

A systematic study on the design, development, and characterization of high-momentum, high-bandwidth microactuators for high-speed flow control is described in this paper. Beginning with building-block experiments, multiple resonant flow phenomena are used in the actuator design to arrive at an actuator configuration that provides the desired flow properties. The first-generation actuator design consists of an underexpanded source jet incident upon a cavity. The lower surface of this cavity contains micronozzles through which the unsteady microjets (400 μm) issue. Results show that microjets produced by this actuator have a high mean momentum (300–400 m/s) and a significant unsteady component (20–30% of the mean). Experiments were conducted over a large range of parameters in terms of cavity length, source jet nozzle pressure ratio, and impingement distance. The results unequivocally demonstrate the ability to vary the frequency and the amplitude of the mean and unsteady momentum of microjets issuing from this actuator. By varying the dimensions of the actuator by few hundred microns and/or source jet pressure by roughly 1 atm, one is able to vary the frequency rather precisely over a range of 5–20 kHz. A correlation based on Strouhal number and jet column length is suggested for the design of actuators. Actuators in the frequency range of a few to well over 50 kHz have been designed and characterized. It is believed that the frequency range may be extended down to $\mathcal{O}$(100 Hz) and up to $\sim\mathcal{O}$(100 kHz) using this actuator approach.

I. Introduction

DESIGN and development of active flow control systems have received wide attention in the recent years due to their ability in reducing or eliminating a number of adverse and parasitic effects associated with aerodynamic flow and providing potentially substantial gains in performance. A number of such systems have been developed and tested over the years by many researchers, some of which were found promising in a limited range of flow conditions. Ideally, the desired control effect (e.g., noise reduction, flow separation control, and turbulent mixing) must be achieved with minimal energy input. Active control of high-speed flow demands high-amplitude and high-bandwidth actuation techniques for the effective and efficient manipulation of such high-energy/high-momentum flows and structures that are often responsible for the adverse flow characteristics. An example of such a flowfield is associated with a supersonic cavity. Various active and passive control strategies have been explored to control the aeroacoustically induced cavity flow oscillations (Zhuang. et al. [1] and Ukeiley et al. [2]). Another high-speed flowfield that requires proficient active control is associated with supersonic impinging jets (Krothapalli et al. [3], Alvi et al. [4], and Kumar et al. [5]). A short takeoff and vertical landing aircraft during its hovering mode, especially in close proximity to the ground, produces a highly unsteady flowfield that produces intense unsteady aeroacoustic loads that can lead to ground erosion and structural damage to the near-field structures. The above examples point to the necessity of developing energy-efficient and effective actuator systems for a number of aeroacoustic problems. In addition, progress in the area of microelectronics has given rise to more challenging problems associated with the thermal management of microdevices (Ro and Loh [6]). Development of effective microactuator systems that are scalable and capable of addressing some of these issues may potentially be beneficial toward solving these problems as well.

Flow control methods are generally classified into active and passive based on the involvement of external energy in the control process. Passive methods do not require external energy input but make use of the energy associated with the primary flow for the purpose of control. Variations in nozzle geometry, i.e., rectangular, triangular, elliptic, etc. (Sfeir [7], Sforza et al. [8], and Schadow et al. [9]), use of mechanical tabs of different shapes and the use of splitter plates (Zaman et al. [10] and Reeder and Samimy [11]) are examples of various passive control methods adopted for the control of jet noise. On the other hand, in active flow control schemes, an external energy source is used for tailoring the natural behavior of a shear-layer or a boundary-layer flow according to the control objectives. The ability to efficiently adapt to changing flow conditions (the ultimate goal of active control schemes) makes them more attractive than passive methods.

Mechanical systems such as vibrating ribbons and cantilevered beams and electromechanical devices such as piezoelectric diaphragms, voice coils, and speakers are used as external energy sources in various active flow control schemes. The vibration of a piezoelectric material is used for generating a low-momentum air jet with zero net mass flux (synthetic jets) for the control of cavity flows (Cattafesta et al. [12]) and shear flows (Wiltse and Glezer [13]). Actuators based on synthetic jets have also been used for separation control over airfoils and cylinders (Amitay et al. [14]). A number of researchers in the past modified the Hartmann tube and used it as a flow actuator, demonstrating reasonable success over a limited range of flow conditions (Raman and Kibens [15], Kastner and Samimy [16], and Dziuba and Rossmann [17]). Although relatively successful at low speeds, many actuators are not very efficient when the primary flow velocities are high, in particular supersonic. Optimal manipulation of the shear or boundary layer of high-speed flows requires aeroacoustic disturbances with high momentum or energy, and actuators whose steady and unsteady components can be manipulated. A simple and robust actuator, with high mean and unsteady momentum that can be easily integrated into practical high-speed flow applications and subsystems is essential for efficient active flow control schemes. The present studies are motivated and driven by this goal.

Presented as Paper 2008-3042 at the 14th AIAA/CEAS Aeroacoustics Conference, Vancouver, British Columbia, Canada, 5–7 May 2008; received 28 December 2009; revision received 21 May 2010; accepted for publication 8 June 2010.

*Graduate Research Assistant, Florida Center for Advanced Aeropropulsion, Department of Mechanical Engineering. Student Member AIAA.

†Research Scientist, Florida Center for Advanced Aeropropulsion, Department of Mechanical Engineering. Senior Member AIAA.

‡Professor, Florida Center for Advanced Aeropropulsion, Department of Mechanical Engineering. Associate Fellow AIAA.

Over the last decade, supersonic impinging-jet flows have been the subject of extensive study at our laboratory. To reduce the feedback-driven unsteadiness in the impinging-jet flowfield, an array of *supersonic steady microjets*, were mounted circumferentially around the main jet. This control technique proved to be very effective, reducing the overall pressure fluctuations and noise levels by as much as 10–15 dB for cold and hot impinging jets. One of the reasons for the success of this technique is likely due to the fact that the high momentum associated with the supersonic microjets allows them to penetrate the primary jet shear layer sufficiently to disrupt the feedback loop (Alvi et al. [4], Kumar et al. [5], and Lou et al. [18]). Furthermore, the small diameter of the supersonic microjets dramatically reduces the mass flow requirement while producing very high-momentum jets. This microjet-based control scheme was equally successful when applied for reducing the unsteady pressure loads in a supersonic cavity flow (Zhuang et al. [1]). The pressure spectra depicting the effect of microjet control on a supersonic impinging jet (Kumar et al. [5]) and supersonic cavity flow (Zhuang et al. [1]) are shown in Fig. 1.

These spectra show the presence of strong, discrete tones in the baseline flow approximately in the range of 4–10 kHz. With steady microjet control, the amplitude of the tones was reduced significantly but not completely eliminated. It is anticipated that actuators with a strong unsteady component in this frequency range could further enhance the control efficacy of microjet-based control of such flows. Motivated by the success of steady supersonic microjets for flow control, and the lessons learned from our previous research and those of others, a program was initiated to develop *pulsed microjet actuators* that produce unsteady microjets with high mean and unsteady momentum and whose actuation frequency would be variable over a large range. Here, we describe an experimental program, where high-speed microjets are combined with a cavity and other geometric features to generate a highly unsteady, pulsed flow. Such a flow could be used to produce high-momentum, unsteady jets, which can be used as fluidic actuators. Furthermore, the unsteady component (frequencies) of such actuators can be tuned for specific applications.

II. Experimental Apparatus and Procedures

The experiments were conducted in the Advanced Aero-Propulsion Laboratory at the Florida State University. Measurements include flowfield visualization using a lens-based microschlieren system and unsteady pressure measurements using an ultraminiature Kulite pressure transducer. Measurements were made for the actuator source jet operating over a range of nozzle pressure ratios (NPR) equal to jet stagnation pressure/ambient pressure of 1.9–6.8, corresponding to moderate to strongly underexpanded jets and over a range of geometrical parameters. The details of the measurement techniques employed are described below.

A. Microschlieren System

Since the length scales associated with the present actuator system are too small ($\sim$10 μm) to be resolved by a conventional schlieren system, a specifically designed lens-based microschlieren system (similar to the one used in Phalnikar et al. [19]) with very high magnification and sensitivity is used for the present study. The flowfield is visualized at an optimized combination of the critical parameters that determine the quality of the schlieren images, such as magnification, resolution, field of view, and sensitivity. The microschlieren system uses high-magnification, in-line achromatic lens-based optics, coupled with a graded filter (to minimize diffraction effects) and a Kodak Megaplus ES 1.0 camera with a charge-coupled-device array of resolution of 1008 $\times$ 1018 pixels. A white light stroboscopic lamp with adjustable frequency (up to 1 kHz) and intensity was used as the light source. The resultant magnification obtained from the lens-based system was as high as 4–5. More details of the optics used in the microschlieren system are available in Phalnikar et al. [19].

B. Unsteady Pressure Measurements

The unsteady flow issuing out of these microjets was measured using a probe (1.5 mm diameter) with a 100 psia range, ultra-miniature (1.3 mm diameter) Kulite model XCE-062 pressure transducer. The unsteady pressure signals were acquired through high-speed National Instruments digital data acquisition cards using LabVIEW software. The transducer output was conditioned using a low-pass Stanford SR640 filter (cutoff frequency of 60 kHz) and sampled at 200 kHz. Standard DFT (discrete Fourier transform) analysis was used to obtain narrowband pressure spectra using 4096 points/DFT. A total of 100 DFTs so computed, without overlap, were averaged to obtain statistically reliable narrowband spectral estimates.

C. Measurement Uncertainties

The important geometrical and flow parameters involved in the present study are the nozzle to cavity distance h, length of the cavity L and the nozzle pressure ratio NPR. The cavity length L was machined with tolerances of $\pm$10 microns. Precise measurement of h during experiment was achieved using microtraverses with an accuracy of $\pm$12.5 microns. The pressure sensors used for these experiments were carefully calibrated. An Omega transducer PX303-200 G5V was used to measure jet total pressure and the uncertainty associated with the total pressure measurement was $\pm$1 psi. The unsteady pressure measurements made using the Kulite sensor were accurate within $\pm$0.1 psi.

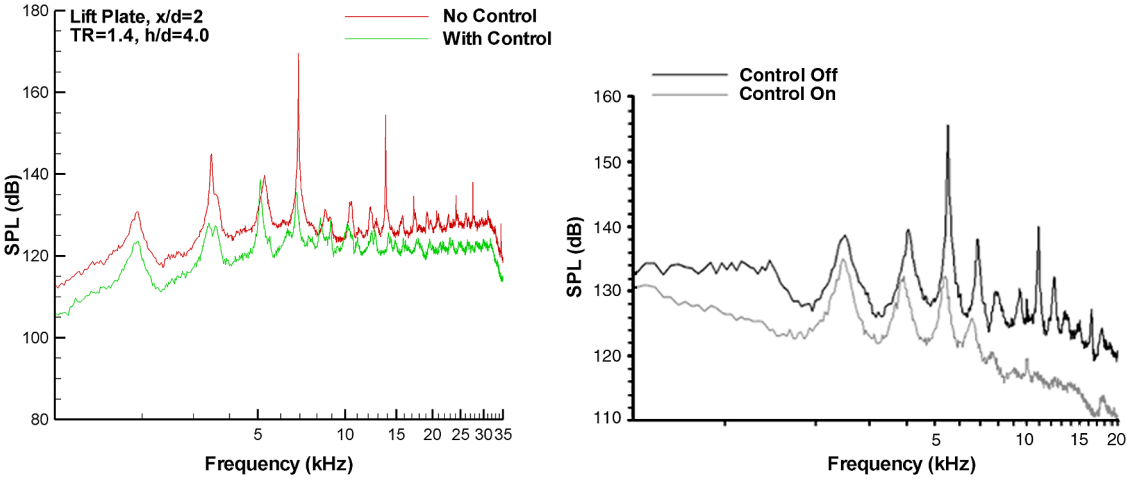

a) Mach 1.5 Impinging jet (Kumar et al. [5]) b) Mach 2 Cavity flow (Zhuang et al. [1])

Fig. 1 Pressure spectra illustrating the effect of steady microjet control of supersonic flows.

III. Building-Block Experiments for Microactuator Development

The initial inspiration for this actuator design came from our extensive studies of larger supersonic impinging jets (Krothapalli et al. [3] and Alvi et al. [4]). As seen in Fig. 1a, such jets produce a highly unsteady flowfield with significant energy at discrete frequencies, seen as high-amplitude peaks in Fig. 1 and commonly referred to as impingement tones. Furthermore, the frequency of these tones can be varied by varying the jet NPR and/or the distance between the nozzle and the impingement surface. Our studies of steady microjets, which were used to control the larger impinging jets, revealed the striking similarities in the mean flow properties between the larger impinging jets and impinging microjets (Phalnikar et al. [19]). Given these similarities, the question was asked whether the unsteady flow properties of *impinging microjets* are also similar to their larger counterparts: i.e., do they produce highly unsteady, discrete frequency-dominated flowfields? If so, then one may possibly use these as a basis for a high control authority, tunable, unsteady actuator. This initial idea led to the development of the present pulsed microjet-based actuators in a systematic process involving building-block experiments and the methodical addition of design elements to produce the first-generation actuator. In this section, we briefly discuss some initial experiments that were conducted using simple canonical configurations. The aim of these studies was to gain some insight and guidance toward the design of the final pulsed microactuators, which is discussed later in Sec. IV.

A. Supersonic Impinging Microjets

As discussed above, large scale supersonic impinging jets produce highly unsteady flowfields that exhibit discrete acoustic tones of high intensity (Powell [20] and Krothapalli et al. [3]). The impinging-jet flowfield of a microjet is examined as a first step to understand how the microscaling of the geometry and the resulting lower Reynolds numbers affect this unsteadiness. Figure 2 shows the configuration and narrow band pressure spectra of a microjet impinging on a flat surface for various nozzle-to-plate h_i/d distances, where h_i is the distance between the nozzle exit plane and the impingement surface, and d is the nozzle diameter at the throat. The jet is moderately underexpanded (NPR = 5.8) and impinging on a flat surface normal to the jet axis. A Kulite sensor is flush mounted to measure the unsteady surface pressures. The narrow band spectra shown above demonstrate the presence of high-amplitude, discrete tones in the frequency range of 25–55 kHz over the range of h_i/d (1.8 to 2.8) tested.

These results confirm the presence of a resonance loop, as observed for larger impinging jets, and suggest that this property may be leveraged for our actuator development. However, due to the small physical scales, the frequency range of these tones is much higher than those required for the development of microactuator for our applications (see Fig. 1). Hence, a modification to the impinging-jet configuration is needed to produce unsteady microjets in the desired frequency range.

B. Microjets with Hole Tones

The unsteady flowfield characteristics of edge/hole tones and the effect of various geometric parameters have been studied in detail by Powell [21] for larger jets. To leverage the understanding gained from prior research, experiments were conducted on microjets grazing through a circular hole. In the present study, a 1 mm diameter d jet and a sharp-edged orifice of 1.6 mm diameter D was used (Fig. 3a). Given that the feedback mechanisms in governing impinging jets, screeching jets, and hole tones are very similar (see Krothapalli et al. [3]), the geometry was designed such that the shear layer of the microjet grazes the edges of the circular hole to generate large-amplitude tones, often referred to as hole tones. We chose a $D/d = 1.6$ based on the previous studies (Phalnikar et al. [19]) on microjet impingement and its shear-layer growth to ensure such grazing flow. A Kulite probe located at a distance of $5d$ from the orifice was used for the unsteady pressure measurement.

As seen in the pressure spectra (Fig. 3b), the presence of the orifice has increased the overall unsteadiness in the jet by about 6 dB, in comparison with a free jet under the same conditions. The maximum unsteadiness in the jet is observed when the orifice is located at $h_o/d = 1.3$, where h_o is the distance from the source jet nozzle exit to the orifice. The interaction of the shear layer with the orifice edge leads to an amplification of the flow instabilities and the resulting pressure fluctuations may lead to resonance and a global unsteadiness in the flow. This behavior may be leveraged for the actuator design. Combining the configurations discussed above and adding little more geometric complexity, the impinging characteristics of a jet in a short cavity was investigated, as discussed next.

C. Microjets in a Cavity

Motivated by above results for microjets and the well-known characteristics of a Hartmann tube [22], we next explored the unsteady flowfield of microjets impinging in a cylindrical cavity. The results corresponding to a 1 mm diameter jet normally incident in a cylindrical cavity of length $L = 4.7$ mm and diameter $D = 1.4$ mm

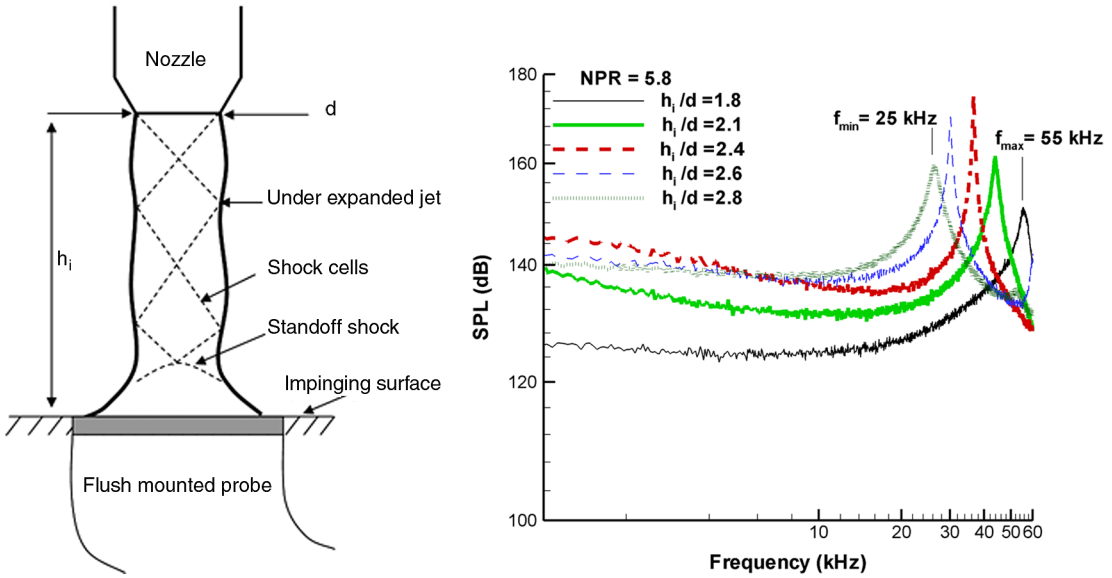

a) Configuration **b) Unsteady pressure spectra**

Fig. 2 Impinging-microjet (1 mm) configuration and corresponding pressure spectra at various impingement distances h_i/d.

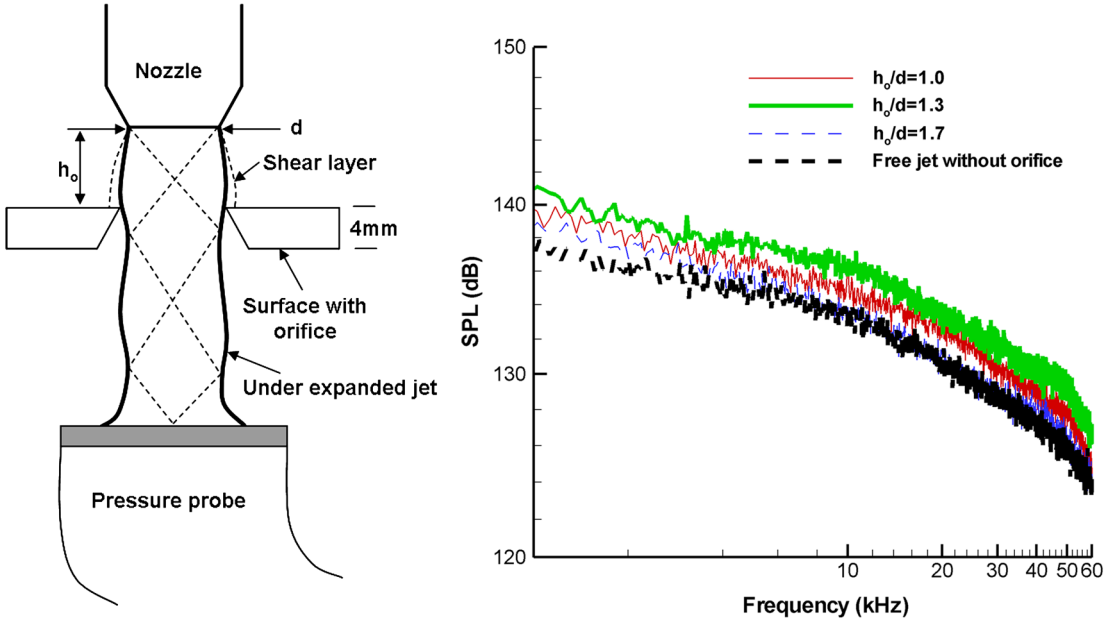

a) Configuration b) Unsteady pressure spectra

Fig. 3 Microjet–orifice configuration and corresponding pressure spectra at various impingement distances h_o/d.

are presented here. Figure 4a shows a schematic of this arrangement and the corresponding pressure spectra produced for microjets impinging into this cavity over a range of NPR (1.9–6.3) for a fixed nozzle to cavity distance $h_c = 1.6$. As seen here, the spectra (Fig. 4b) show distinct high-amplitude peaks (or tones) in the frequency range of 6–11 kHz for an NPR range of 4.1–6.3 for this configuration. These results were very encouraging both in terms of the high amplitudes and the associated tonal frequency range, which lies in the range needed for the lab-scale supersonic cavity and impinging-jet control applications (see Fig. 1). The experimental results discussed so far form the basis for a preliminary design of an actuator system that can provide high-momentum microjets with significant unsteady amplitudes, whose frequency can be varied. The design of a microactuator system and experimental results using this system are discussed in the following.

IV. Pulsed Microactuator Design

The results of the building-block experiments described in the previous section are very encouraging. They provide ample evidence of the potential to produce unsteady, high-momentum microjets by expanding upon the simple canonical configurations shown in Figs. 2–4. Based on these results a first-generation microactuator was designed, a schematic of which is shown in Fig. 5. The microactuator consists of three main components: 1) A larger, underexpanded *primary source jet*, which supplies air to 2) a *cylindrical cavity* in which the source jet resonates, and 3) multiple *micronozzles* (i.e., microjet orifices) at the bottom of the cylindrical cavity, from which the high-momentum, *unsteady microjets* issue.

In the present design, the source jet issued from a 1-mm-diam converging nozzle and the micronozzle array at the bottom of the cavity consists of four 400 μm micronozzles in the pattern shown in

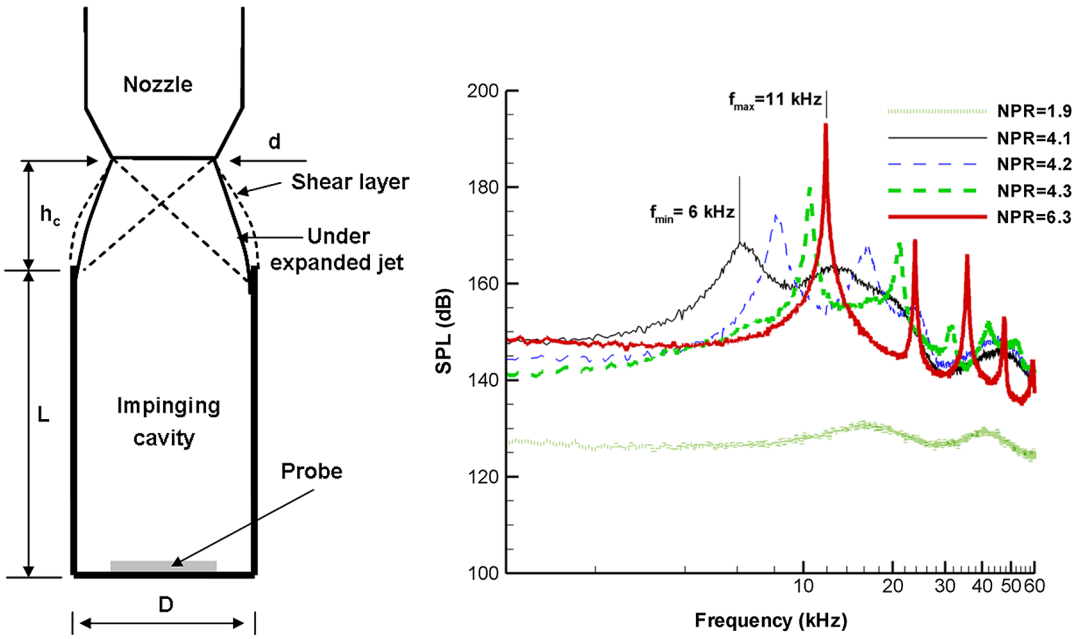

a) Configuration b) Pressure spectra

Fig. 4 Microjet–cavity configuration and corresponding pressure spectra at various NPR.

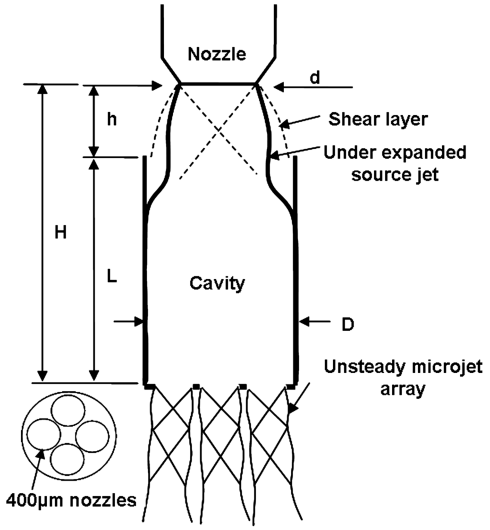

Fig. 5 Schematic of microactuator.

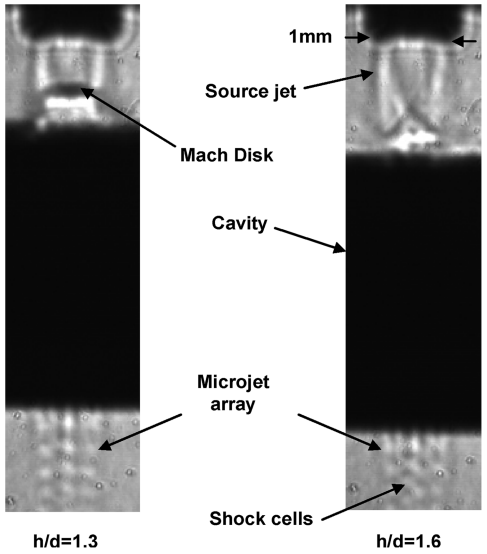

Fig. 6 Schlieren images of the flowfield at NPR = 4.8 and $L/d = 3$.

Fig. 5. The aim was to obtain the maximum flow rate through this actuator and four was maximum number of orifices that could be machined in the present configuration. (We have subsequently explored alternate cavity designs that allowed for a larger number of orifices and a corresponding increase in flow rate; the results of these ongoing studies will be published separately, once the experiments are completed.) As previously mentioned, the cavity diameter D (1.6 mm, kept constant in this study) was chosen such that the shear layer of the source jet grazes the lip/entrance of the orifice. The unsteady microjet flow was visualized using the high magnification microschlieren system discussed in Sec. II.A. The flow properties of the microjets were measured using a Kulite total pressure probe, fabricated using a Kulite XCE-062-100A (100 psia) transducer. Given the very small size of the microjets ($\sim$0.016 in.) some spatial averaging will undoubtedly occur. However, as discussed later, measurements made with the probe tangential to (i.e., grazing the unsteady microjet plume) confirm that the unsteady properties discussed in the following represent the overall unsteady microjet behavior.

V. Actuator Flowfield Properties

The main parameters that govern the flow properties of the microjet array issuing from the actuator assembly are: a) the distance from the source jet h, b) the length of the cylindrical cavity, L and c) the source jet pressure ratio, NPR. Experiments were conducted over a wide range in terms of geometric and flow parameters, where h/d is varied from 1 to 2, L/d from 1 to 5 and NPR from 1.9 to 6.3. The objective was to examine and understand the effect of these parameters on the flowfield issuing from the actuator array and to identify the optimal range and combination of these parameters that produce the desired microactuator flow. Furthermore, we aim to develop a preliminary design approach and scaling laws for such actuators. In subsequent discussion, the flowfield characteristics and the unsteady properties of the secondary microjets are presented as these parameters are varied.

A microschlieren system was extensively used to understand the flow features of the microactuator throughout the development process. In fact, a significant amount of insight into the flow physics involved in the microactuator system is gained from these images. Figure 6 shows representative instantaneous schlieren images of the flowfield associated with a microactuator at NPR = 4.8 for two values of h/d (1.3 and 1.6).

At $h/d = 1.3$, large oscillations of the Mach disc (see Fig. 6) of the primary jet at the entrance of the cavity were observed, which led to a strong tone in the pressure spectra, presented in the next section. There were no visually observable oscillations in the flow at $h/d = 1.6$, a property confirmed by the corresponding pressure spectra being devoid of any discrete tones (shown later). The presence of shock cells in the microjets issuing from the bottom of the actuator clearly confirms that the flow is supersonic. The flowfield for $h/d = 1.3$ is further analyzed in Fig. 7, in which we show images corresponding to different phases of flow oscillation. One interpretation of these images based on the shock structure of the source jet and the strength of microjets is as follows. As the primary jet fills up the cavity (Fig. 7a); flow oscillates in the cavity, where it appears to move up as in Figs. 7b and 7c and down as in Fig. 7d, and is discharged through orifices producing highly unsteady microjets. Similar flow features were observed at other test conditions in which the level of unsteadiness in the flow was dependent upon the geometric and flow parameters of the actuator.

As mentioned earlier, the geometric parameters involved in the microactuator flow are the distance from the source jet h and the length of the cylindrical cavity, L and the flow parameter is the source jet pressure ratio, NPR. In the subsequent sections, we present results based on the nondimensionalized quantities, L/d and h/d, which also represent control knobs in the microactuator performance. These parameters were systematically varied to better understand their influence on microactuator flow properties from which to formulate the design criteria.

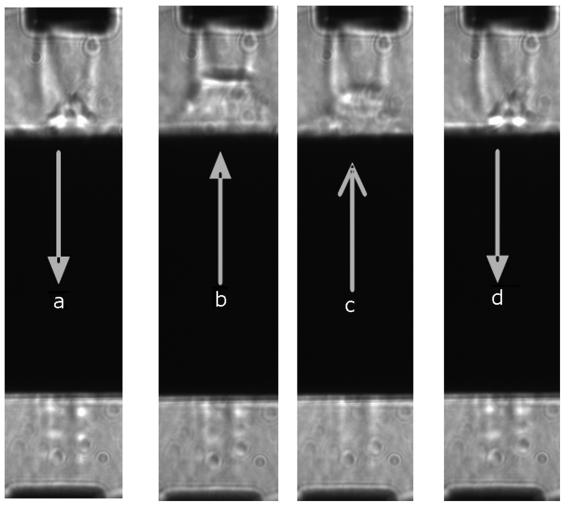

Fig. 7 Schlieren images of various phases of flow oscillations at $h/d =$ 1.3 and NPR = 4.8.

VI. Microactuator Frequency Properties: A Parametric Study

The pressure spectra of the flow issuing from the microjet actuators for a cavity length $L/d = 1$ is shown in Fig. 8. Figure 8a shows the effect of varying h/d while NPR is kept constant (NPR = 4.8), and Fig. 8b shows the effect of varying the NPR for a fixed value of $h/d = 1.4$. Unless otherwise noted, all subsequent pressures shown were measured using the Kulite probe described in Sec. III.

The spectra in both figures clearly show the presence of high-amplitude peaks indicating the presence of highly unsteady flow issuing from the actuators. Equally noteworthy is the trend in the peak frequency variation seen in Fig. 8a, in which a modest variation of h/d (from 1.3 to 2) leads to a significant shift in the peak frequency. For example, at $h/d = 1.3$ a spectral peak with an amplitude of ~157 dB occurs at a frequency of approximately 58 kHz, whereas at $h/d = 1.8$ the peak has shifted to a lower frequency of ~42 kHz and with an amplitude of roughly 141 dB. Furthermore, the spectral peaks systematically broaden with increasing h/d and beyond $h/d = 1.8$, there is no measurable discrete peak. The presence of narrow spectral tones is expected as this actuator design leverages a number of flow-acoustic resonance phenomena to enhance the flow unsteadiness; some of these have already been discussed in Sec. III. Similarly, the shift to lower frequencies with increasing spatial lengths or distances is also expected. Likewise, if one is using impinging-jet resonance, then the feedback loop governing such phenomenon is expected to become weaker beyond some critical distance due to the decay in the strength of the flow instabilities. For the present case, this critical distance appears to be $h/d = 2$, which may be due to the fact that only the shear layer is impinging/grazing the cavity lip while the core of the jet enters the cavity. A variation in NPR also produces a shift in peak frequency (Fig. 8b): at NPR = 4.5, the high-amplitude tone is at approximately 51 kHz, whereas at NPR = 4.8, it is shifted to 54 kHz. It is to be noted that a minimum jet pressure is required to produce high-amplitude tones; in the present case this corresponds to NPR > 4.2. This issue is further discussed in Sec. VIII.

The results in Fig. 8 are promising in that they clearly show the capability of this actuator to produce highly unsteady flow. Equally important, we see the presence of simple control knobs (namely, NPR and h/d), which allows one to vary the frequency and amplitude of the unsteady flow from these actuators. Keeping in mind that the two applications in which we first plan to implement and test such actuators in our laboratory, i.e., the supersonic impinging jet and cavity flowfield, require frequencies in a range of 6–10 kHz (see Fig. 1), we next examine ways of reducing the unsteady frequencies to this range.

Figures 9 and 10 show pressure spectra for longer cavities: $L/d =$ 2 and 3, respectively. The trends observed are very similar to the one with $L/d = 1$ except that the output frequency range is shifted to lower values. As seen in Fig. 9, for $L/d = 2$, an h/d variation from

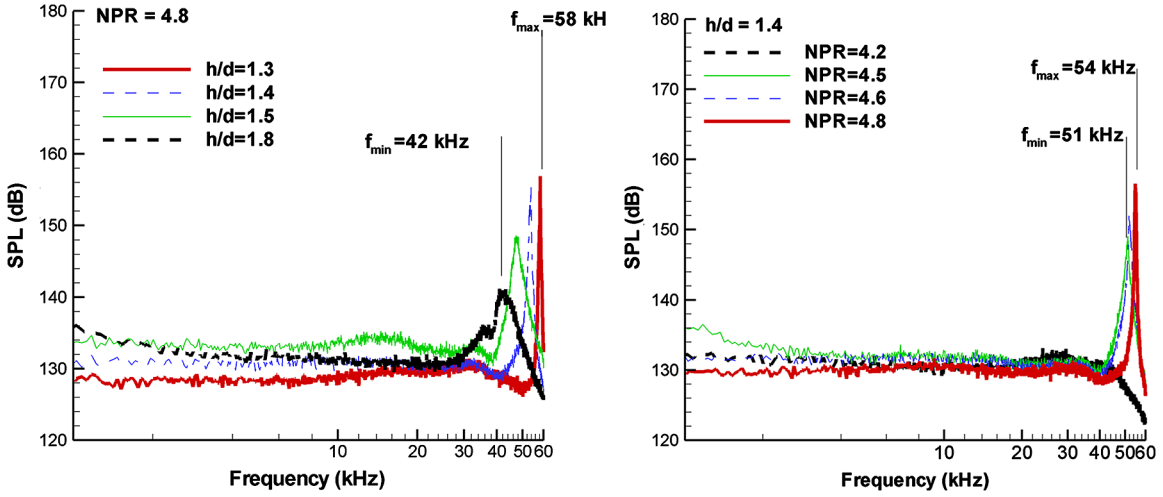

a) Fixed *NPR*, *h/d* variation b) Fixed *h/d*, *NPR* variation

Fig. 8 Pressure spectra for microactuator with $L/d = 1$, where NPR and h/d are varied: a) h/D varied at NPR = 4.8 and b) NPR varied at $h/d = 1.4$.

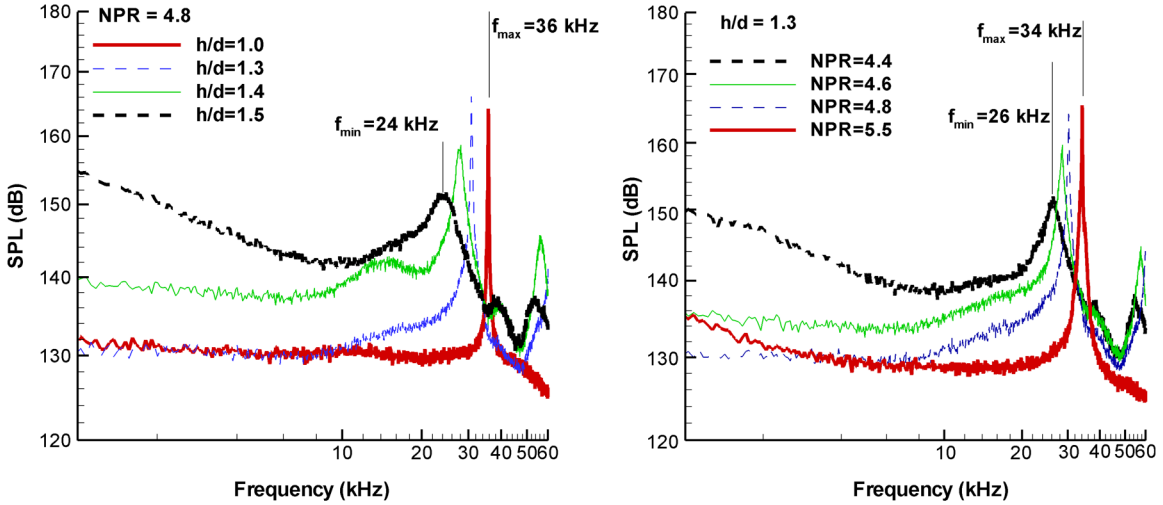

a) Fixed *NPR*, *h/d* variation b) Fixed *h/d*, *NPR* variation

Fig. 9 Pressure spectra for microactuator with $L/d = 2$, where NPR and h/d are varied: a) h/D varied at NPR = 4.8 and b) NPR varied at $h/d = 1.3$.

1.0 to 1.5 has resulted in a frequency response of 36 to 24 kHz with discrete frequency amplitudes of 162 and 150 dB, respectively. Similarly, increasing the NPR from 4.4 to 5.5 (Fig. 9b) shifts the frequency from 26 to 34 kHz while increasing the peak amplitude by roughly 15 dB. The frequency range is further reduced to 14–24 kHz for a longer cavity length $L/d = 3$ (Fig. 10). A closer look at these spectra also reveals that the large-amplitude discrete tones are associated with lower broadband unsteadiness, whereas the spectra consisting of higher broadband levels have lower-amplitude discrete tones. This indicates some redistribution of the total energy with these control parameters. This effect needs further exploration and is being presently studied. Based on the above experiments, the frequency of a microactuator and its relation to the geometrical parameters was established. It was anticipated that $L/d = 5$ will result in a frequency range of 6–12 kHz, suitable for the applications of our interest. A microactuator with $L/d = 5$ was then fabricated and tested over a range of NPR = 4.5 to 5.5, where the h/d was varied from 1.3 to 1.8; these results are shown in Fig. 11.

As we hoped, the spectra show dominant tones in a frequency range of 6–11 kHz, with flow characteristics very similar to those of shorter cavities discussed earlier.

In all of the experiments discussed so far, unsteady pressure measurements were obtained with the Kulite probe placed normal to the jet axis. A few tests were conducted with a probe placed parallel to the unsteady microjet (Fig. 12a), in which the microjet plume just grazes this sensor. These spectra are compared in Fig. 12b. These tests were conducted in part to verify that the fluctuations measured by the Kulite probe were not in fact due to resonance induced by impingement on the probe itself. As seen here, peaks are observed at the same frequency in both cases. However, as expected, the amplitudes are lower for the tangential probe. These results verify that the unsteady microjet flow measured by the Kulite is due to the aeroacoustic coupling within the actuator which significantly enhances the unsteady component of the supersonic flow issuing from these actuators.

The results obtained by varying geometric and flow parameters are summarized in Fig. 13 which shows a variation of the peak frequency as a function of L/d, for a range of h/d and NPR variations. As seen here, by changing the cavity length, L/d from 1 to 5, the resonance frequency of the actuator can be shifted from ~50 kHz to ~4 kHz. For a given actuator design, i.e., fixed L/d, very small change in h/d (open symbols) and/or NPR (filled symbols) one can sweep or tune the actuator frequency over a large range ($\Delta f_{\text{actuator}} \sim$ 5–20 kHz).

Using the trends summarized in Fig. 13, one may design an actuator in the frequency range of roughly 1–60 kHz (the upper limit has not been explored to date), the frequency of which can be tuned by fine control knobs (h/d and NPR) around the design envelop frequency based on L/d. A closer look at the results in Fig. 13 show

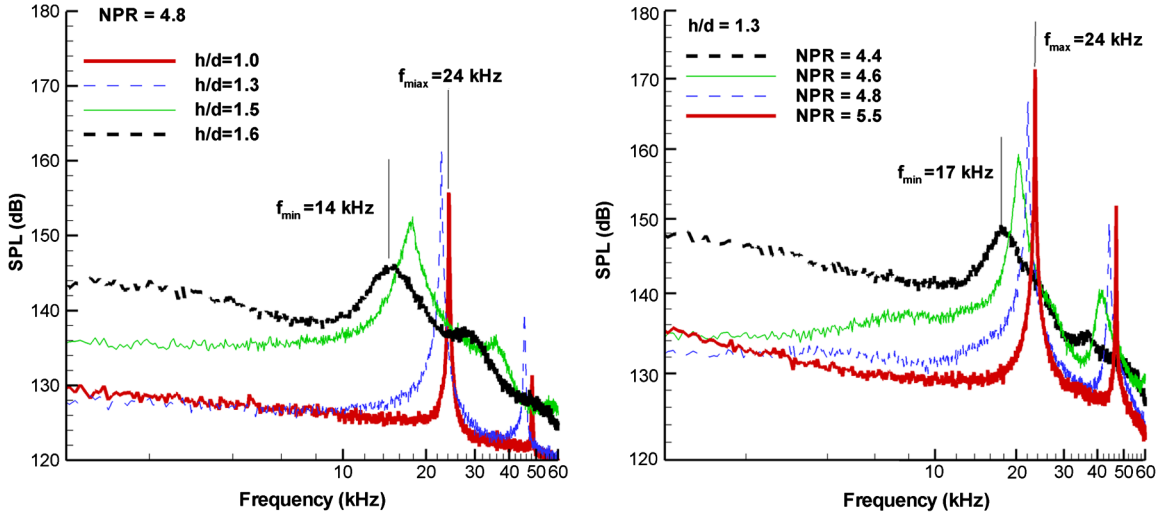

a) Fixed *NPR*, *h/d* variation

b) Fixed *h/d*, *NPR* variation

Fig. 10 Pressure spectra for microactuator with $L/d = 3$, where NPR and h/d are varied: a) h/D varied at NPR $= 4.8$ and b) NPR varied at $h/d = 1.3$.

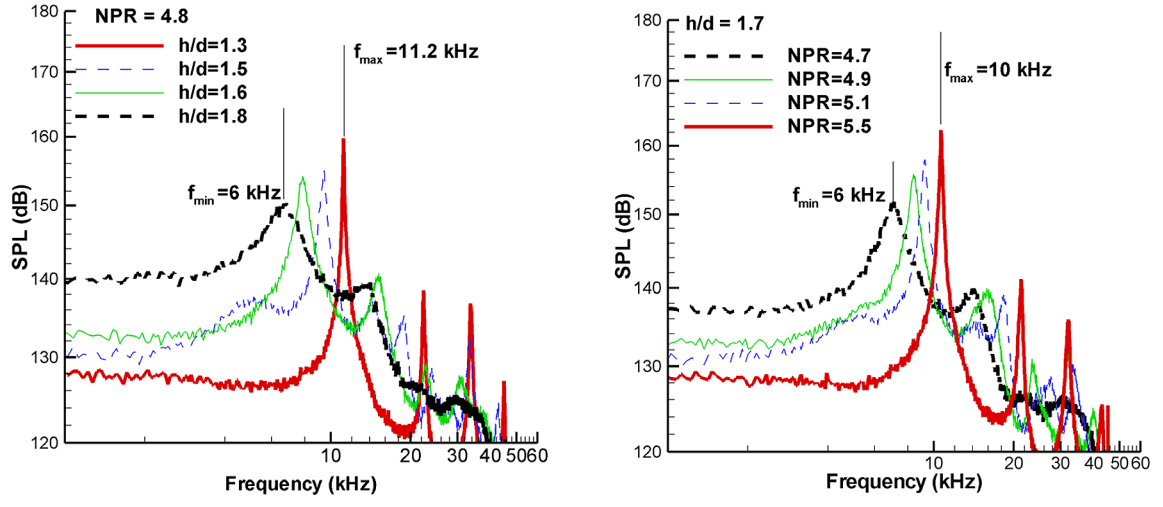

a) Fixed *NPR, h/d* variation

b) Fixed *h/d, NPR* variation

Fig. 11 Pressure spectra for microactuator with $L/d = 5$, where NPR and h/d are varied: a) h/D varied at NPR $= 4.8$ and b) NPR varied at $h/d = 1.7$.

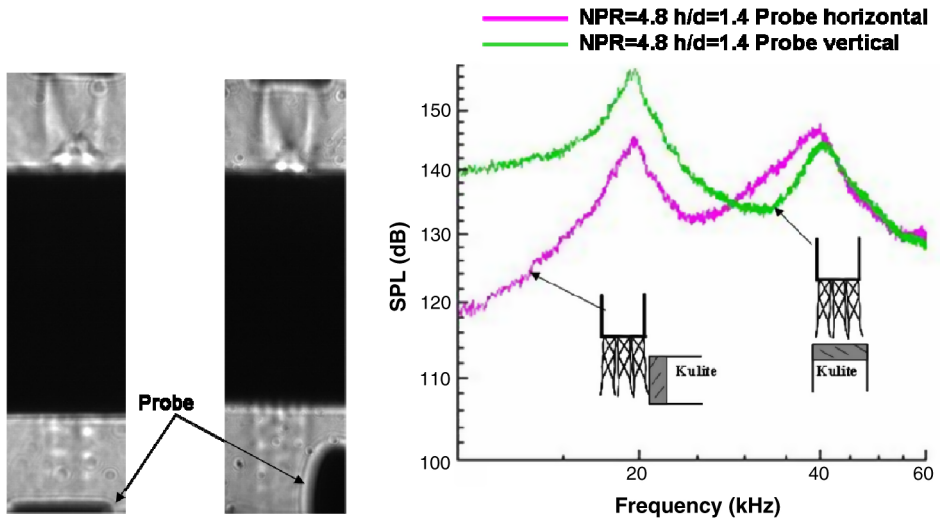

a) Probe location b) Spectra

Fig. 12 Effect of probe direction on pressure spectra.

that an h/d variation from 1.0 to 1.7, at a constant NPR, has resulted in a decrease in the frequency, a trend similar to that of variable L. This suggests that jet column length may be a better combined parameter that describes the effect of both h/d and L/d. Hence, we define a new variable $H = h + L$. This parameter H represents the total length of the jet column, from the source nozzle exit to the bottom of the cavity. The results shown in Fig. 13 are replotted in dimensionless parameters, Strouhal number St_{ideal} and H/d. For St_{ideal}, the actuator frequency is non dimensionalized using the ideally expanded jet velocity based on the primary source jet NPR as

$$St_{\text{ideal}} = fd/U_{\text{ideal}} \tag{1}$$

In Eq. (1) f is the frequency of the actuator, d is source jet diameter and U_{ideal} is the ideally expanded jet velocity of the underexpanded source jet. Interestingly, these new variables collapse the data reasonably well into a single curve, as seen in Fig. 14. The collapsed curve is approximated by the correlation

$$St_{\text{ideal}} = 0.4(H/d)^{-1.45} \tag{2}$$

Rewriting Eq. (2) in terms of NPR results in

$$f = \frac{0.4}{d}\left(\frac{2}{\gamma - 1}((\text{NPR})^{\frac{\gamma-1}{\gamma}} - 1)\right)^{1/2}\sqrt{\gamma R T_o (\text{NPR})^{\frac{1-\gamma}{\gamma}}}(H/d)^{-1.45} \tag{3}$$

where γ is the specific heat ratio, T_o is the stagnation temperature of the source jet and R is the universal gas constant.

This correlation can in turn be used as a guide for designing actuators with a high bandwidth and tunable frequency. Microjet actuator arrays designed using the above approach can potentially be used for a number of supersonic (and subsonic) flow control applications which require high unsteady and mean components, such as those produced herein.

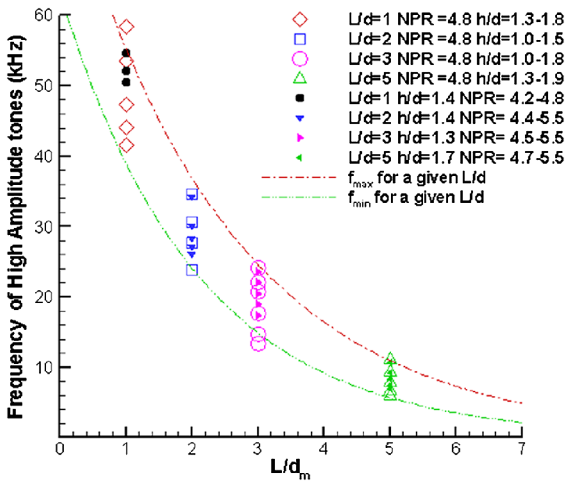

Fig. 13 Summary of actuator performance in terms of geometric, L/D and h/D, and flow parameters.

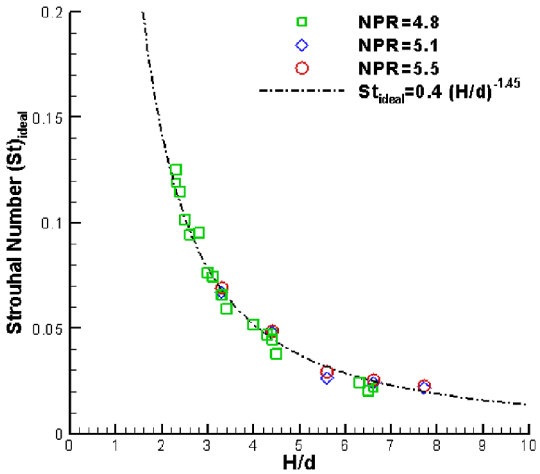

Fig. 14 Actuator dynamics in nondimensional frequency and modified parameter H/d, where $H = h + L$.

VII. Comparison of Present Microactuator Properties with Other Designs

As noted in the introduction, a number of past studies used flow resonance phenomena to design actuators for various flow control applications. In the current actuator design we have a supersonic microjet entering a partially open cavity. Since a Hartmann tube is a closed cavity and closely resembles the present geometry, it may be useful to compare the predictions of Hartmann and Trolle [22] and other actuator designs based on Hartmann's principles with the present actuator. Figure 15 shows the variation of the peak frequencies as a function of jet column length H/d (where $H = L + h$) for the present microactuator along with the data from literature. Here, we compare the present microactuator frequency with Hartmann predictions and the experimental data of Raman and

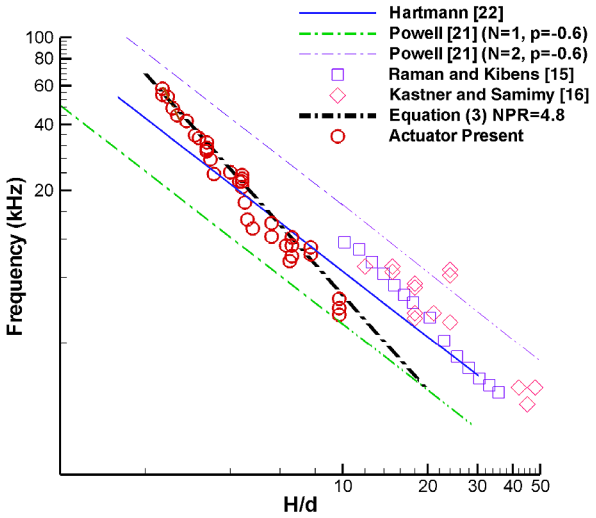

Fig. 15 Comparison of microactuator frequency with other designs and predictions.

Kibens [15] and Kastner and Samimy [16]. Both of these designs were based on the original Hartmann approach. In the plot in Fig. 15, the results from the present actuator are shown as circles, while data from Raman and Kibens [15] and Kastner and Samimy [16] are shown as polygons.

In addition, the frequency predictions of Hartmann [22] are shown as a solid line. It is clear from this plot that Kastner and Samimy's [16] and Raman and Kibens's [15] actuator designs, which are closely based on the Hartmann approach, produced tones of frequencies that agree reasonably well with Hartmann's predictions, in particular for longer cavity lengths. In contrast, the microactuator frequencies, while similar in magnitude, exhibit a different H/d dependence than predicted by the Hartmann correlation.

Another comparison is made with Powell's feedback correlation [20] (shown as dash-dot lines) that predicts the frequency of impinging or hole tones. The rationale behind this comparison is the similarity between these two flow phenomena. In the current actuator design, the primary jet is impinging on a flat surface, the bottom of cavity, with a number of orifices in it, resembling an impinging-jet flow. In addition, as seen in Fig. 4, the shear layer of the actuator source jet grazes the edges of the cylindrical cavity resembling a hole tone configuration, that may also enhance the feedback-loop-driven instabilities creating unsteadiness in the main jet. This comparison reveals that the actuator frequency falls within the first and second mode of Powell's prediction assuming a phase lag of −0.6. It is worth noting that, with an appropriate choice of a phase lag value, the Hartman prediction and Powell's correlation collapse to one single line. This points toward the influence of feedback-loop-driven instabilities in both of these configurations. In summary, although the present flow displays trends similar to feedback-driven flows examined by Hartmann [22] and Powell [20], it does not agree with either. This is because it is likely a combination of a number of flow resonance phenomena and is better captured by Eqs. (2) and (3).

VIII. Microactuator Amplitude: A Parametric Study

For any actuator system, the amplitude of unsteadiness is as important as its frequency response. The total energy in the unsteady component of the microactuator flow can be captured by the rms of the total pressure measured, P_{rms}. In the following, we describe how the geometric and flow parameters affect the unsteady amplitude of the present microactuator system.

A. Effect of h/d

At a fixed NPR (=4.8), the variation of P_{rms} with h/d for different cavity lengths is shown in Fig. 16a. It is observed that initially an increase in h/d results in an increase in P_{rms}. Beyond a threshold h/d, P_{rms} remains nearly constant over significant a range of h/d, decreasing at larger values. For example, at $L/d = 1$, the P_{rms} is 144 dB at $h/d = 0.75$, it reaches nearly 168 dB at $h/d = 1.1$ and remains nearly constant up to $h/d = 1.6$, it then decays to 158 dB at higher h/d values. As seen in Fig. 16a, this entire variation occurs within an h/d range of 1 to 1.6, a change of only 0.6 mm, and is seen for all the cavity lengths examined. This suggests the existence of a region in which the flow is particularly unsteady and in which the instabilities are amplified: i.e., a region of instability (ROI).

An examination of the schlieren images, similar to those shown in Figs. 6 and 7, corresponding to this ROI range of h/d, reveals that for most of these unstable cases, the cavity entrance is in the compression region of the shock cell structure of the source jet where the local static pressure has begun to increase due to the compression fans in the shock cells. Hence, in addition to the cavity diameter being such that its edges graze the source jet shear layer, the cavity entrance should be located in the compression region of the source jet. This placement with respect to the source jet flowfield leads to large oscillations in the source jet and its Mach disk as seen in Fig. 7. This in turn provides the unsteady source flow/function for the actuator cavity.

Figure 16b shows a variation of P_{rms} with jet column length H/d, where $H = h + L$. Using this variable, which accounts for the length of the cavity, L and h/d, the dependence of P_{rms}, on the total actuator length is more systematically and more clearly revealed. These results once again confirm that there is a range of h/d over which the unsteadiness levels are high for all cases of cavity lengths (L) used in this study. It is also worth noting that while the unstable frequencies change by nearly an order of magnitude between the actuator with the

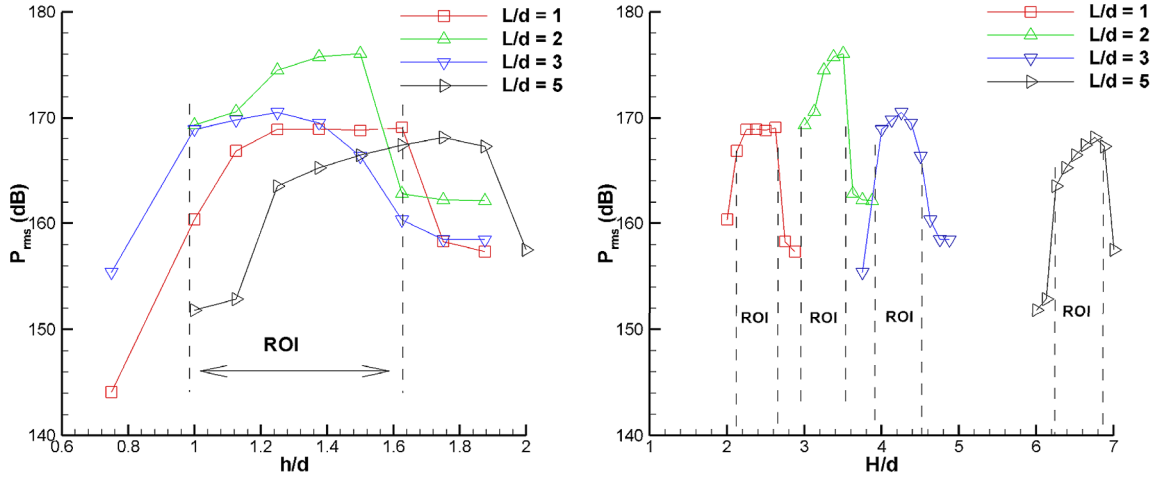

a) Effect of *h/d* **b) Effect of *H/d***

Fig. 16 Unsteady amplitude variation as a function of geometric parameters for a fixed NPR = 4.8.

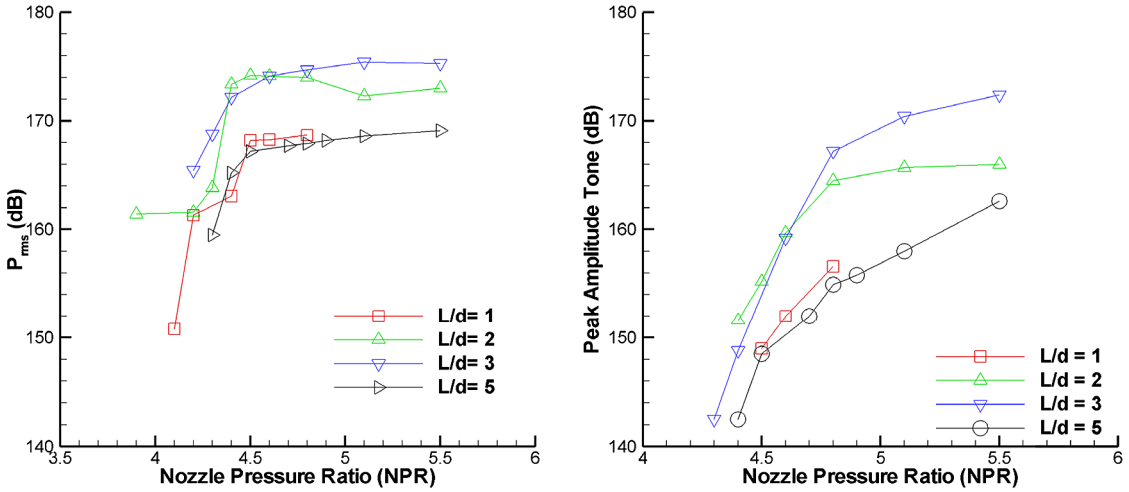

a) P_{rms} b) Tonal amplitude

Fig. 17 Effect of nozzle pressure ratio on flow unsteadiness of microactuator.

shortest cavity ($L/d = 1$) and the longest cavity ($L/d = 5$), the total energy in the unsteady component, i.e., P_{rms}, is relatively constant over the ROI.

While discussing the pressure spectra of the microactuator flow (Figs. 8–11) the emergence of distinct, sharp frequency tones when h/d is varied from 1.0–1.6 was observed. It was noted that high P_{rms}, levels in the same h/d range. It is clear (and perhaps obvious) that the discrete peaks in the pressure spectra, which are indicative of significant unsteadiness, are responsible for the high P_{rms}. The conclusion is that for a sufficiently high NPR, there exists a region of instability within which the variations of h/d give rise to highly unsteady secondary jets with energy concentrated in a limited frequency range. Furthermore, the dominant frequency range for a fixed NPR can be controlled by selecting the appropriate h/d and cavity length L.

B. Effect of NPR

The variation of P_{rms} with nozzle pressure ratio (NPR) is shown in Fig. 17a. In the present experiments, at a fixed value of L/d and h/d (corresponding to highly unsteady flow), the NPR is varied from 4 to 5.5. It is observed that at each L/d, once NPR is increased above 4.2, there is a sharp increase in OASPL. However, this value saturates beyond NPR = 4.5 over the range of conditions tested. This once again suggests the possibility of a region of instability leading to high-amplitude unsteadiness. To further understand the effect of NPR, the peak tonal amplitude is shown in Fig. 17b. It is observed that discrete measurable tones are observed in the spectra beyond NPR = 4.2 and their amplitude increases with increasing NPR. These results confirm that although increasing NPR (beyond 4.5) increases the peak tonal amplitude, the overall unsteadiness in the microactuator system remains nearly constant.

IX. Conclusions

There exists a significant need for high-momentum high-bandwidth microactuators for various high-speed applications, such as jet noise and cavity flows. In this paper, we describe a systematic approach for designing microactuators with high unsteady and mean momentum efflux. Beginning with a simple configuration, i.e., supersonic impinging microjets, we systematically add more complexity to the actuator design, resulting in higher but predictable and controllable unsteady output, to finally arrive at an actuator configuration that provides the desired flow properties. Our first-generation actuator design consists of a primary source jet, incident upon a cylindrical cavity. The lower surface of this cavity contains micronozzles through which the unsteady microjets issue. The results clearly show that the microjets produced by this actuator possess very high mean momentum (they are supersonic for most cases, with velocity of greater than 300 m/s) as well as a very significant unsteady component (50–100 m/s). Using this design, experiments were conducted over a large range of parameters, in terms of cavity length, source jet NPR, and source jet impingement distance. The results unequivocally demonstrate the ability to vary the frequency and the perturbation amplitude of the unsteady microjets issuing from this actuator. By varying the dimensions of the actuator by only a few hundred microns, we are able to finely sweep the frequency of the unsteady component over intervals of 5–20 kHz. We have provided a simple design criterion to develop any actuator over the frequency range of roughly 1–60 kHz by suitably selecting the geometric parameters (we believe that higher frequencies are also possible). The ability to produce unsteady flow with significant mean and unsteady components, where the dynamic range can be easily varied makes these actuators promising for a number of high and low speed flow control applications. The notable characteristics of this design are its simplicity, robustness, scalability and the flexibility in controlling the frequency and amplitude suitable for the application of interest.

Acknowledgments

The authors would like to thank Florida Center for Advanced Aero-Propulsion and the U.S. Air Force Office of Scientific Research for the financial support for this research.

References

[1] Zhuang, N., Alvi, F. S., Alkislar, M. B., and Shih, C., "Supersonic Cavity Flows and Their Control," *AIAA Journal*, Vol. 44, No. 9, 2006, pp. 2118–2128. doi:10.2514/1.14879

[2] Ukeiley, L., Sheehan, M., Coiffet, F., Alvi, F. S., Arunajatesan, S., and Jansen, B., "Control of Pressure Loads in Geometrically Complex Cavities," *Journal of Aircraft*, Vol. 45, No. 3, 2008, pp. 1014–1024. doi:10.2514/1.33324

[3] Krothapalli, A., Rajkuperan, E., Alvi, F. S., and Lourenco, L., "Flow Field and Noise Characteristics of a Supersonic Impinging Jet," *Journal of Fluid Mechanics*, Vol. 392, 1999, pp. 155–181. doi:10.1017/S0022112099005406

[4] Alvi, F. S., Shih, C., Elavarasan, R., Garg, G., and Krothapalli, A., "Control of Supersonic Impinging Jet Flows Using Supersonic Microjets," *AIAA Journal*, Vol. 41, No. 7, 2003, pp. 1347–1355. doi:10.2514/2.2080

[5] Kumar, R., Lazic, S., and Alvi, F. S., "Control of High-Temperature Supersonic Impinging Jets Using Microjets," *AIAA Journal*, Vol. 47, No. 12, pp. 2800–2811. doi:10.2514/1.39061

[6] Ro, I. P., and Loh, G. B., "Feasibility of Using Ultrasonic Flexural Waves as a Cooling Mechanism," *IEEE Transactions on Industrial Electronics*, Vol. 48, No. 1, 2001, pp. 143–150.

doi:10.1109/41.904574
[7] Sfeir, A. A., "Investigation of Three Dimensional Turbulent Rectangular Jets," AIAA Paper 1185, 1978.
[8] Sforza, P. M., Steiger, M. H., and Trentacoste, N., "Studies on Three Dimensional Viscous Jets," *AIAA Journal*, Vol. 4, No. 5, 1966, pp. 800–806.
doi:10.2514/3.3549
[9] Schadow, K. C., Gutmark, E. J., Wilson, K. J., and Smith, R., "Non Circular Inlet Duct Cross-Section to Reduce Combustion Instabilities," *Combustion Science and Technology*, Vol. 73, No. 4, 1990, pp. 537–553.
doi:10.1080/00102209008951669
[10] Zaman, K. B. M. Q., Reeder, M. F., and Samimy, M., "Control of an Axisymmetric Jet Using Vortex Generators," *Physics of Fluids*, Vol. 6, No. 2, 1994, pp. 778–793.
doi:10.1063/1.868316
[11] Reeder, M., and Samimy, M., "The Evolution of a Jet with Vortex Generating Tabs: Real Time Visualization and Quantitative Measurements," *Journal of Fluid Mechanics*, Vol. 311, 1996, pp. 73–118.
doi:10.1017/S0022112096002510
[12] Cattafesta, L. N., III, Garg, S., Choudhari, M., and Li, F., "Active Control of Flow-Induced Cavity Resonance," AIAA Paper 97-1804.
[13] Wiltse, J. M., and Glezer, A., "Manipulation of Free Shear Flows Using Piezoelectric Actuators," *Journal of Fluid Mechanics*, Vol. 249, 1993, pp. 261–285.
doi:10.1017/S002211209300117X
[14] Amitay, M., Kibens, V., Parekh, D. E., and Glezer, A., "Flow Reattachment Dynamics over a Thick Airfoil Controlled by Synthetic Jet Actuators," AIAA Paper 99-1001.
[15] Raman, G., and Kibens, V., "Active Flow Control Using Integrated Powered Resonance Tube Actuators," AIAA Paper 2001-31330.
[16] Kastner, J., and Samimy, M., "Development and Characterization of Hartmann Tube Fluidic Actuators for High-Speed Flow Control," *AIAA Journal*, Vol. 40, No. 10, 2002, pp. 1926–1934.
doi:10.2514/2.1541
[17] Dziuba, M., and Rossmann, T., "Active control of a Sonic Transverse Jet in a Supersonic Cross Flow Using a Powered Resonance Tube," AIAA Paper 2005-897.
[18] Lou, H., Alvi, F. S., and Shih, C., "Active and Adaptive Control of Supersonic Impinging jets," *AIAA Journal*, Vol. 44, No. 1, 2006, pp. 58–66.
doi:10.2514/1.13347
[19] Phalnikar, K. A., Kumar, R., and Alvi, F. S., "Experiments on Free and Impinging Supersonic Microjets," *Experiments in Fluids*, Vol. 44, 2008, pp. 819–830.
doi:10.1007/s00348-007-0438-4
[20] Powell, A., "The Sound Producing Oscillations of Round Underexpanded Jets Impinging on Normal Plates," *Journal of the Acoustical Society of America*, Vol. 83, No. 2, 1988.
[21] Powell, A., "On Edge Tones and Associated Phenomena," *Acoustica* Vol. 3, 1953.
[22] Hartmann, J., and Trolle, B., "A New Acoustic Generator," *Journal of Scientific Instruments*, Vol. 4, No. 4, 1927, pp. 101–111.
doi:10.1088/0950-7671/4/4/303

M. Glauser
Associate Editor

Design and Characterization of High-bandwidth, Resonance Enhanced Pulsed Microactuators: A Parametric Study

John T Solomon[1], Chase Foster[2] , Farrukh S Alvi[3]

Florida Center for Advanced Aero propulsion
Florida A&M and Florida State University, Tallahassee, Florida, 32310

An extensive study on a microactuator that can generate high momentum, high frequency perturbations over a large bandwidth is presented in this paper. Such an actuator can potentially be used for the active control of various shear and boundary layer flows that involve separation, mixing, and noise generation. The resonance enhanced microjet actuator described in this paper is a simple micro fluidic system consisting of an underexpanded source jet flowing into a specially configured cavity integrated with multiple micro nozzles, through which unsteady pulsed supersonic jets issue. The resonance frequency of these microjets could be varied over a large range (approx. 1-60 kHz) by changing the geometric and flow parameters of the microactuator system. Mean and unsteady properties of the microactuator are examined, including time-resolved flow visualizations and synchronous pressure and noise measurements; collectively they provide a better understanding of the actuator dynamics. The present study also explores the design space and performance as well as some of the design limitations of this actuator. Based on this parametric, a correlation is suggested that may be used for designing such actuators for various applications.

I. Introduction

Active control of shear and boundary layer flows by means of unsteady momentum addition has drawn the

[1]Post-Doctoral Research Associate, Adjunct Assistant Professor, Department of Mechanical Engineering, Member AIAA
[2]Graduate Research Assistant, Department of Mechanical Engineering, Student Member AIAA
[3]Professor, Department of Mechanical Engineering, AIAA Associate Fellow

attention of flow control researchers in recent years. The natural flow characteristics such as transition, turbulence, flow separation, mixing etc. can potentially be controlled: suppressed, attenuated or enhanced, more efficiently through schemes that use such actuators. As an example, flow separation over an airfoil is an important practical problem where unsteady actuation techniques have been extensively studied for its control. Seifert et al. [1] have shown that periodic excitation by momentum addition, with a frequency higher than the natural vortex shedding frequency, may achieve similar gains in performance in comparison with steady blowing, with 99% less momentum. McManus et al. [2] used pulsed angular injection to create co-rotating vortices to attach separated flow. This actuation technique reportedly worked well for high angles of attack and is referred to as pulsed vortex generators. Bryant et al. [3], Wiltse et al. [4] and Smith et al. [5] used piezoelectric actuators for imparting unsteady momentum for flow separation control. These actuators, also called synthetic jets, produce zero net mass flux jets with velocities in the range of 10-80 m/sec at a frequency range up to 1 kHz. This technology has been developed further with input from many others on the modeling, design and fabrication of compact ZNMF actuator systems (Cattafesta et al. [6] and Joslin et al. [7]). Some of the actuators mentioned above were found promising for a number of subsonic flow control applications but were ineffective when the flow velocities are very high. The highly unsteady flowfield of an impinging supersonic jet or the flowfield inside a cavity, such as a weapon/cargo bay of a fighter aircraft subjected to cruise conditions from high subsonic to supersonic, are examples of flows that demand unsteady, high-amplitude actuation techniques. Such high speed flows require actuators that can provide high mean and unsteady momentum. Moreover, in most applications, the unsteady properties of the base flows largely depend on operating conditions that vary over a wide range of frequencies. An actuator with high unsteady momentum whose frequency can be tuned over a large bandwidth will be useful for such applications.

Plasma actuators were reported to have the capability for boundary layer separation control by imparting near wall flow momentum (List et al. [8], Jacob et al [9], and Corke et al. [10]). Ganiev et al. [11] used plasma jet injection for reducing the drag over a cone-cylinder model by a factor of two. Kelley et al. [12] used an AC dielectric barrier discharge plasma actuator for the leading edge flow separation control of a high subsonic flow. The high voltage requirement, EMI, complexities associated with plasma systems and limited bandwidth are some issues that may restrict the implementation of these devices into practical systems. Sparkjet actuators use an electric discharge to generate high pressure within a chamber and produce an air discharge through the orifice (Grossman et al [13]). Similar to plasma actuators these devices also require a very high voltage to operate. Another variant,

described as pulsed detonation actuator, has been recently developed and characterized by Cutler and Drummon [14]; it can generate a perturbation up to 1.5 kHz. A mixture of reactants (hydrogen and air) burns inside a resonating tube equipped with a high speed valve resulting in pulsed flow of hot combustion gases through the orifices. LAFPAs, localized arc filament plasma actuators, are another recently introduced design that is being examined for controlling high-speed flows (Samimy et al., 2011 [15]). Even though high control authority actuation may be achieved using some of these designs and as such hold promise for the future, other alternatives that are perhaps less complex, robust with a high dynamic range are still desirable.

Yeung et al. [16] proposed that in turbulent flows there exist a bi-directional coupling between the large scale and fine structures and this coupling can be excited by coherent high frequency forcing either at large or at fine scales. Exciting the shear layer at a frequency higher than its dominant natural frequency may provoke an accelerated transfer of energy from large to small scales, in subsonic flows (Wiltse and Glezer) [17]. This argument has led to studies on the 'high frequency forcing control' concept in recent years. Stanek et al. [18] employed 'high frequency forcing' to suppress supersonic cavity oscillations using powered resonance tubes as actuators. Interestingly, they reported that high frequency excitation caused deceleration of the turbulent energy cascade contrary to the findings of previous researchers. The design and development of robust and tunable actuators that can deliver sufficient unsteady momentum at higher frequencies over a large range remain as a challenge.

The original concepts of powered resonance tubes were introduced by Hartmann in 1927 [19] who described the device as a novel acoustic generator. Though it was not originally intended for the active flow control, subsequently many researchers (Raman et al. [20], Stanek et al. [18], Kaster and Samimy [21], Dziuba and Rossmann [22]) used the resonance tube concept as a source for high energy and high frequency acoustic perturbations for active flow control. A detailed study of this device can be found in Brocher et al. [23]. Kastner and Samimy [21] studied the effect of forcing frequency on the control of an impinging high speed jet by using a Hartmann tube fluidic actuator. They noticed that by forcing the base jet with a frequency 7.5 kHz or above, or using a steady mass injection, the dominant tone and its harmonics were suppressed. They also reported that at a lower mass flow rate, the high frequency actuators were found to be more effective than the comparable steady mass injection. A major drawback associated with this actuator is the very large mass flow requirement.

The potential capability of steady microjets as actuators for high speed flow control has been studied over a number of years in the Advanced Aero Propulsion Laboratory (AAPL) located at Florida State University. A control

strategy based on steady microjet injection near the nozzle exit of a supersonic impinging jet reduced the over all sound pressure level (OASPL) as much as 10dB for both cold and hot jet conditions over a range of operating conditions (Alvi et al. [24], Kumar et al. [25]). This is accompanied by higher reduction in the tonal components. A similar control approach, based on steady microjet injection, was very effective in controlling the resonating flowfield associated with a supersonic cavity as well. By injecting steady microjets at the leading edge of a Mach 2 cavity, Zhuang et al. [26] demonstrated a reduction of more than 8 dB OASPL inside the cavity and a 20 dB reduction in the cavity tones. The control effectiveness of steady microjets on these two problems is shown in Figure 1.

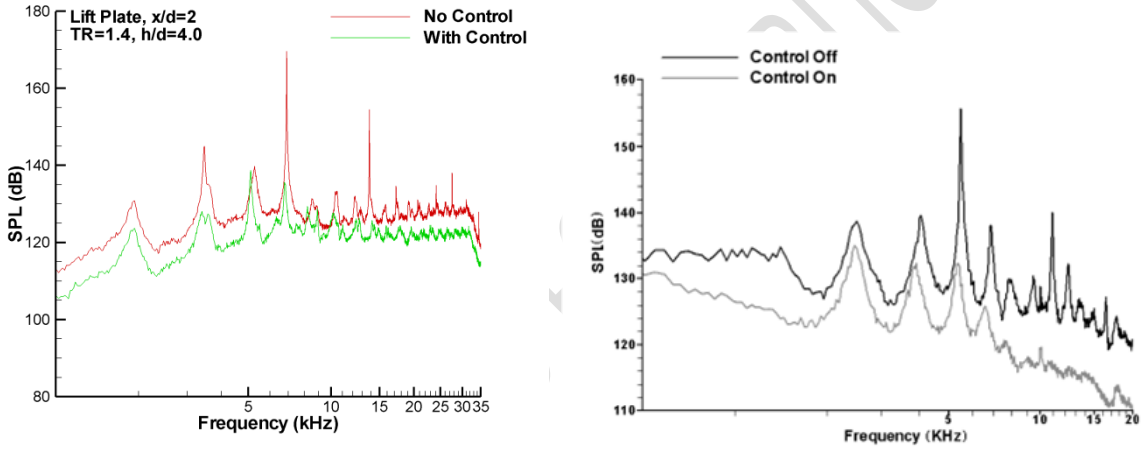

(a) **(b)**

Fig. 1 Flow control using steady microjets as actuators (a) Pressure spectra of an impinging supersonic jet with and without microjet control (Kumar et al. [25]) (b) Pressure spectra inside a supersonic cavity with and without steady microjet control (Zhuang et al. [26])

Figure 1 shows the efficiency of steady microjets on high speed flow control. However, the spectra also show that although the tonal features were reduced, they were not eliminated completely indicating that additional improvements are possible. To improve the effectiveness of microjet based control approach, a robust and novel micro fluidic actuator was developed recently by Solomon et al. [27] at the AAPL that can produce pulsed microjets over a wide range of frequencies (1-60 kHz). The advantage of this high-bandwidth, resonance enhanced microjet

(REM) actuator system lies in its simple and compact design and the ability to generate tunable, supersonic pulsed microjets at a frequency that can be selected in light of the base flow dynamics. Moreover, since these pulsed microjets possess high mean and unsteady momentum, they are expected to penetrate into the shear/boundary layer potentially allowing one to manipulate their instability properties in a favorable manner. Solomon et al. [27] described the basic characteristics of this actuator and suggested a simple correlation for the design. In this paper, an extensive experimental study of the REM actuator is described over a very large range of design and flow parameters. As a result, further insight into the actuator aero-acoustics is gained and the results allowed exploring more generalized features that are necessary for designing actuators with more complicated geometry for a wide range of flow control applications.

II. Experimental Apparatus and Procedures

The experiments presented were conducted in AAPL located at the Florida State University. Measurements include: flow visualization –using a specialized lens based microschlieren system that uses laser-induced breakdown in argon as a pulsed light source; unsteady pressure measurements using ultra-miniature *Kulite*^{TM} pressure transducers; and near field noise using microphones. Measurements were obtained for the actuator source jet operating over a range of Nozzle Pressure Ratios (*NPR* = jet stagnation pressure / ambient pressure) of 1.9-8, corresponding to moderate to strongly under-expanded jets and over a range of geometrical parameters. The details of the measurement techniques employed are described below.

A. Unsteady Pressure Measurements

The unsteady microjet flow issuing out of these actuators was measured using a probe (diameter = 1.5 mm) with a 100psia range, ultra-miniature (1.3 mm diameter) Kulite pressure transducer Model XCE-062. A similar Kulite transducer with a 50psi range was used to measure the pressure inside the actuator cavity. The unsteady pressure signals were acquired through high speed National Instruments digital data acquisition cards using *Labview*^{TM} software. The transducer output was conditioned using a low-pass *Stanford*^{TM} SR640 filter and sampled at 100 kHz. Standard DFT (Discrete Fourier Transform) analysis was used to obtain narrowband pressure spectra using 4096 points/DFT. A total of 100 DFTs, without overlap, were averaged to obtain statistically reliable narrowband spectral estimates.

B. Laser based Microschlieren System

Images were acquired using the laser based microschlieren system shown in Figure 2. In order to obtain the requisite nanosecond pulse duration needed to 'freeze' the flow, laser-induced breakdown in argon was used as a broadband light source for the microschlieren system. A similar technique has been previously adopted by Volpe & Settles [29] and Beutner & Adelgren [30]. A New Wave Gemini PIV laser was used to generate breakdown due to its short pulsed duration of 3-5 ns; this was found to sustain the plasma for approximately 10 ns by Volpe & Settles [29]. The laser light is focused using a 50.8mm, f/1.5 plano-convex lens. A tank of compressed argon was regulated to supply argon at approximately 4 L/min in a cell where the beam is focused and the plasma is generated. The use of argon was found by Volpe and Settles [29] to increase the light output of the plasma 3-4 times compared to generating plasma in air and decreases the jitter of the plasma in the beam direction of the laser. The light generated from the breakdown is focused onto a rectangular slit using a 50mm/1.4 camera lens. From here a lens based schlieren system similar to Phalnikar et al.'s [31] is used with 50.8 mm diameter f/2.5 lenses. A 28-200 mm variable focal length camera lens coupled with a Kodak Megaplus camera (1018 x 1008 pixels) was used to acquire the images. More details of this laser based microschlieren system are available in Foster [32].

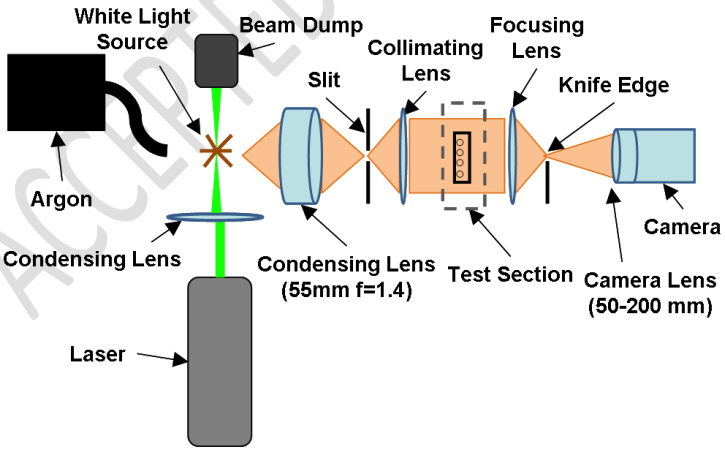

Fig. 2 Laser based microschlieren system used in this study for micro flow visualization

C. Measurement Uncertainties

The important geometrical and flow parameters involved in the present study are the nozzle to cavity distance *h*,

length of the cavity *L,* the actuator source jet diameter *d*, total actuator volume *V*, cavity diameter *D*, and the nozzle pressure ratio *NPR*. The cavity dimensions were machined with tolerances of ±10 microns. Precise measurement of length scales involved in the experiment was achieved using micro traverses with an accuracy of ±12.5 microns. An *Omega*^{TM} transducer PX303-200 G5V was used to measure jet total pressure and the uncertainty associated with the total pressure measurement was ±1 psi. The unsteady pressure measurements using the Kulite sensor were accurate within ±0.1 psi.

III. Resonance enhanced microjet (REM) actuator

In order to orient the reader and put the present study in context, a brief review of previous studies on REM actuator is discussed in this section. Figure 3*a* shows the schematic of the REM actuator developed and studied by Solomon et al. [27]. The most basic version of the microactuator (first generation) consists of a cylindrical cavity with multiple micronozzles at one end. A source jet underexpanded into the cavity will generate pulsed microjets under suitable flow and geometric conditions. The detailed characterization of this geometry is available in [27]. The frequency and amplitude of pulsed/unsteady microjets were measured over a range of flow and geometric parameters such as *NPR*, *h/d* and *L/d*. *NPR* is the source nozzle pressure ratio, *h* is the distance of cavity lip from the source nozzle, *L* is length of the cavity and *d* is the diameter of the source jet nozzle. For the simple geometry as shown in Figure 3*a*, a strong correlation between frequency of the actuator and its geometric parameters *h* and *L* was reported. An empirical relation that captures this was suggested for the non dimensional frequency of the actuator in terms of the jet column length, *H=L+h*, as given in equation (1), this is also represented in Figure 3*b* [27].

$$St_{ideal} = 0.4(H/d)^{-1.45} \tag{1}$$

Where,

$$St_{ideal} = fd/U_{ideal} \tag{2}$$

Rewriting equation (1) in terms of *NPR* results in:

$$f = \frac{0.4}{d}\left(\frac{2}{\gamma-1}\left((NPR)^{\frac{\gamma-1}{\gamma}}-1\right)\right)^{1/2}\sqrt{\gamma RT_o(NPR)^{\frac{1-\gamma}{\gamma}}}\,(H/d)^{-1.45} \tag{3}$$

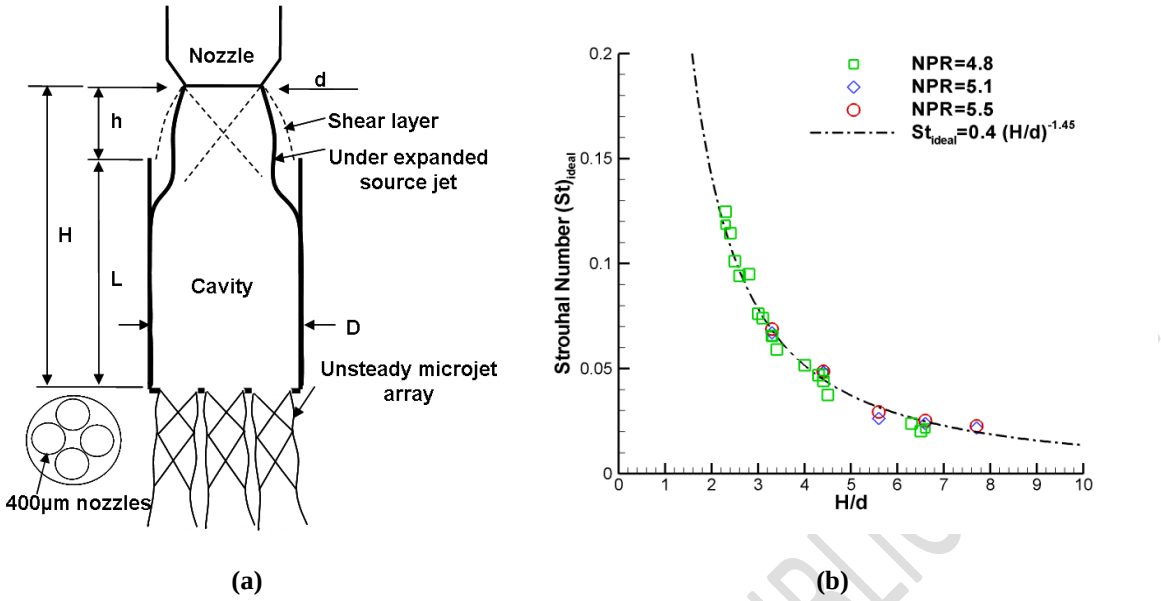

Fig. 3 REM actuator (a) Schematic (b) An empirical Correlation suggested for the microactuator design (Solomon et. al. [27])

The correlation given in equation (3) was derived for the simple geometry shown in Figure 2*a*. However, for implementation of these actuators in practical applications, the geometry often becomes more complex. Therefore a more generalized approach, based on other parameters where, as subsequent results show, an additional principal parameter turns out to be the actuator volume *V*, maybe useful for the accurate prediction of actuator frequency. In the present study, in addition to actuator volume, the influence of other parameters, such as source and exit jet diameter on actuator performance is also studied. It is expected that these results will be useful for the optimization of actuator design for a broader variety of applications. In addition to the detailed flow visualization, multiple miniaturized *Kulite*^{TM} unsteady pressure probes and microphones were used simultaneously in this study to characterize the unsteady flowfield generated by the microactuator for a better understanding of the resonance phenomena. The details of these studies are described next.

IV. Parametric studies of actuator properties

(a) Effect of volume on REM properties

The effect of actuator volume on its frequency is investigated here. In the previous studies described in [27] the actuator geometry was a simple cylindrical cavity where, as shown in Figure 3*a*, the actuator volume is a direct function of the cavity length *L* as the cavity diameter *D* was kept constant. Hence any inference regarding the actuator frequency dependence on cavity length can also be extended to its volume. The correlation suggested for this cylindrical design (Equation 3) indicates that the actuator frequency has a strong dependence on jet column length *H*. This parameter essentially captures the effect of cavity length *L*, which is directly related to the volume *V* of the actuator, and the nozzle to actuator distance *h*. As discussed in Solomon et al. [27], the actuator frequency *f* can be varied by the parameter *h* and/or *L*. Note that for a fixed cavity length *L*, the actuator frequency can be varied by changing *h* and in such a variation, volume of actuator is constant but the 'effective jet column length' *H= 'L+h'* changes. Since a change in cavity length changes the volume of the actuator as well as *H*, it is important to delineate the dependence of frequency on actuator volume from the effect of cavity length *L* or jet column length *H*. Such an experiment should keep the parameters *L* and *h* constant while actuator volume will be varied. One such geometry is shown in Figure 4.

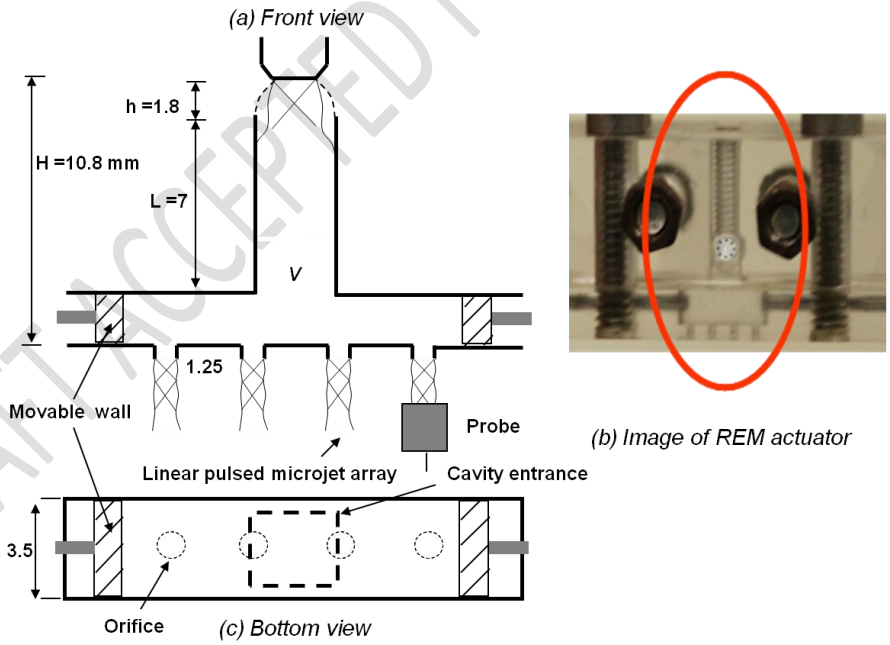

Fig. 4 Schematic of variable volume actuator used for volume-frequency experiments a) Front view b) An image of REM actuator c) Bottom view

In this configuration, the actuator has a square cross section cavity that opens to a rectangular spreader. Four micro nozzles (orifices) are located at the bottom of the spreader in a linear array pattern as shown in Figure 4*c*. In this way the pulsed microjets can be distributed in different configurations for various flow control applications. The square cross section is chosen to provide optical access inside the cavity as well to flush mount a Kulite sensor in the cavity wall inside the actuator for unsteady pressure measurements. The volume of the actuator can be varied by adjusting the two screws attached on either end of the spreader (Fig. 4*a*). In this way the cavity length (*L*) and the jet column length (*H*) can be kept constant while the volume of the actuator (*V*) is varied. In the present study, the actuator volume is varied from 34 mm^3 to 73 mm^3 while all other parameters are kept constant.

Figure 5 represents the pressure spectra of the actuator for different actuator volumes as measured by a Kulite probe located 2mm from the exhaust orifice of one of the unsteady/pulsed microjets as shown in Figure 4*a*. As seen in Figure 5*a*, for a fixed *H/d*=10.8 and constant volume of 34 mm^3, an *NPR* variation from 5.1 to 5.5 changes the actuator frequency from 5 to 6 kHz. Figure 5*b* shows that an increase in the volume to 54 mm^3 further changes the frequency range to 3 to 4.1 kHz for the same *H/d* value. At a higher volume (73 mm^3) the frequency response decreased to the 1.9-2.3 kHz range as shown in Figure 5*c*. In summary, changes in actuator volume from 34 to 73mm^3 have shifted the frequency from 1.9 to 6 kHz. This experiment clearly confirms importance of actuator volume as a critical parameter that determines the resonance frequency of the microactuator. The trend observed – decrease in frequency with increase in volume – is similar to studies reported earlier [27].

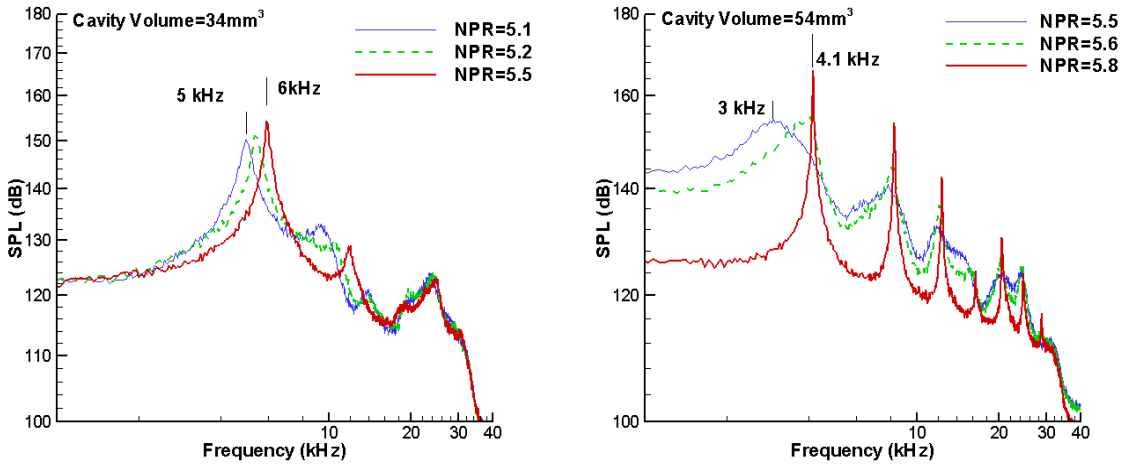

(a) Cavity Volume=34 mm^3 (b) Cavity Volume=54 mm^3

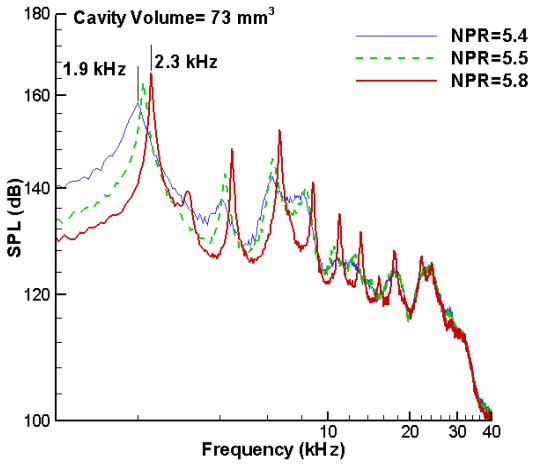

(c) Cavity Volume=73 mm^3

Fig. 5 Pressure spectra showing the influence of cavity volume in actuator performance for the actuator geometry shown in Figure 4 for a) Volume =34 mm^3, b) Volume =54 mm^3 c) Volume =73 mm^3

Actuator flowfield

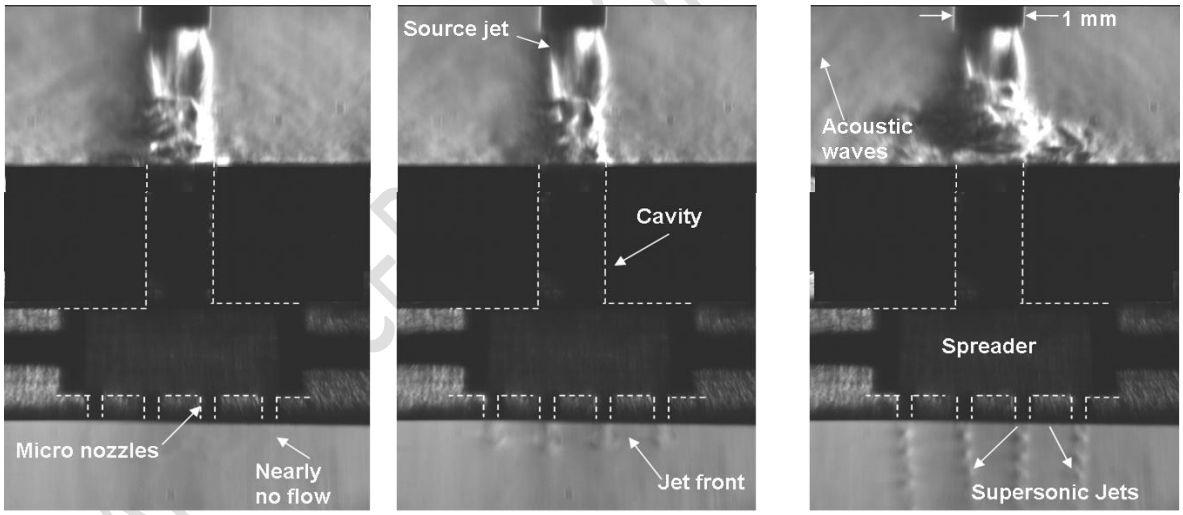

(a) **(b)** **(c)**

Fig. 6 Instantaneous microschlieren images showing various phases of the flowfield from the variable volume actuator (*h/d*=3 and *NPR*=8.2, V=34 mm^3 @ 5 kHz) (a) Phase where the microjet velocity is minimum (near zero velocity) (b) Phase that shows the beginning of jet front (c) Phase where microjets are supersonic (shock cell pattern inside the jet indicate the supersonic nature of the jets)

Several instantaneous microschlieren images of the actuator flowfield are shown in Figure 6. Note that this actuator was made with plexiglass side-walls with the hope of visualizing the internal flow; however, the optical distortions introduced due to internal strains in the material rendered this impractical. (An outline of the actuator cavity, as shown in Figure 4, has been superimposed on these images). As seen in Figure 6*a*, an under expanded source jet from a 1mm nozzle flows into the actuator cavity that opens to a rectangular spreader that has 4 micronozzles on the lower surface. A study of series of similar phase-conditioned visualizations reveals the following dynamics: The source jet initially "fills up" the actuator volume; this pressurizes the actuator cavity and initiates a discharge through the pulsed microactuators on the lower surface of the actuator. Roughly concomitant with the discharge from the nozzles on the lower surface, some 'spilling' of the source jet occurs at the top due to the high back-pressure that has developed in the actuator cavity. This repetitive 'filling' and 'spilling' process is essentially responsible for the highly unsteady properties of the microjet flows out of the actuator cavity. The decrease in the resonant frequency with increasing actuator volume may, to a first order, be explained with respect to this observation. For a fixed mass flow rate into the actuator (constant NPR), a larger volume essentially require a higher 'filling' time and results in a lower frequency response. A detailed numerical simulation of a similar REM flowfield, demonstrating the physical mechanism involved as well as the detailed aeroacoustic properties of the flow inside and outside the REM actuator, is reported recently by Uzun et al. [33]. The computed flowfield clearly demonstrates the actuator behavior discussed above. Figure 6*a-c* represents various phases of the resonating flow that produces pulsed microjets and high energy acoustic radiation. Very high unsteadiness is seen in the source jet flowfield, an observation similar to earlier studies [27]. The pulsing nature of microjets is also very evident from these images. Figure 6*a* shows the beginning phase of pulsing microjets where the velocity is at a minimum (almost near to zero velocity). Figure 6*b* shows jet fronts that indicate the evolution of pulsed jets. Figure 6*c* represents a phase where microjets are clearly supersonic with a high exhaust velocity. These flow visualizations indicate that the amplitude of velocity fluctuations of pulsed microjet is more than 300m/sec for this case, which is notable and unique at this high frequency (~5 kHz). The unsteady source jet field is also characterized by oscillation of source jet Mach disc. This oscillatory behavior is highly correlated to the unsteady behavior of microjets issuing from the actuator. A detailed description of the phase correlations between the unsteady properties of source jet and pulsing microjets, carried out using a phase locked flow visualization study, is available in Foster [32].

(b) Effect of inflow-out flow area ratio, n(S_m/S_c), on properties

Section IV*a* discusses the importance of actuator volume as an important parameter for REM actuator design. In this section the influence of another parameter on actuator frequency is discussed. An area ratio parameter, $n(S_m/S_c)$ is introduced here for this purpose where S_c is the area of the cross section of the cavity that the source jet flows into, S_m is the area micro nozzle/orifice (see Fig. 7*a*), and n is the number of microjets. This parameter mainly determines the exhaust mass flow rate from the REM actuator and is useful for the output optimization of this actuator system from a mass flow perspective. The area ratio parameter also represents the blockage of the flow inside the actuator. Actuators described in section III & IV were designed to have four pulsed microjets at its output/exhaust. However, in this section an actuator with a single variable diameter microjet nozzle (n=1) at its output is studied. In such a case, if S_m is zero, the flow entering the cavity will be completely blocked. On the other hand if S_m/S_c =1, the geometric blockage is zero, i.e. the flow entering the cavity can leave through the other end without flow accumulation inside the actuator. An actuator with a simple geometry –a cylindrical cavity with a single orifice, as shown in Figure 7*a* –is used for this study; the two limiting cases are shown on either side (Figure 7*b*&*c*). The goal of this experiment is to understand the dependence of area ratio (S_m/S_c) on the actuator frequency and to explore the limits of resonance. The jet column length H and the actuator volume V are kept constant at 10.8 mm and 18 mm^3, respectively for the present experiments while the area ratio (S_m/S_c) is varied from 0.01-1.

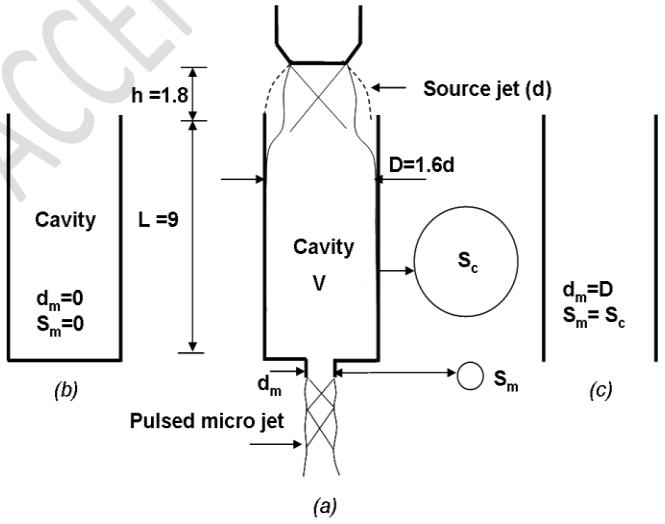

Fig. 7 Actuator configuration used to study the dependence of parameter $n(S_m/S_c)$ on frequency, n=1

Table1: Geometrical details of actuators used to study the effect of inflow-outflow area ratio (S_m/S_c) on REM properties

d_m (mm)	S_m (mm²)	S_c (mm²)	S_m/S_c	V (mm³)	f_{max} (kHz)
0.18	0.025	2.01	0.01	18.1	8.5
0.4	0.126	2.01	0.06	18.1	8.3
1.0	0.785	2.01	0.39	18.1	8.3
1.3	1.33	2.01	0.66	18.1	5.8
1.6	2.01	2.01	1.0	18.1	No resonance

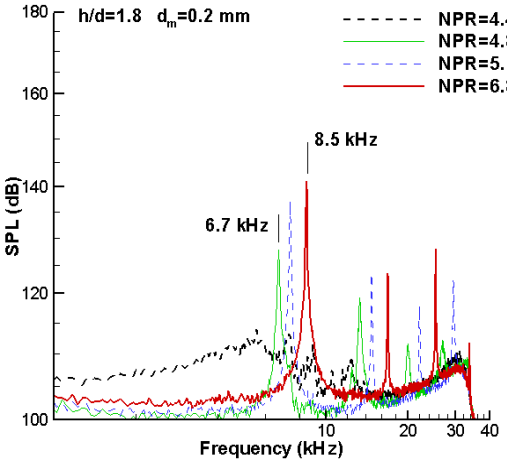

(a) S_m/S_c= 0.01

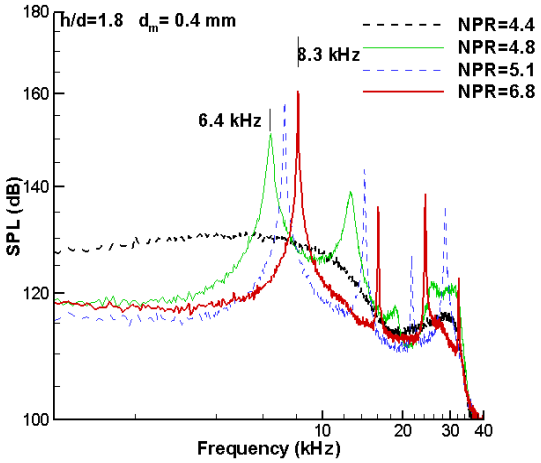

(b) S_m/S_c=0.06

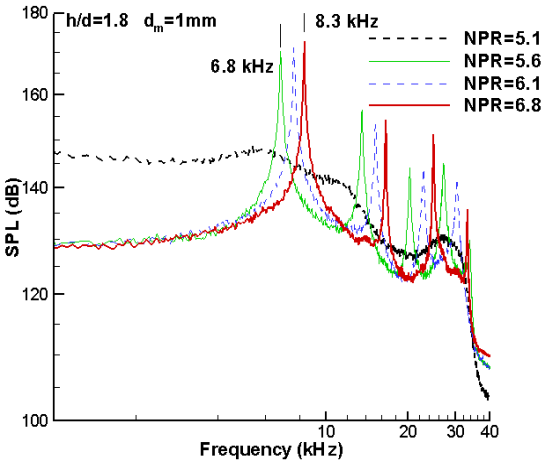

(c) S_m/S_c=0.39

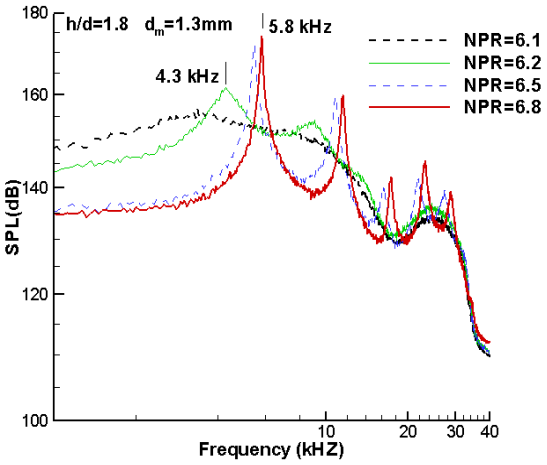

(d) S_m/S_c=0.66

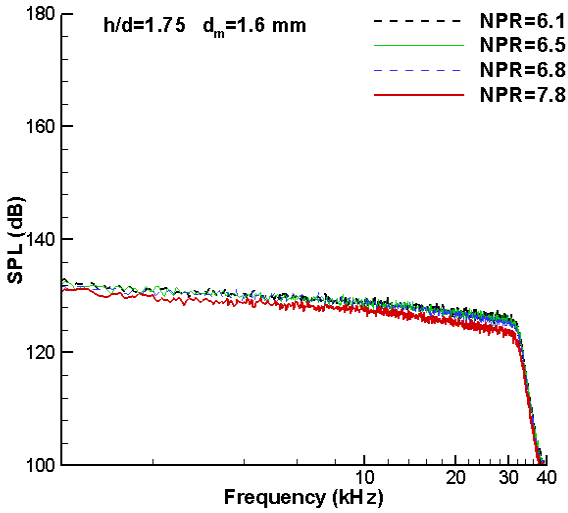

(e) S_m/S_c =1

Fig. 8 Pressure spectra of actuator with single orifice at different $n(S_m/S_c)$ ratios

The cavity and the source jet diameter are 1.6 and 1 mm respectively, similar to the dimensions used in previous experiments, further details are provided in Table 1. The pressure spectra measured at the actuator exit for this single orifice actuator at different S_m/S_c values are shown in Figure 8*a-e.*

As shown in Figure 8*a*, for the actuator with area ratio S_m/S_c=0.01, the amplified frequency varies from 6.7-8.5 kHz, for an *NPR* variation of 4.4-6.8. The frequency range remains nearly same for the next two cases i.e. for S_m/S_c=0.06 and 0.39 as seen in Figure 8*b* and *c* respectively. This shows that for relatively low area ratios, the frequency of the actuator mainly depends on other parameters such as volume *V* and the jet column length *H*, which were discussed previously. For a higher area ratio, S_m/S_c=0.66, the amplified frequency was reduced to a range of 4.3-5.8 kHz. Resonance was not observed for the last case where the area ratio is equal to 1 i.e. $S_m=S_c$ (Figure 8*e*).This is the case where the inflow area and the out flow area are equal, so that there is no flow accumulation inside the actuator. To better understand the effect of area ratio parameter $n(S_m/S_c)$ on actuator frequency, the resonance frequency of this actuator at *h/d*=1.8 and *NPR*=6.8 is plotted in Figure 9. In the case of lower area ratios, $n(S_m/S_c) < 0.4$, the frequency remains nominally constant, while for a higher area ratio, it shifts and is reduced significantly. In the limiting case (S_m/S_c =1) no resonance is observed. This experiment highlights the importance of the parameter $n(S_m/S_c)$ in determining the REM actuator properties.

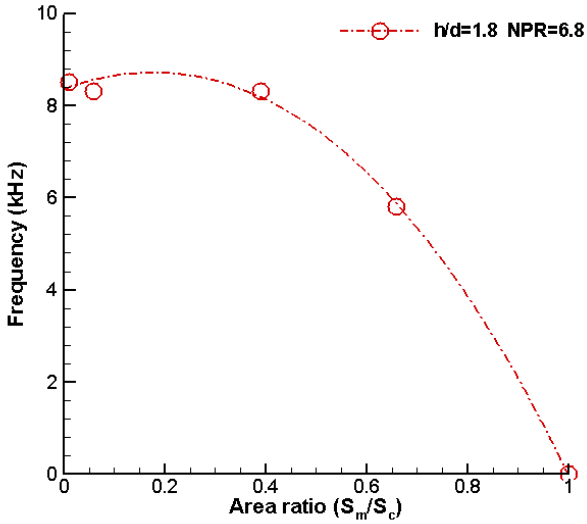

Fig. 9 Frequency variation with area ratio parameter $n(S_m/S_c)$ for actuators with single microjet output at h/d=1.8 and NPR=6.8

Another feature to be noted from Figure 8 is the shift in resonance triggering *NPR* values, (i.e., minimum *NPR* value to initiate pulsed flow from the REM actuator) for different area ratios of the actuator for a fixed *h/d* value. For lower S_m/S_c values, (0.01 and 0.06) resonance phenomena began at *NPR*~4.8. At higher area ratios 0.39 and 0.66, NPR_{crit} has changed to a higher value ~5.6 and 6.2, respectively. This observation is shown explicitly in Figure 10. This points to the fact that an actuator with a higher flow throughput (larger number of pulsed microjets or a larger diameter of micro nozzles) requires higher mass flow into the system to trigger the resonance phenomena. This is possible by either increasing the source jet nozzle diameter or increasing the nozzle pressure ratio *NPR*. Since a higher *NPR* would result in elongation of the shock cell pattern in the source jet, the selection of NPR requires a judicious selection of parameter *h/d* to keep the cavity lip of the actuator within the pressure recovery region of the first shock cell of the source jet, as this is the region where source jet instability is triggered. (See Solomon et. al [27] for further discussion)

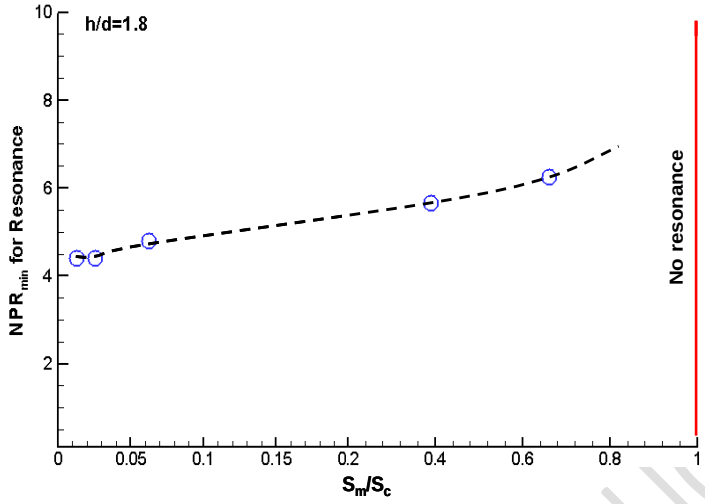

Fig. 10 Dependence of resonance triggering *NPR* on area ratio parameter S_m/S_c

(c) REM actuator design- An improved model for complex actuator configuration

In general, the results presented so far indicate that the actuator volume V and the area ratio parameter, S_m/S_c (in case of actuators with n number of microjet output, this will be $n(S_m/S_c)$, are important variables that need to be taken into account while designing actuators with complex geometries. The studies reported earlier [27] can now be seen as a particular case of this generalized configuration, where the cylindrical volume of the first generation of actuators was a direct function of the internal cavity length L. Table 2 summarizes the details of various parameters of actuators used in the present and previous studies. In order to better understand and utilize the larger parametric space tested for the REM actuator (Table 2) and to develop more general design tools for its design, the resonance frequencies with maximum amplitude of various actuators discussed in section III and IV are plotted against the parameter V. These results are compared with a semi empirical relation (Equation 4) derived for the maximum resonance frequency of REM actuator, based on a lumped element modeling approach used by Solomon [28]. This comparison is shown in Figure 12 where the parameters used in Equation 4 are indicated in Figure 11.

Table 2: Geometric details of REM actuators used for the present and previous studies

Actuator	ℓ'_c mm	ℓ_m mm	n	V mm^3	S_c mm^2	S_m mm^2	$n(S_m/S_c)$	
A	1	0.5	4	2	2	0.13	0.26	Previous study [27] Fig. 3a
B	2	0.5	4	4	2	0.13	0.26	
C	3	0.5	4	6	2	0.13	0.26	
D	5	0.5	4	10	2	0.13	0.26	
E	9	1.0	1	18	2	0.03 0.13 0.79 1.33 2.01	0.02 0.06 0.39 0.66 1.00	Present study Section IV b Fig. 7
F	9	0.5	6	27	2	0.13	0.39	Reference [34] Fig. 11
G	9	0.5	4	34	2.6	0.13	0.2	Present study Section IV a Fig. 4
H	9	0.5	4	54	2.6	0.13	0.2	
I	9	0.5	4	73	2.6	0.13	0.2	

$$f_{\max} = \frac{c_0}{2\pi}\left\{\left(\frac{nS_m\ell'_c + S_c\ell'_m}{\ell'_m\,\ell'_c\,V}\right)\left(1-\frac{nS_m}{S_c}\right)\right\}^{1/2} \tag{4}$$

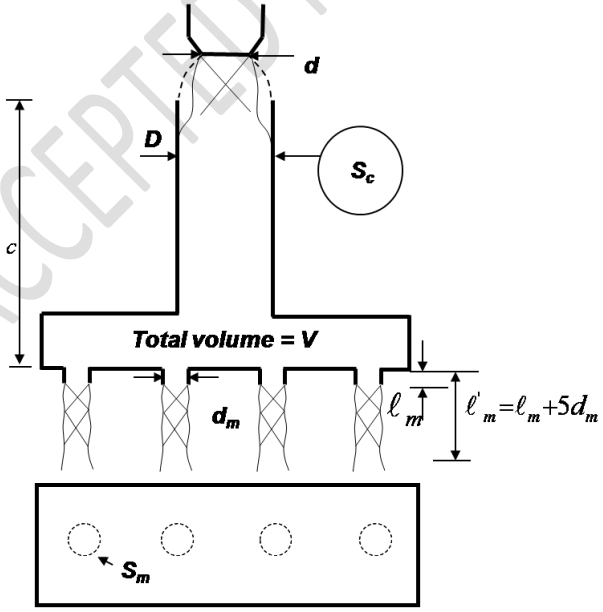

Fig. 11 Parameters used in Equation 4 to determine the actuator resonance frequency with maximum amplitude [28].

Actuators A-D have a simple cylindrical geometry with 4 microjet output, as shown in Figure 3*a*. This geometry was used in the previous study [27]. Actuator E is cylindrical with circular cross-section, used in the present study having a single microjet output (Figure 7a). Geometry F is a cylindrical cavity with rectangular spreader at the bottom, similar to Figure 11, but it has six microjet output. This actuator design was used by Ali et al [34] to control the resonant flow inside a cavity subjected to supersonic flow. The geometric details of actuators G-I were discussed earlier in section III *b* (Figure 4). From the above discussions it is evident that the semi empirical correlation based on actuator volume and the area ratio parameter, i.e., equation (4), is more general and comprehensive for predicting the most amplified resonance frequency for actuators with complex geometry. Using this improved model, REM actuators may be designed for practical applications that require more complex actuator configurations.

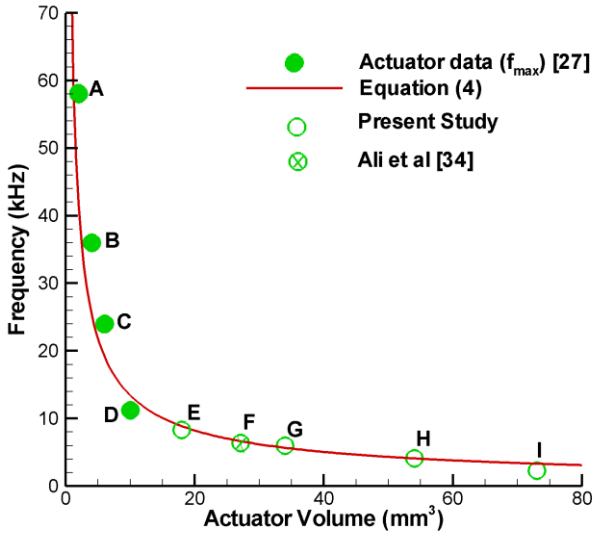

Fig. 12 Resonance frequencies with maximum amplitude of various actuators are compared with the semi empirical equation given in Equation 4

The flow features of various REM actuator designs discussed so far indicate that the physical mechanisms are very similar, irrespective of the actuator geometry. To better understand the resonance mechanism and the unsteady properties of REM actuator, synchronous measurements were carried out using multiple ultra-miniature unsteady pressure sensors and microphones; details are presented next.

V. Actuator Dynamics

The pressure measurements discussed so far were obtained using the Kulite probe located outside the actuator and directly exposed to the pulsing microjets as indicated in Figure 4. To better understand the actuator aeroacoustic and the physical mechanism involved, synchronized measurements of unsteady pressure inside and outside the actuator and the acoustic radiation in the near field were also acquired.

(a) Spectral Properties

The pressure fluctuations inside the cavity and that associated with the pulsed microjets are measured with two Kulite sensors –one flush mounted in one of the interior walls of the actuator cavity and the other located at the actuator exit and exposed to the pulsing microjets– simultaneously. The near field acoustic spectrum is synchronously measured with the Kulite measurements using a *B &K* microphone. The configuration of the actuator with Kulite sensors and microphone is shown in Figure 4.

Figure 13*a* shows the spectra measured by the Kulites while the geometric parameters of the actuator are kept constant (h/d=1.8, V=34 mm^3 and H=9 mm) and the *NPR* is varied from 5.1 to 6.8. The spectra show the same frequency and frequency range (4 to 6 kHz) measured by both Kulite sensors for a given condition. Although the tones occur at the same discrete frequencies the amplitudes are different; the pressure fluctuations inside the cavity have higher amplitudes than those measured for the pulsed microjets. These results clearly reveal that there exists a strong coupling between the unsteady pressure fluctuations inside the cavity and the unsteadiness measured in the microjets. This is anticipated because, as noted in our discussion of the flow visualizations in Figure 6, the flow through the micro nozzles is driven by the flow accumulating inside the actuator cavity and then being discharged through the micronozzles. Pressure fluctuations inside the cavity will strongly influence the microjets characteristics. Figure 13*b* shows the unsteady spectra measured by both Kulites and the nearfield microphone for *NPR*=6.1. All three sensor record the same frequency, 6.1 kHz at this *NPR*, confirming the global nature of perturbations generated by the actuator.

To further examine this, the coherence between the measurements made by the three sensors is evaluated for one of the test cases, *NPR*=5.8, and is shown in Figure 14. First, as expected, high coherence values are measured between the Kulites and the microphone at the actuator resonant frequency of 5.5 kHz (see Fig. 13a; resonant frequency is 5.5 kHz at *NPR*=5.8), indicating a strong correlation at these frequencies. However, equally noteworthy, and perhaps somewhat unexpected, is the very high coherence between the internal (cavity) and

external Kulite (probe) sensors (red spectra) for a much wider range of frequencies, suggesting a direct correlation between the actuator internal flow dynamics and the microjets produced at its exhaust.

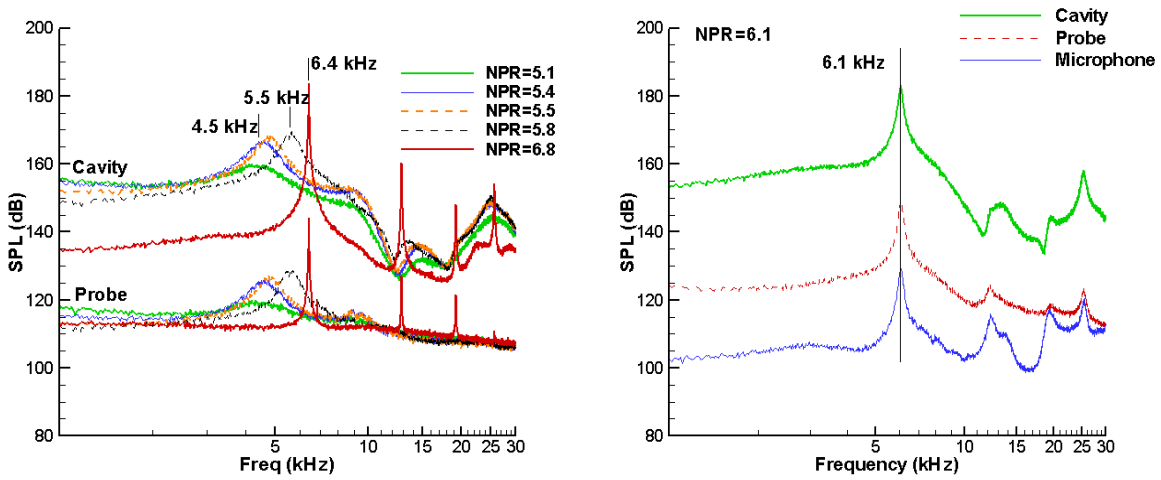

a) **b)**

Fig. 13 a)Pressure spectra measured inside the cavity and in the microjets (probe) at various *NPR*; b) synchronized unsteady pressure measured inside the cavity, in microjets (Probe) and in nearfield (microphone) at *NPR*=6.1

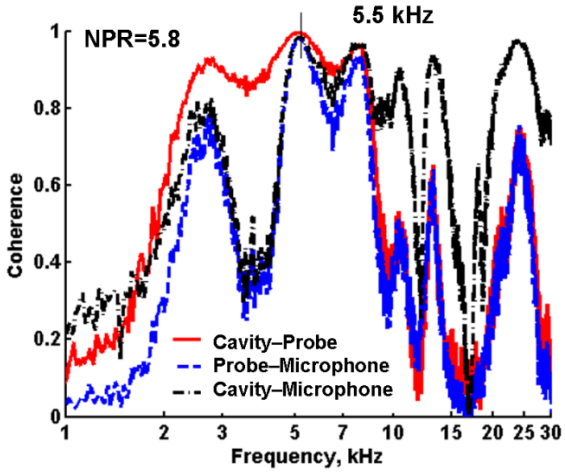

Fig. 14 Coherence of unsteady pressure spectra measured by Cavity Kulite, Kulite probe and the microphone in the nearfield

From a practical perspective, this allows one to reliably estimate actuator performance using internal sensors when such actuators are used for flow control in complex applications where external sensors may not be easily implemented.

(b) Time History

Figure 15 shows the time history of the pressure measured by the Kulite inside the actuator cavity for a *NPR*= 6.8. Using this sensor, the mean pressure and the p_{rms} were measured to be ~21.7 psia and 22.7 psia, respectively. This pressure history clearly shows large periodic pressure fluctuations within the cavity which in turn drive the pulsed microjets at the actuator output. As seen here, two consecutive peaks are separated by approximately 157 micro-seconds that correspond to a frequency of 6.4 kHz. This corresponds to the largest amplitude tone seen in Figure 13a. The pressure history also clearly depicts the very large pressure oscillations inside the cavity where the pressure varies from a minima of ~13psia to a maxima of ~37psia where the higher cavity pressures are more than sufficient to produce supersonic pulsed microjets at the actuator output, as seen in Fig 6. The cyclic variation in the actuator cavity pressure once again supports the previous observation of a filling and spilling phenomena discussed in the context of Fig. 6

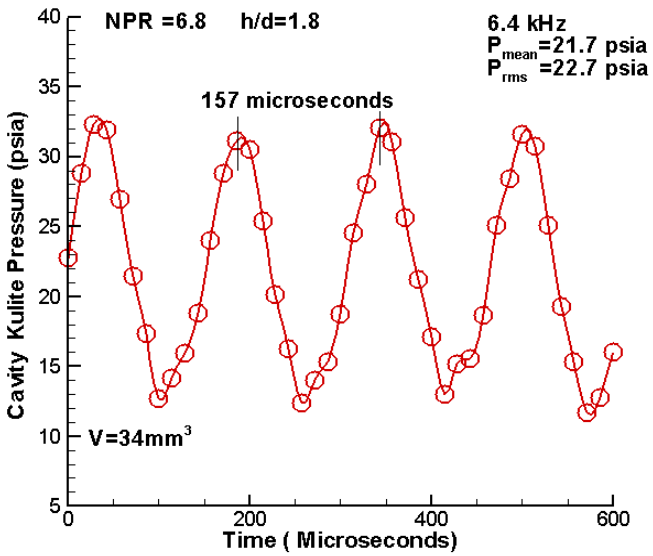

Fig. 15 Pressure fluctuations inside the cavity measured by the cavity Kulite

(c) Mean and unsteady pressure

Figure 16 shows the mean and rms pressures using the two Kulite sensors, for a source jet *NPR* variation from 0-8, at *h/d*=1.8, *V*=34 mm^3 and *H*=9 mm (Figure 4). The circles show the mean pressure variation inside the cavity where a linearly increasing trend is seen as *NPR* varied from 0-4.8. Further increase in *NPR* (*NPR*>4.8) results in a decreased mean pressure inside the cavity until ~ *NPR*=6.1. For *NPR* 6.1 to 8, again an increasing trend in the mean cavity pressure is observed. Note that previously discussed results (Figure 5a) indicate that the resonance behavior of actuator begins approximately at this *NPR* (4.8).

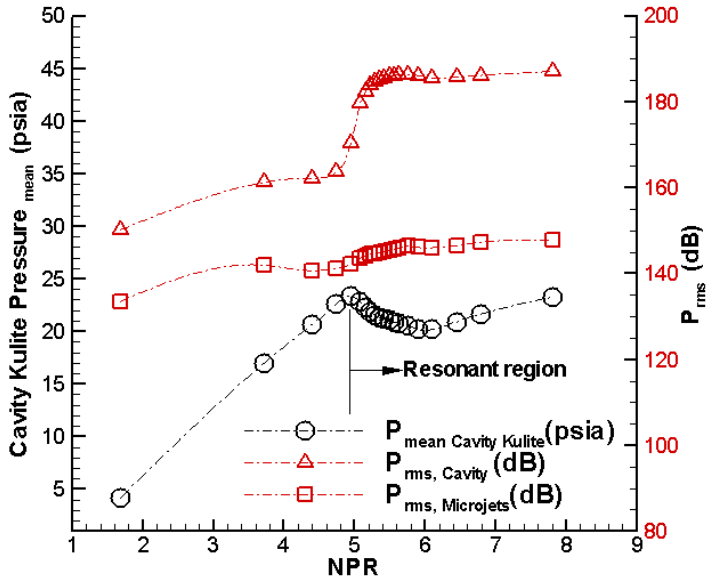

Fig. 16 Mean and RMS pressure measured inside the cavity and in the microjets at various source jet *NPR*.

It was reported earlier (Solomon et al. [27]) that for a given h/d, the resonance phenomenon in the actuator will be triggered when the cavity lip of the actuator lies in the pressure recovery region of the first shock cell of the source jet. Hence, the present critical value of *NPR* (~4.8) applies only for the current *h/d* (=1.8), whereas resonance will be triggered at a lower *NPR* for a smaller *h/d*. It is interesting to note in Fig. 16 that once resonance is triggered, the measured mean pressure inside the cavity decreases with increasing *NPR*. That is, once the actuator flow becomes globally unstable, adding more energy through the source jet does not necessarily increase the mean momentum associated with the microjets. However, a concomitant increase in the P_{rms} measured inside the cavity

(red triangles in Fig. 16) reveals that in the resonance mode, a larger portion of the energy input to the actuator system is used to increase the unsteady component inside the actuator - the higher value of P_{rms} measured inside the cavity for *NPR*>4.8 is a clear indicator of this behavior. Also, note that beyond a certain threshold, *NPR*~ 5.5 in this case, further increments in *NPR* did not produce significant changes in the of cavity unsteady pressure. P_{rms} measured in the pulsed microjet plumes (green circles) shows a trend similar to that of P_{rms} measured inside the cavity. In summary, Figure 16 provides insight into the relationship between the mean and unsteady flow inside the REM actuator and its impact on the unsteady properties of the microjets emanating from the actuator.

VI. Summary and Conclusions

A detailed study of a high-bandwidth resonance enhanced microactuator that can generate pulsed, high momentum (supersonic) jets over a frequency range of ~1-60 kHz is described in this paper. The actuator essentially consists of an underexpanded source jet entering a cavity with multiple micronozzles that allow pulsed microjets to flow out of the cavity. One of the main goals of this study was to better understand the dynamics of this compact actuator, including its frequency dependence on the actuator flow and geometry parameters. The actuator volume is one of the main performance parameters; this was varied from 2 mm^3 to 74 mm^3 producing pulsed supersonic microjets in a frequency range of 1-60 kHz. The effect of blockage of the source jet flow was also found to be a relevant parameter; this was explored through the variation of an 'area ratio parameter', which is the area ratio of outlet and inlet openings of the actuator geometry. It is found that a minimum threshold of blockage was needed to initiate resonance in the actuator flowfield; without flow blockage (area ratio parameter =1) no resonance phenomena is triggered. The actuator frequency is also strongly influenced by this parameter. Unsteady pressure measured inside the actuator shows highly periodic, nearly sinusoidal, oscillations with large amplitudes. Cross correlation analysis of sensors at various locations in the flow reveal the global nature of the flow unsteadiness generated by the actuator where the fluctuations in the source jet, cavity and the microjets are intimately related. Finally, a more general relationship that accounts for the relevant actuator parameters, is proposed for predicting the actuator design frequency. This correlation can in principle be used to help design actuators with more complex geometry for use in practical applications.

Acknowledgments

This work was in part supported by Florida Center for Advanced Aero Propulsion (FCAAP) and AFOSR, managed by Dr. D. Smith. The authors would like to thank FCAAP and AFOSR for supporting this research and Dr. Rajan Kumar and Dr. Jonas Gustavson for their valuable suggestions for this study.

References

1. Seifert, A., Darabi, A., and Wygnanski, I., "Delay of Airfoil Stall by Periodic Excitation," *Journal of Aircraft*, Vol. 33, No. 4, 1996, pp. 691-698.

2. McManus, K., and Magill, J., "Separation Control in Incompressible and Compressible Flows using Pulsed Jets," AIAA Paper 1948, 1996.

3. Bryant, R. G., Fox, R. L., Lachowicz, J. T., and Cheri, F.J., "Piezoelectric Synthetic Jets for Aircraft Control Surfaces," SPIE Paper 3674, 1999.

4. Wiltse, J. M., and Glezer, A., "Manipulation of Free Shear Flows Using Piezoelectric Actuators," *Journal of Fluid Mechanics,* Vol. 249, 1993, pp. 261-285.

5. Smith, B, L., and Glezer, A., "The Formation and Evolution of Synthetic Jets," *Physics of Fluids*, Vol. 10, No. 9, 1998, pp. 2281-2297.

6. Cattafesta, L., Mathew, J., Wang, W., and Kurdila.A., "Modeling of Piezoelectric Actuators for Fluid Flow Control," SAE Paper 01-5534, 2000.

7. Joslin, R. D., Horta, L. G., and Chen, F.J., "Transitioning Active Flow Control to Applications," AIAA Paper 3575, 1999.

8. List, J., Byerley, A., McLaughlin, T., and Dyken, R. V., "Using a Plasma Actuator to Control Laminar Separation on a Linear Cascade Turbine Blade," AIAA Paper 1026, 2003.

9. Jacob, J. D., Rivir, R., Carter, C., and Estevadeordal, J., "Boundary Layer Flow Control using AC Discharge Plasma Actuators," AIAA Paper 2128, 2004.

10. Corke, T. C., Enloe, C. L., and Wilkinson, S. P., "Dielectric Barrier Discharge Plasma Actuators for Flow Control," *Annual Review of Fluid Mechanics*, Vol. 42, 2010, pp 505-529.

11. Ganiev, Y. C., Gordeev, V. P., Krasilnikov, A. V., Lagutin, V. I., Otmennikov, V. N., Panasenko, A. V., "Theoretical and Experimental Study of The Possibility of Reducing Aerodynamic Drag by Employing Plasma Injection," AIAA paper1999-0603.

12. Kelley, C., Bowles, P., Cooney, J., He, C., Corke, T., "High Mach number Leading-Edge Flow Separation Control Using AC DBD Plasma Actuators," AIAA paper 0906, 2012.

13. Grossman, K. R., Cybyk, B. Z., and Van Wie, D. M., "Spark Jet Actuators for Flow Control," AIAA Paper 57, 2003.

14. Cutler, A., Drummon, J. P., "Toward a High-Frequency Pulsed-Detonation Actuator," AIAA paper 555, 2006.

15. Samimy, M., Kearney-Fisher, M., Kim, J., and Sinha, A., "High speed and High Reynolds Number Jet Control Using Arc Filament Plasma Actuators for Noise Mitigation and for Flow and Noise Diagnostics," AIAA paper 2011-22.

16. Yeung, P. K., Brasseur, J. G., and Wang, Q., "Dynamics of Direct Large-Scale Couplings in Coherently- Forced Turbulence: Concurrent Physical-Space and Fourier-Space Views," *Journal of. Fluid Mechanics*, Vol. 283, 1995, pp 43-95.

17. Wiltse, J. M., and Glezer, A., "Direct Excitation of Small Scale Motions in Free Shear Flows," *Physics o. Fluids*, Vol. 10, No. 8, 1998, pp 2026-2036.

18. Stanek, M. J., Raman, G., Kibens, V., Ross, J. A., Odedra, J., and Peto, J. W., "Control of Cavity Resonance Through Very High Frequency Forcing," AIAA paper 1905, 2000.

19. Hartmann, J., and Trolle, B., "A new acoustic generator," *Journal of Scientific Instruments*, Vol. 4, No. 4 ,1927, pp 101-111.

20. Raman, G., and Kibens, V., "Active Flow Control using Integrated Powered Resonance tube Actuators," AIAA Paper 3024, 2001.

21. Kastner, J., and Samimy, M., "Development and Characterization of Hartmann tube fluidic actuators for high-speed flow control," *AIAA Journal*, Vol. 40, No.10, 2002, pp. 1926-1934.

22. Dziuba, M., and Rossmann, T., "Active control of a Sonic Transverse Jet in a Supersonic Cross Flow using a powered Resonance tube," AIAA Paper 897, 2005.

23. Brocher, E., Maresca, C., and Bournay, M. H., "Fluid Dynamics of the Resonance Tube," *Journal of Fluid Mechanics*, Vol. 43, Part 2, 1970, pp 369-384.

24. Alvi, F. S., Shih, C., Elavarasan, R., Garg, G., and Krothapalli, A., "Control of Supersonic Impinging Jet Flows using supersonic microjets," *AIAA Journal*, Vol. 41, No. 7, 2003, pp. 1347-1355.

25. Kumar, R., Lazic, S., and Alvi, F. S., "Control of High-Temperature Supersonic Impinging jets Using Microjets," *AIAA Journal*, Vol. 47, No. 12, 2009, pp. 2800-2811.

26. Zhuang, N., Alvi, F.S., Alkislar, M.B., and Shih, C., "Supersonic Cavity Flows and their Control," *AIAA Journal*, Vol. 44, No. 9, 2006, pp. 2118-2128.

27. Solomon, J. T., Kumar, R., and Alvi, F. S., "High-Bandwidth Pulsed Microactuators for High-Speed Flow Control," *AIAA Journal*, Vol. 48, No. 10, 2010, pp. 2386-2396.

28. Solomon, T, J., "High-bandwidth Unsteady Actuators for Active Control of High-Speed Flows," PhD Dissertation, Florida State University, 2010.

29. Volpe, J., and Settles, G., "Laser-induced Gas Breakdown as a Light Source for Schlieren and Shadowgraph Particle Image Velocimetry," *Optical Engineering*, Vol. 45, 2006, pp. 080509-3.

30. Beutner, T., Adelgren, R., and Elliott, G., "Characterization of Schlieren Light Source Using Laser-Induced Breakdown in Argon," *AIAA Journal*, Vol. 44, 2006, pp.399-402.

31. Phalnikar, K. A., Kumar, R., and Alvi, F. S., "Experiments on Free and Impinging Supersonic Microjets," *Experiments in Fluids*, Vol. 44, 2007, pp. 819-830.

32. Chase Foster., "Characterizing High Frequency Microscale Flows Using Optical Methods," Masters Thesis, Florida State University, 2011.

33. Uzun, A., Foster, C. H., Solomon, J.T., Oates, W. S., Hussaini. M.Y., and Alvi, F.S., "Simulations of Pulsed Microactuators for High Speed Flow Control," AIAA paper 2938, 2011.

34. Ali, M.Y., Solomon, J.T., Gustavsson, J., Kumar, R., Alvi, F.S., "Control of Supersonic Cavity Flows Using High Bandwidth Micro actuators," AIAA paper 197194-564, 2010.

50th AIAA Aerospace Sciences Meeting including the New Horizons Forum and Aerospace Exposition
09 - 12 January 2012, Nashville, Tennessee
AIAA 2012-0065

Implementing Resonant Enhanced Pulsed Micro-Actuators for the Control of Supersonic Impinging Jets

Garrett M. Strickland[1], John T. Solomon[2], Jonas P. R. Gustavsson[3], and Farrukh S. Alvi[4]
Florida Center for Advanced Aero-Propulsion (FCAAP)
Florida A & M University and Florida State University, Tallahassee, FL, 32308

Recent work at the Advanced Aero-Propulsion Laboratory (AAPL) at Florida State University has produced a micro-actuator design utilizing micro scale cavity resonance phenomena for active control of various high-speed flowfields such as supersonic impinging jets and cavity flows. These micro-scale actuators are capable of producing pulsed supersonic microjets over a wide range of design frequencies which can be chosen depending on the frequencies that are relevant to the application. Pulsed microjet control has the potential to produce improved flow and/or noise control as has been shown with steady microjet control, while introducing less mean momentum into the system by actuating at the natural frequency of the system. This study focuses on the design, characterization, and implementation of these actuators into the STOVL impinging jet flowfield. The results of this implementation are compared to the no control case, steady control, and the first generation implementation of pulsed microjets into our STOVL facility. By operating these pulsed microjet actuators at 6.1 kHz, impinging tones were reduced by up to 23 dB, and overall sound pressure levels were reduced by up to 7 dB as compared to the baseline flow. Compared to steady microjet control, pulsed control showed improved reduction of discrete tones of about 5 dB and overall sound pressure levels within 2 dB of those found in the steady case. Additionally, this second generation implementation does not exhibit the new peaks generated by first generation control, and further reduces OASPL by about 5 dB.

I. Introduction

FLOW control techniques for supersonic impinging jets have been the topic of considerable discussion and development in recent years resulting in the development of a wide range of both passive as well as active devices.[1] It has been shown that many undesirable effects associated with certain complex flowfields, such as impinging jets and cavity flows, can be reduced or eliminated with the proper use of flow control actuators.[2] These flowfields are of great importance in many applications, such as Short Takeoff and Vertical Landing (STOVL) aircraft where the resulting impingement tones can cause large scale unsteadiness and powerful acoustic disturbances. These disturbances result in unwanted effects such as sonic fatigue to parts of the aircraft and ground erosion. Some of these features can be seen in the shadowgraph image shown in Fig. 1. These unsteady effects are a result of a feedback mechanism in which disturbances in the shear layer at the jet exit grow into large scale vortical structures which then convect downstream to the ground plane. Upon impingement, these generate acoustic waves that propagate back up to the nozzle exit through the ambient air exciting further instabilities in the jet shear layer closing the feedback loop.[3,4]

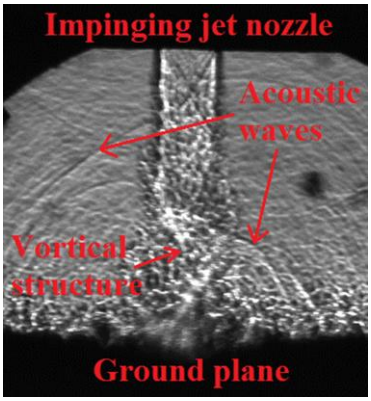

Figure 1. Shadowgraph image of the impinging jet flowfield.

[1] Graduate Research Assistant, Department of Mechanical Engineering, Student Member AIAA
[2] Post-doctoral Research Associate, Adjunct Assistant Professor, Department of Mechanical Engineering, Member AIAA
[3] Associate Research Scientist, Department of Mechanical Engineering, AIAA Senior Member
[4] Professor, Department of Mechanical Engineering, Associate Fellow AIAA

Various passive as well as active control methods have been investigated for control of these phenomena including microtabs,[2] wire devices,[5] porous ground plane surfaces,[6] plasma actuators,[7] Hartmann tube fluidic actuators,[8] and hybrid control schemes involving both passive and active control methods.[2,6] Recent research at the Advanced Aero-Propulsion Laboratory (AAPL) at Florida State University (FSU), which is part of the state-wide Florida Center for Advanced Aero-Propulsion (FCAAP), has focused primarily on active control because there is no thrust penalty to the main jet when the control is inactive, as well as its ability to adjust dynamically depending on the flow conditions. Plasma actuators, an active control method that has seen some treatment in recent research,[7] have the benefit of very fast response times enabling phase-based control, however they require large power supplies and involve high voltages which can lead to EMI related issues and may prove difficult to implement into applications with tight space and weight restrictions. With these restrictions in mind, research at the AAPL has focused on microjet actuators designed to be driven by pressurized air already present in the engines of aircraft, using relatively small supply systems with minimal mass flow requirements. These actuators use micro-scale supersonic air jets introduced at the supersonic nozzle exit to disrupt the system's feedback mechanism and have shown significant reduction in flow unsteadiness, impingement tones, as well as overall noise levels.[9,10]

Having shown the effectiveness of steady microjet injection, ongoing research has focused on creating pulsed microjet actuators in an effort to produce similar or even better results while introducing less mean momentum flux into the system. This could potentially reduce the mean pressure cost significantly and increase the overall efficiency of microjet control by both increasing effectiveness and decreasing the mass requirements. Additionally, if pulsed actuators are operated at or near the dominant flow frequency it may allow one to leverage the base flow instabilities producing greater benefit. Future research also aims to develop phase-based control of the flowfield using pulsed actuators. The Resonance Enhanced Micro-actuators (REM) developed by Solomon[11] in recent years show potential to produce such pulsed microjets for control of a variety of high-speed resonance flows.[12] These active, resonant actuators create pulsed micro-scale jets with high mean momentum flux and a wide amplitude range extending from nearly no flow to significantly underexpanded with the added benefit of requiring no moving parts. This paper will discuss further development of these unsteady microjet actuators driven by their implementation into an impinging jet flowfield and comparisons with both steady and previous attempts at implementing unsteady microjet flow control actuators.

II. REM actuator – Previous research

Steady microjet control, discussed later in this paper, shows reduction of impinging tones on the order of 15 dB as well as overall sound pressure level reduction of 3 to 8 dB agreeing well with previous work.[9] While already promising, these results could potentially be improved upon with proper application of pulsed microjet control. The goal of unsteady microjet control is to equal or surpass the reduction of impinging tones, overall noise levels and unsteadiness with less mass and momentum introduced into the system. Additionally, the successful development of unsteady actuators enables the future development of phase-based control potentially providing even more efficient and effective control. In order to accomplish these goals, an actuator has been developed which is capable of producing unsteady microjets oscillating at frequencies on the same order as those of the main impinging jet flow.[13] For the STOVL facility at the AAPL, the primary resonant frequencies of the impinging jet are in the range of 5-8 kHz corresponding to Strouhal numbers with respect to the nozzle throat diameter in the range of 0.25 to 0.4.

Rather than rely on moving parts, which could prove to be problematic due to size constraints and the high frequencies required, research at the AAPL has produced a fluidic actuator which uses cavity resonance principles combined with impinging microjet resonance to generate unsteady pressures inside of a cavity. These pressure fluctuations in turn cause an array of highly unsteady microjets to emanate from the bottom of the spreader section of the cavity[11,13] (see Fig. 2). These microjets have been shown[14] to be highly unsteady and by varying their geometry and the stagnation pressure of their source jet, they can be tuned across a very wide range of frequencies. These properties, along with their small size and low mass flow requirements, make them useful as high bandwidth, high mean momentum flow control devices.

By careful selection of several key parameters including cavity volume, source Nozzle Pressure Ratio (NPR_{mj}), and height of the source jet above the cavity opening normalized by the source nozzle diameter (h/d_{mj}), these actuators can be designed for frequencies ranging from 1-60 kHz.[14] Figure 2 is a schematic of one of the early designs of this type of actuator and Fig. 3 shows representative acoustic spectra of the response from such an actuator operating at h/d_{mj} = 1.7, and NPR_{mj} ranging from 4.7 to 5.5.[11] These pressure spectra show that for a constant distance between the source nozzle and the impingement cavity, simply varying the source jet pressure changes the frequency response of the actuator. This allows the actuator's frequency to be fine-tuned over a range of frequencies simply by adjusting the source jet pressure. Additionally, as Fig. 3 shows, increasing the source pressure

narrows the bands in which the peak frequencies occur, resulting in high-amplitude disturbances over a narrower frequency being produced from the actuator.

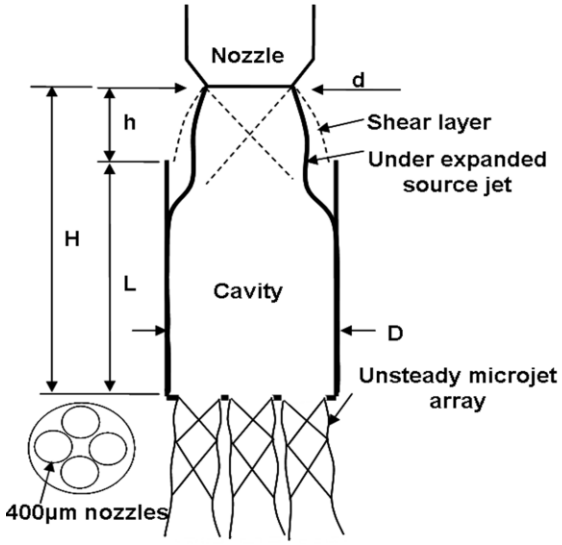

Figure 2. Schematic of REM actuator.[11]

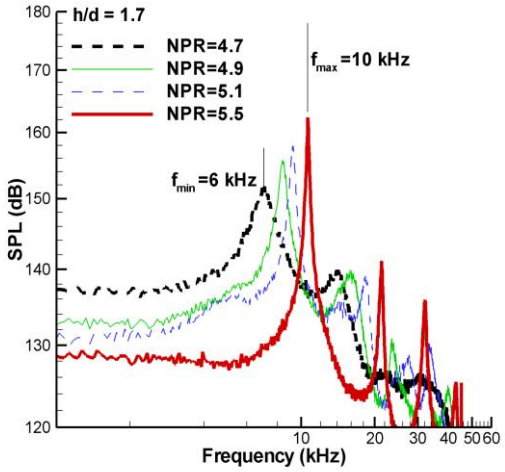

Figure 3. Sample spectra of REM actuator.[11]

A similar study[15,16] has been conducted in which four of these actuators were implemented around the nozzle of a supersonic impinging jet arranged as shown in Fig. 4a. This arrangement was selected due to the size and geometric requirements of the lift plate assembly in the STOVL facility, and similarity to the benchtop actuators which had been characterized at the time. The setup in Fig. 4a resulted in a decrease in Overall Sound Pressure Level (OASPL) of 3 - 4 dB, and elimination of the impingement tones generated, however new tones of similar amplitude appeared in the spectra that matched neither the tones of the impinging jet, nor the tones of the actuators integrated into the lift plate. Representative results from Solomon et al.[15] are shown in Fig. 4b.

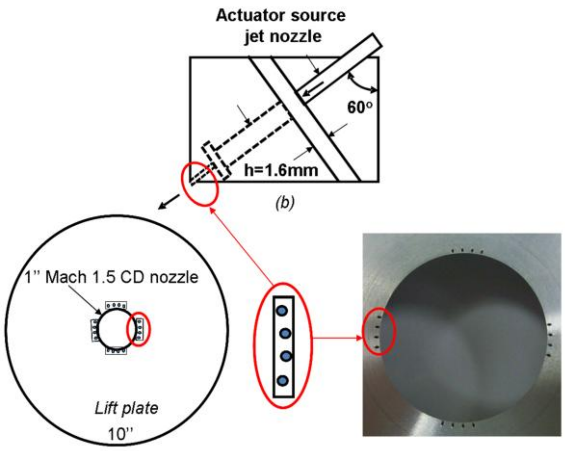

a) REM Actuator assembly

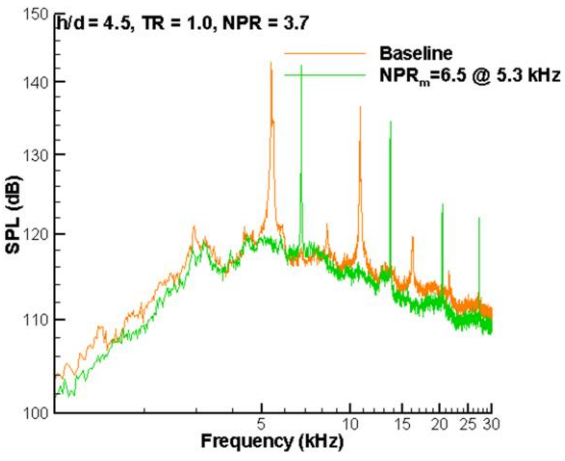

b) Effect of unsteady control with this assembly

Figure 4. Assembly details and spectra of the REM actuator modules used in Solomon et al.[15] The four actuators generated 16 pulsed microjets. These microjets were unevenly distributed along the periphery of the main jet. The spectra show the new tones present with unsteady actuation and uneven microjet distribution.

III. Description of Facility

The STOVL impinging jet facility at FSU uses a converging-diverging nozzle with throat diameter of one inch to produce a supersonic jet that then impinges on a ground plane. This ground plane can be raised and lowered so as to adjust the distance between the impingement surface and the nozzle exit. Around the main jet nozzle is a circular plate mounted flush with the exit plane designed to mimic the bottom surface of a STOVL aircraft. A simplified schematic of the STOVL setup is presented in Fig. 5. In both steady as well as unsteady microjet control schemes, microjet nozzles are positioned around the edge of the main jet nozzle so as to exhaust into the shear layer of the main jet immediately below the exit plane. A more detailed description of the STOVL facility can be found in Wiley[16] and a detailed description of sensors and signal conditioning used will be presented later.

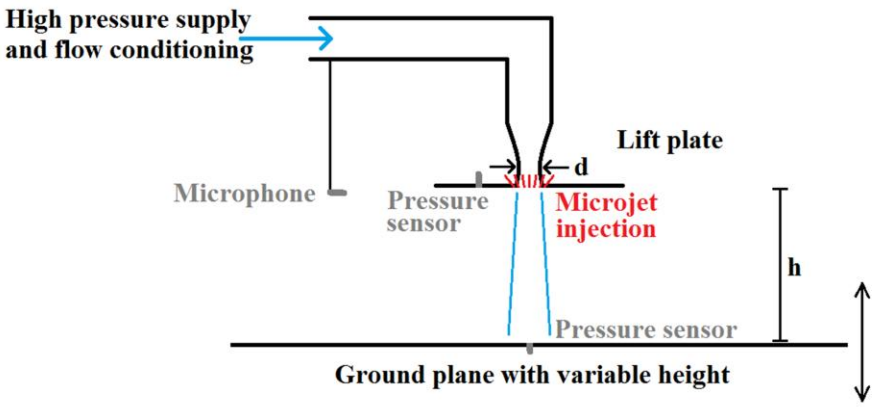

Figure 5. Schematic of the STOVL facility at the AAPL.

One of the concerns of the previous study was that the pulsed actuators only acted upon a small section of the jet periphery, which may have compromised the effectiveness of control. This design was originally chosen to more closely match the benchtop actuators being tested at the time, and served only as a first generation implementation to determine if the actuators would operate as predicted when implemented into the STOVL facility. The new design used in this study can only incorporate two microjets per actuator to keep the actuator frequency close to the main jet frequency based on frequency predictions made by Solomon.[17] This lengthens the actuator cavities significantly in order to place all sixteen microjets evenly around the nozzle as shown in Fig. 6. There have been several studies conducted using steady microjet control in which the microjets were evenly spaced, resulting in very significant reduction of unsteadiness, tones, and overall noise levels.[2,9,10] The design used in this study attempts to space the microjet nozzles evenly, as in the literature in an effort to make direct comparisons with past and current steady control results, and possibly increase the effectiveness of pulsed microjet control in the process.

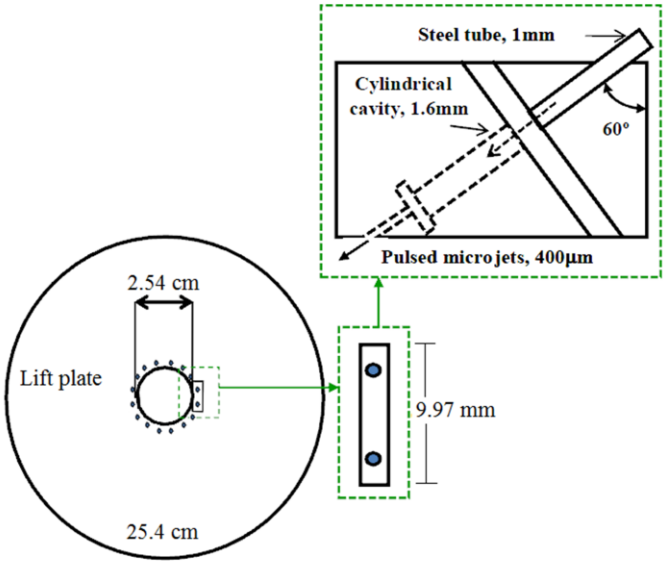

Figure 6. Schematic of new lift plate design with evenly spaced microjet actuators used in the current study.

IV. Benchtop Design and Characterization of REM Actuators

Before implementing these actuators into a STOVL/impinging jet configuration, benchtop testing was conducted to characterize the actuators' frequency response, as well as to determine the effects, if any, of multiple actuators operating in close proximity as is the case in many implementations. The distances between source jets and microjets used in benchtop tests were selected to be similar to those required in the STOVL implementation. Impingement of the source jet on the cavity opening results in resonance, producing strong tones as well as significant spillage in the form of an unsteady wall jet around the top of the actuator. Possible interactions between adjacent actuators as a result of these effects have been investigated through simultaneous unsteady pressure measurements in the cavities of adjacent actuators. The goal of this exercise was to determine if the wall jets produced during the periodic pulsing of the actuators affected the relative phase of adjacent actuators, or otherwise changed their behavior.

A. Design of the REM actuators

The design of the REM modules used in this study are based upon two factors: the geometry of the impinging jet setup in the AAPL facility, and the lumped element model (LEM) developed by Solomon.[17] The former sets the circumferential distance between the microjets, the actuator cavity locations, and various other size constraints, and the latter provides a range of expected output frequencies for a given actuator geometry. The design frequency of the REM modules was chosen to be on the same order as the primary tones produced by the impinging jet itself as in Solomon et al.[15] and Wiley[16], typically in the range of 5-8 kHz depending on the flow conditions selected. Based on these guides and the geometrical requirements of the STOVL facility, the benchtop model shown in Fig 7. was developed for characterization prior to its final implementation.

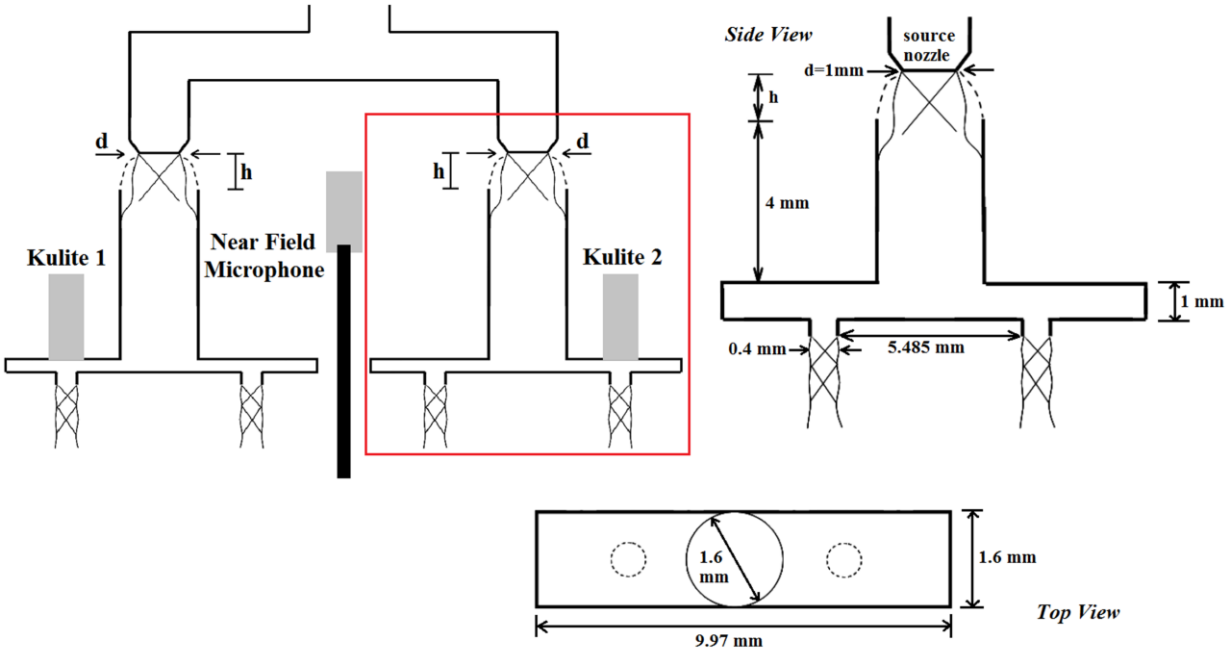

Figure 7. Schematic of REM actuators for benchtop testing. Two actuators were tested side by side from a split source nozzle. The dimensions of the two identical actuators are shown on the schematic on the right.

The actuator design shown in Fig. 7 was fabricated as a set consisting of two modules side-by-side for the purpose of benchtop characterization. The volume, distance between microjets, and distance between source jets was designed to mimic those required by the STOVL lift plate design, but otherwise the design was somewhat simplified to allow for optical access to the source jets as well as the microjets in a microschlieren setup. Details of the microschlieren setup used for benchtop flow visualization can be found in Foster.[18]

B. Benchtop characterization of REM actuators

This actuator was tested for a range of impingement height nondimensionalized by nozzle diameter, $(h/d)_{mj}$, and nozzle pressure ratio, NPR_{mj}, to determine the frequency response, and the optimal conditions producing strong,

distinct disturbances from the actuator in the desired frequency range. As these control knobs are adjusted, both the actuator's frequency response and the width of the resulting peaks in the frequency spectra change significantly. Figure 8 shows these changes with varying NPR_{mj}. The frequencies recorded by the cavity pressure transducers agreed very well, though only one is shown here, and closely matched those recorded by the external microphone, indicating that the oscillations at the peak frequencies were global in nature as well as common to both cavities operating simultaneously. This result was expected because the two actuators were designed to be as similar as possible and operated under as similar conditions as possible. The condition of $(h/d)_{mj}$ =1.5 and NPR_{mj}=7.6 was chosen as the optimal case for the benchtop model as it produced sufficiently strong, discrete disturbances in the form of pulsed microjets from the actuator for the lowest mass flow.

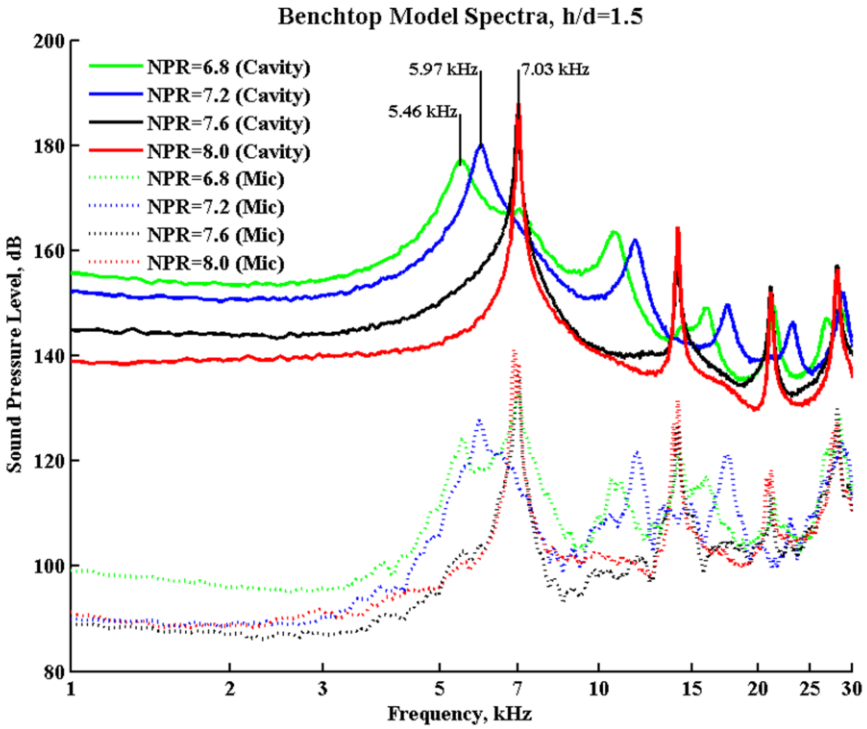

Figure 8. Benchtop actuator frequency response for a range of NPR_{mj}.

Additionally, the flowfields produced by these actuators were imaged using a microschlieren system with sufficient spatial and temporal resolution to resolve features of the source jet as well as the microjets.[18] Figures 9a and 9b are representative phase-locked, phase-averaged images of the actuators in operation. These images were phase-locked using the unsteady pressure signal from the Kulite in the right actuator and the camera trigger was then delayed by a fraction of the period to lock onto various phases. These images were all taken during the same continuous run, and then averaged to show the structure of the mean flow for a given phase. From these images, 180 degrees apart, it is clear that the microjets oscillate significantly, where their amplitude varies from nearly no flow to considerably underexpanded supersonic jets. The blurring of the flowfield through the left actuator, and the fact that the left actuator's mean flow structure is nearly unchanged between the two averaged images indicates that the left actuator's frequency is slightly different from that of the right cavity or that there is some phase wandering relative to the actuator on the right, thus causing the resulting flow images to be averaged across different phases. This is a good indication that the two actuators operating in close proximity do not influence each other's phase to a significant degree.

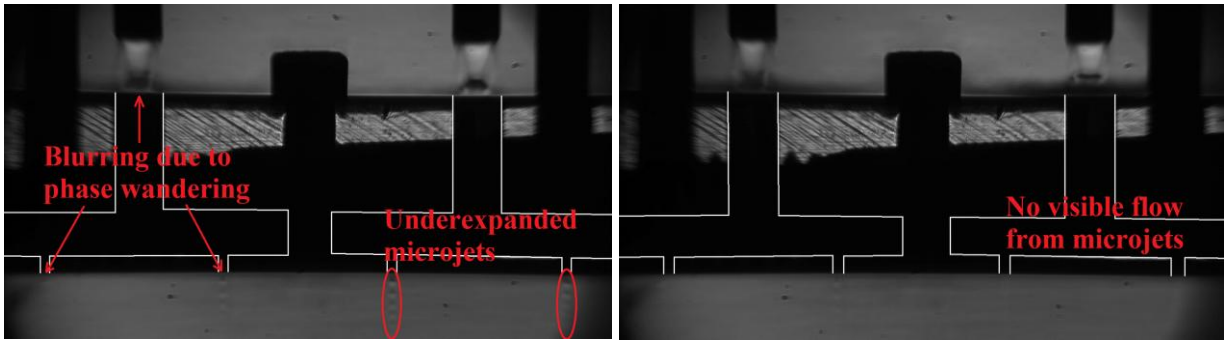

a) Phase-averaged image at 0 degrees b) Phase-averaged image at 180 degrees

Figure 9. Two phase-averaged images 180 degrees out of phase based on the periodic pressure signal from the right-most actuator. Actuator conditions were $(h/d)_{mi}$=1.5, and NPR_{mi}=7.4.

The results of the benchtop characterization of the microjet actuators show good agreement with the LEM prediction, and produce strong tones in the same frequency range as the STOVL impinging jet. Additionally, flow visualization of the actuators in operation show that there is no significant cross talk or phase forcing between adjacent actuators at these separations. Overall, the design shows good promise for implementation.

V. Design and Characterization of Lift Plate Incorporating REM Actuators

Based on the benchtop results, a lift plate was designed incorporating the REM actuators with sixteen micronozzles evenly spaced around the periphery of the main jet nozzle. The even separation between the microjets was designed to be similar to previous studies involving steady microjet control.[2,9,10] A schematic of the design used in this study can be found in Fig. 6. The main difference between the design used in this study and the one used in Solomon[15] is the microjet spacing, however the geometry of the actuators themselves is also different. In this study, eight actuators with two microjet nozzles each have been evenly spaced around the main jet exit plane so as to provide equal spacing between each of the sixteen microjet nozzles. In Solomon,[15] there were four actuators with four microjet nozzles each grouped unevenly over a fraction of the circumference of the main jet (as in Fig. 4a).

The lift plate incorporating the microactuators was first characterized without the main jet flow before being used for control of the STOVL main jet. This design incorporated an unsteady pressure sensor flush mounted inside one of the microjet cavities much like with the benchtop model in order to accurately record the behavior of the actuator while the microjets are operational. The spectra produced for the primary NPR_{mj} used in the characterization of the lift plate are shown in Fig. 10. The cases displayed in Fig. 10 were selected to show the broadband nature of actuation at NPR_{mj}=7.0 versus the discrete tones when NPR_{mj} is increased to 7.8 or higher. The frequencies produced by the actuators in the lift plate agree reasonably well with the benchtop results, producing pulsed microjets at similar frequencies with amplitudes just over 180 dB as measured inside the cavities. Based on these results, the primary control case of NPR_{mj}=7.8 was chosen for use in the STOVL tests as this results in strong, discrete tones of around 6.2 kHz, as shown in Fig. 10. Additionally, a broadband case of NPR_{mj}=7.0 was initially selected as well for STOVL testing. It may be noted that based on microphone measurements acquired during testing of the lift plate, not all of the eight actuators operate at exactly

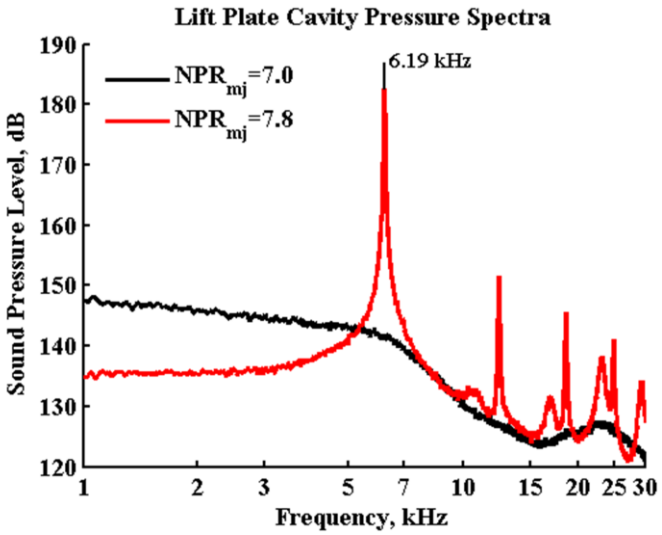

Figure 10. Lift plate REM actuator response for primary NPR_{mj} with no main jet flow.

the same frequency due to machining tolerances and possibly flow leaking around some of the cavities. In general, the actuators tended to still show frequency responses within 250 Hz of the one with the Kulite sensor.

Figure 11 shows the cavity Kulite spectra for the primary microjet pressures while the STOVL main jet is operational. These spectra show that there is a slight change in the actuators' behavior compared to the no flow characterization when the main jet is running. The peak retains the same amplitude, approximately the same frequency at 6.1 kHz, and narrow band behavior at high NPR_{mj}, however the NPR_{mj} required for tonal responses lowered slightly. As a result, the NPR_{mj} selected for broadband cases in STOVL testing was revised to 6.8. This result was likely due to air near the lift plate becoming entrained in the jet flow, effectively reducing the local ambient pressure near the exit of the source jets slightly. The design of the lift plate was such that the venting slots (see Fig. 6) were directed away from the jet as much as possible in an attempt to reduce the interaction with the main impinging jet flowfield.

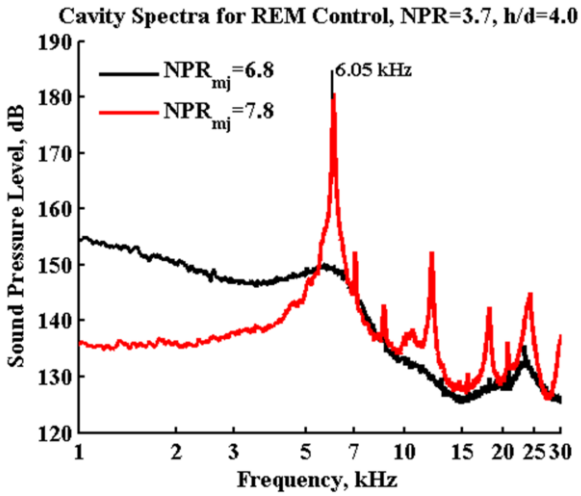

Figure 11. Lift plate actuator response for revised primary NPR_{mj} with the STOVL main jet in operation.

VI. Results of REM Control on STOVL Flowfield

A. Experimental setup for STOVL testing

In an effort to limit the parametric space of this study, all STOVL test cases were operated at the same Mach number and main jet *NPR*. The impinging jet was ideally expanded, corresponding to a nozzle stagnation pressure ratio to ambient pressure (*NPR*) of 3.7, and ratio of stagnation temperature to ambient temperature of 1.0 for a Mach 1.5 converging-diverging nozzle. The nondimensional impingement height (*h/d*) was varied from 3.5 to 8.0 with the height nondimensionalized by the throat diameter. A simplified schematic of the STOVL facility can be found in Fig. 5, and a schematic of the REM actuator lift plate can be found in Fig. 6. Additionally, a more detailed description of the facility can be found in Wiley.[16]

A B&K 4939 microphone coupled with a B&K 2670 preamp located 15 throat diameters from the centerline of the main jet in the nozzle exit plane was used to acquire acoustic data. Additionally, an XCS-052-5D Kulite unsteady pressure transducer with 5 psi range was flush mounted on the lift plate three diameters from the centerline of the main jet, and another Kulite sensor model XTEH-10L-190-100A with 100 psia range was flush mounted on the ground plane directly in the jet axis. A XCQ-062-100G Kulite pressure sensor with 100 psig range was used to measure the unsteady pressure inside the actuator cavity. The microphone signal was amplified and low pass filtered at 30 kHz with a B&K Nexus 2690 conditioning amplifier, and all Kulite signals were amplified with a Hendrick & Associates MX9000 transducer amplifier. For any given condition of *NPR*, *h/d* and control, all sensor signals were low pass filtered with a Stanford model SR640 low pass filter at 30 kHz and all sampled simultaneously at 70 kHz with a National Instruments PXI-6133 card. All data was processed in MatLab, and spectra were produced using the Welch method of FFT averaging over 100 data blocks using Hanning windows with 50% overlap.

Whenever used, steady microjet control was applied with a stagnation pressure of 100 psia, corresponding to steady microjet NPR_{mj}=6.8. Steady control was applied using a separate lift plate which did not incorporate resonance cavities. The steady control lift plate simply has sixteen 0.4 mm nozzles supplied by a single plenum discharging into the main jet shear layer. Pulsed control for tonal response was applied with a source jet stagnation pressure of 114 psia, corresponding to pulsed microjet NPR_{mj}=7.8. Based on the actuators' response while the main jet was operational as shown in Fig. 10, additional test cases with the pulsed microjet array operating in the broadband range were performed with microjet NPR_{mj}=6.8 as well. As will be discussed in the next section, this NPR_{mj} was chosen lower than was indicated by the benchtop results because the actuators exhibited tonal responses at slightly lower NPR_{mj} during main jet operation, requiring lower NPR_{mj} to still produce a broadband response. For this case of NPR_{mj}=6.8, the REM actuators do not exhibit a tonal response, yet the results still show a very significant reduction of noise levels.

B. Measurement Uncertainty

Stagnation pressure of the main jet was measured in the jet stagnation chamber upstream of the nozzle with an Omegadyne PX219-200A5V pressure transducer with an uncertainty of ± 3.4 kPa and the stagnation temperature of the main jet was measured with a K-Type thermocouple amplified with an Analog Devices AD595 monolithic thermocouple amplifier with a combined uncertainty of ± 1 °C. The total uncertainty of *NPR* and the temperature ratio are ± 0.05, and the uncertainty in *h/d* is ± 0.1. The XTEH-10L-100A ground plane Kulite and XCQ-062-100G cavity Kulite have uncertainties of ± 3.45 kPa, the B&K microphone uncertainty is ± 1 dB, and the lift plate Kulite has an uncertainty of ± 86 Pa. Pressure transducers were calibrated with a Druck DPI 605 calibrator with calibration uncertainties of ± 550 Pa for the ground plane and cavity Kulites and ± 28 Pa for the lift plate Kulite. The N.I. Data Acquisition card has an uncertainty of ± 28 Pa for the microphone, ± 210 Pa for the ground plane Kulite, and ± 8 Pa for the lift plate Kulite.

C. Baseline flow and effect of actuation for flow control

Pressure and acoustic spectra for no control, steady control, and pulsed control cases are shown in Fig. 12 for *h/d* of 4.0. Here, for pulsed control, the REM actuators were operated at NPR_{mj}=7.8 resulting in tonal, pulsed microjet injection. Steady microjet control was implemented using steady microjets with a supply NPR_{mj}=6.8. The primary impinging tone at 7.1 kHz and its harmonics are immediately visible in the no control case. Both steady control as well as REM control show significant reduction of the impinging tones. Tone reduction of 16 dB was achieved with steady control and 23 dB with pulsed control as measured from the ground plane sensor. This shows that both steady as well as pulsed microjet control are effective in disrupting the feedback mechanism of the impinging jet, thus almost eliminating the strong impingement tones associated with the system's resonance. Additionally, the broadband noise levels were reduced by 3-6 dB in both control cases. Comparison between the microphone and ground plane Kulite spectra show that most phenomena associated with this flowfield are felt globally, and the microjet control methods reduce both tones as well as broadband noise globally.

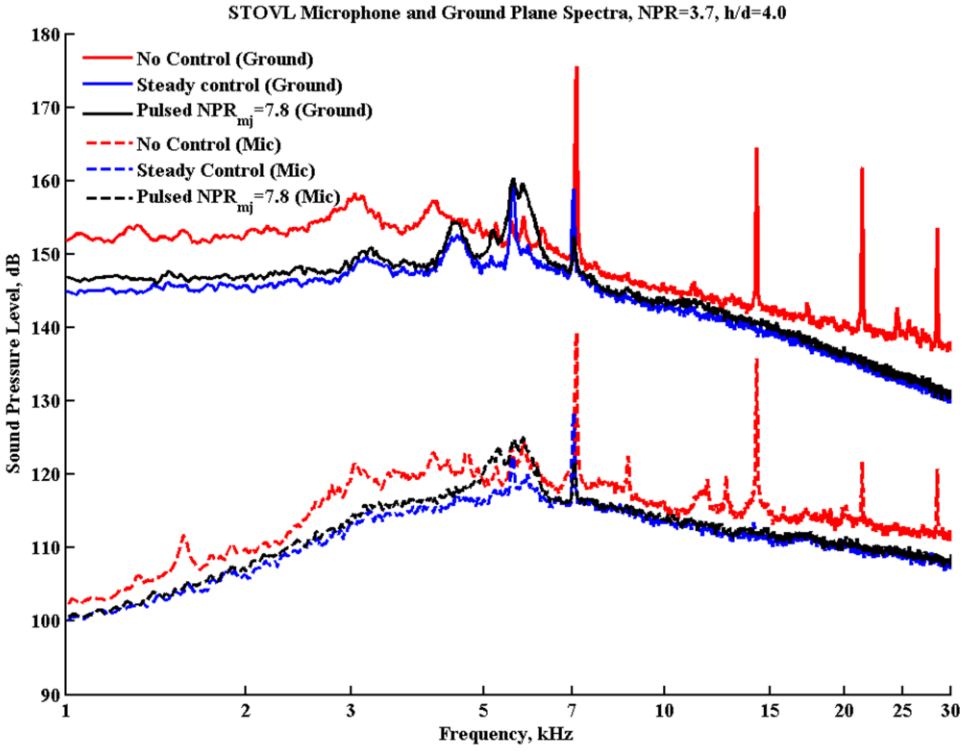

Figure 12. STOVL microphone and centerline ground plane pressure spectra for no control, steady microjet control, and pulsed microjet control at NPR_{mj}=7.8.

Figure 13 plots the actuator Kulite spectra and microphone spectra for *h/d*=4.0 while the main jet was operational. In the no control case, the cavity Kulite clearly picked up the main jet frequency as shown in the simultaneous microphone spectrum. When the actuator was operational at NPR_{mj}=7.8, the cavity Kulite as well as the microphone still show a response at the flow frequency indicating that there is some crosstalk between the main flow and the cavity Kulite even when the actuator is operational. The microphone, however, did not show a single distinct peak at the actuator's frequency when the actuator was operational, only a small, wider peak spanning a range of frequencies from the actuator's tone to just above 5 kHz. This hump is likely the acoustic radiation produced by the actuators. The broadness of this peak is due to the fact that the eight REM actuators in the lift plate operate at somewhat different frequencies ranging over a band of about 500 Hz. While not large, this hump does influence the OASPL negatively because it is the highest amplitude peak in the microphone spectrum once control is activated. Relative to the impinging tones the actuator is designed to reduce, the actuator noise is quite small, and while it is detected by the microphone, it is far below the main jet noise levels at the ground plane Kulite (not shown). This indicates that while the actuator and main jet are operational, the acoustic radiation produced by the REM actuator is not sufficiently strong to be felt throughout the entire flowfield over the broadband noise of the main jet.

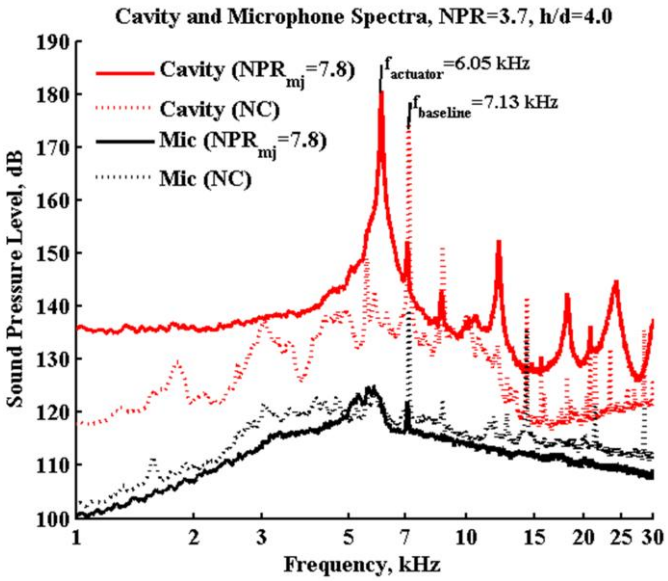

Figure 13. Simultaneous cavity Kulite and microphone spectra without control and for and NPR_{mj}=7.8 cases at *h/d*=4.0, *NPR*=3.7.

Interestingly, when the REM actuators were operated at lower NPR_{mj}, they showed even further reduction in both tonal as well as overall noise level reduction. For NPR_{mj}=6.8, the actuators operate in a broadband range producing no distinct tones (see Fig. 11), yet when this case was compared to the tonal case of NPR_{mj}=7.8 as shown in Fig. 14, the impinging tone was reduced 3 dB further and the broadband noise was reduced further as well. In both cases, all of the primary tone's harmonics were completely eliminated.

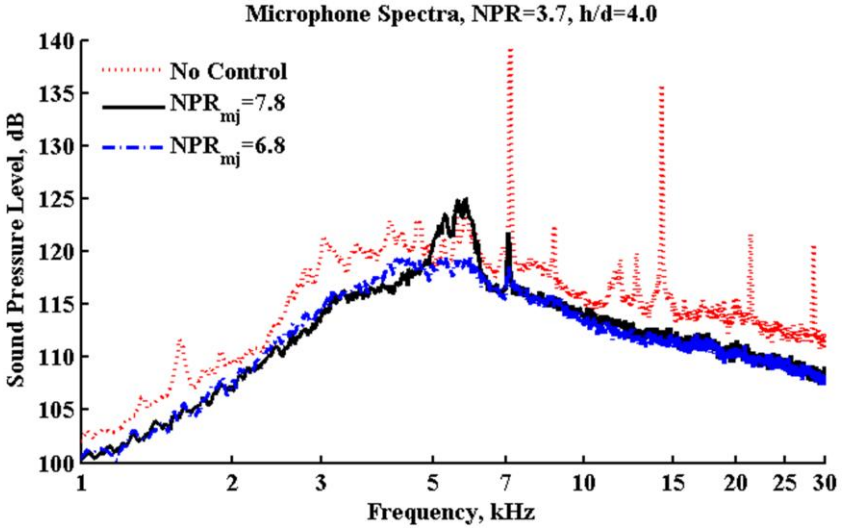

Figure 14. STOVL microphone spectra for no control, NPR_{mj}=6.8, and NPR_{mj}=7.8.

This increase in effectiveness with sub-tonal actuation is likely caused by an interaction with the intermittant way the actuators are operating in this range. For NPR_{mj} below what is required for the actuators to produce distinct tones, the actuators are switching between essentially steady jet production and the pulsing seen at higher NPR_{mj}, at random intervals. Time series plots of the cavity pressure while the actuator is operating for three different NPR_{mj} are shown in Fig. 15. Figure 15a shows the actuator pressure as a function of time for NPR_{mj}=6.4, Fig. 15b shows the cavity pressure for NPR_{mj}=6.8, and Fig. 15c shows the cavity pressure for NPR_{mj}=7.8. Figure 15c exhibits the sinusoidal pressure fluctuations characteristic of the tonal case, which is as expected. However, in Fig. 15a and 15b, there is a relatively steady pressure level that is maintained for a majority of the time the actuator is in operation, interrupted by occasional sharp drops in pressure, likely accompanied by strong pulses in the resulting microjets. When operated in this range of NPR_{mj} the microjets emit loud, audible "crackling sounds" with no clear associated tone. As the supply pressure is increased, bringing NPR_{mj} closer to the tonal range, these "crackles" become more frequent until they merge together into a distinct tone at the actuator's resonant frequency. A possible explanation for the increased effectiveness of sub-tonal actuation is suggested by the mean pressure at different NPR_{mj}. At lower supply pressure, the mean pressure in the cavity is actually higher than when the actuator is tonal, likely resulting in more mean momentum being ejected from the cavity through the microjet nozzles. This increase in momentum flux could be responsible for the increased effectiveness of control.

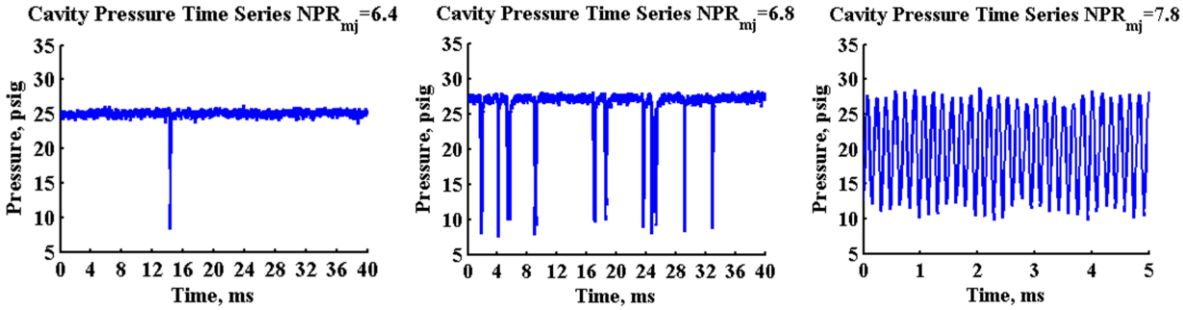

a) Very infrequent fluctuations b) Fluctuations more frequent c) Fully tonal sinusoidal response

Figure 15. Time series plots of the cavity pressure for different NPR_{mj} showing the transition from nearly steady microjet flow to fully periodic pulsed flow.

Plots of the overall sound pressure levels for the full range of *h/d* tested from 3.5 to 8.0 are shown in Fig. 16. As *h/d* increases towards 8.0, the system begins to behave more like a free jet, and the feedback mechanism ceases to dominate the flowfield, thus reducing the effectiveness of both steady as well as pulsed microjet injection. Figure 16a shows that, as measured from the ground plane centerline, steady and low NPR_{mj} control reduce OASPL by about 2 dB more than high NPR_{mj} over almost the entire range of *h/d*, however the microphone measurements in Fig. 16b show relative control effectiveness that is more dependent on *h/d*. Generally, steady control is slightly more effective in reducing OASPL than high NPR_{mj}, and low NPR_{mj} seems to be slightly more effective still.

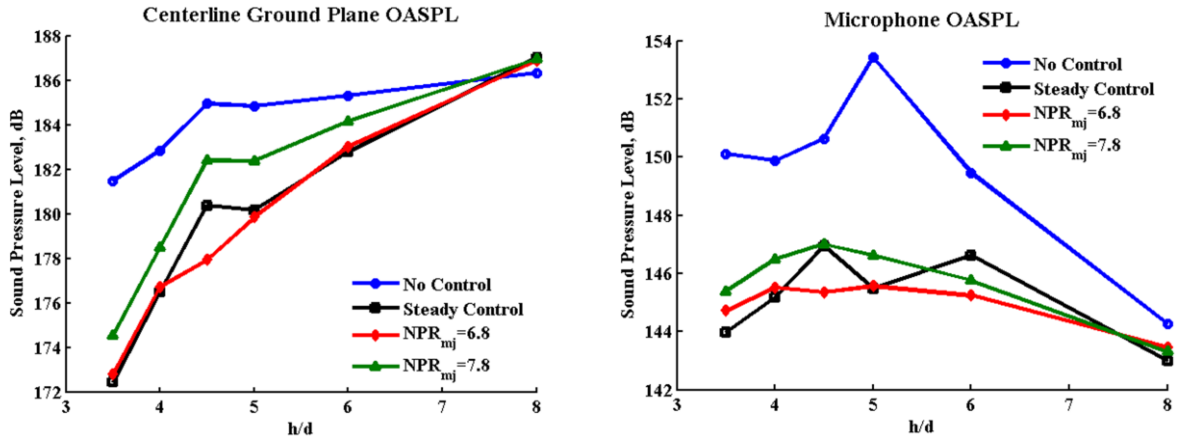

a) Ground plane Kulite OASPL b) Microphone OASPL

Figure 16. Overall sound pressure levels for no control, steady microjet control, and pulsed microjet control with NPR_{mj}=6.8, and NPR_{mj}=7.8 at *h/d*=4.0, *NPR*=3.7.

Figure 17 shows the general trend in OASPL at h/d=4.0 with changing NPR_{mj}. Lower source pressures, to the point where the REM actuators are producing only broadband noise, seem to result in slightly larger reductions of OASPL. It is possible that this is due to an increase in mean momentum being introduced into the main jet flow for lower NPR_{mj}, in the broadband, non-tonal range as seen in Fig. 15. For these cases, the mean cavity pressure is actually higher than that of the tonal cases because the pressure is not pulsing as often. When the actuators are pulsing with a distinct frequency, based on benchtop flow visualization, they are alternating between highly underexpanded and nearly no flow, while when they are producing only broadband noise, they are likely behaving more similarly to steady jets with only moderate, relatively infrequent unsteadiness. This reduces the periods of no flow, but the jets remain choked or nearly choked for a larger percentage of the cycle resulting in a mean increase in mass flow. Literature[12] suggests that for steady jets, effective control can be achieved even with relatively low supply pressures such as the mean pressures present in these microjet cavities at low NPR_{mj}. It is also interesting to note that as shown in Fig. 17, the centerline ground plane Kulite shows generally better OASPL reduction as compared to the baseline for all cases except the low tonal or transitional stages of actuation. This may indicate that periodic actuation near the flow frequency is more effective at reducing jet instability than wider band actuation at slightly higher mean flow rates, however further increasing the mean flow by further reducing NPR_{mj} more than offsets the loss of tonal actuation as seen by the increased effectiveness at sub-tonal NPR_{mj}.

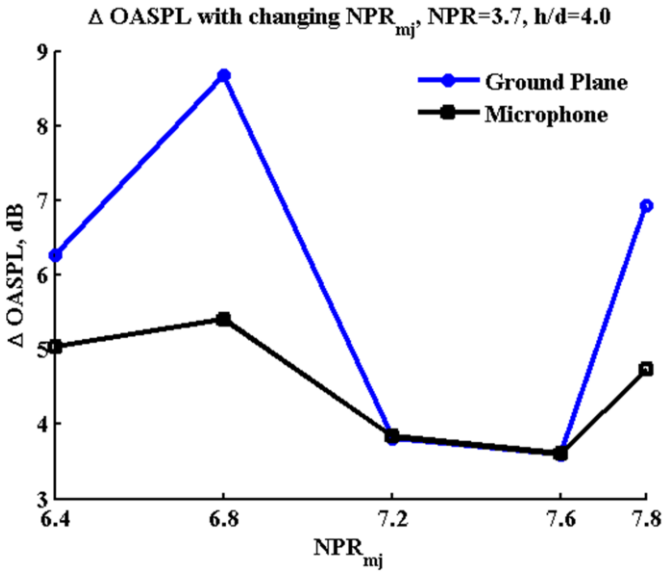

Figure 17. OASPL for microphone and ground plane Kulites, as well as the OASPL inside of the actuator cavity with changing NPR_{mi}.

Figure 18 compares current data from this study using evenly spaced microjets with data from Wiley[16] using unevenly spaced microjets. All of the cases shown were at h/d=4.0, NPR=3.7. Only one case is plotted for steady, evenly spaced microjets because for steady control, supply pressure corresponding to NPR_{mj}=6.8 was the only case tested. This plot clearly indicates that the performance of both steady as well as unsteady microjet control is greatly reduced when the microjets are spaced as shown in Fig. 4a. Also apparent in this plot is the fact that evenly spaced pulsed microjet control is capable, if the correct NPR_{mj} is selected for a given h/d, of even surpassing the results of steady control showing maximum OASPL reduction with REM control of 8-9 dB.

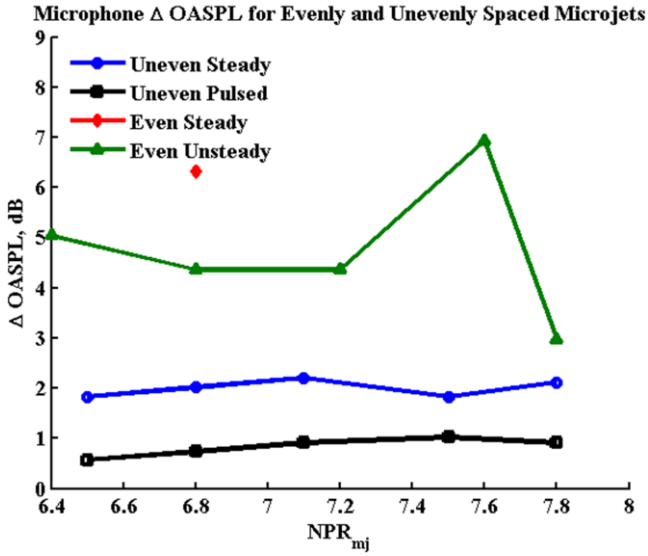

Figure 18. OASPL change for varied NPR_{mj} at h/d=4.0 versus baseline OASPL for evenly and unevenly[16] spaced microjets.

In addition to pressure and acoustic measurements, shadowgraph was also performed on the STOVL impinging jet. Figure 19a is a shadowgraph image of the main jet with NPR=3.7 and h/d=4.0 with no control. The large scale vortical structures are clearly visible propagating

downstream in the jet shear layer. Powerful acoustic waves are also visible being produced by these structures impinging on the ground plane as well as being reflected off of the lift plate. Figure 19b is an image under the same main jet conditions, but with control NPR_{mj}=7.8. In this image, the streaks visible in the main jet shear layer are caused by streamwise vorticity generated by the microjet injection which results in thickening of the shear layer and disruption of the feedback loop responsible for the jet instability.[4] Visually, this result is nearly indistinguishable from NPR_{mj}=6.8 REM control and steady control (not shown). These shadowgraph images further reinforce the conclusions drawn from the pressure and acoustic data, and very closely match shadowgraph images from the literature.[9]

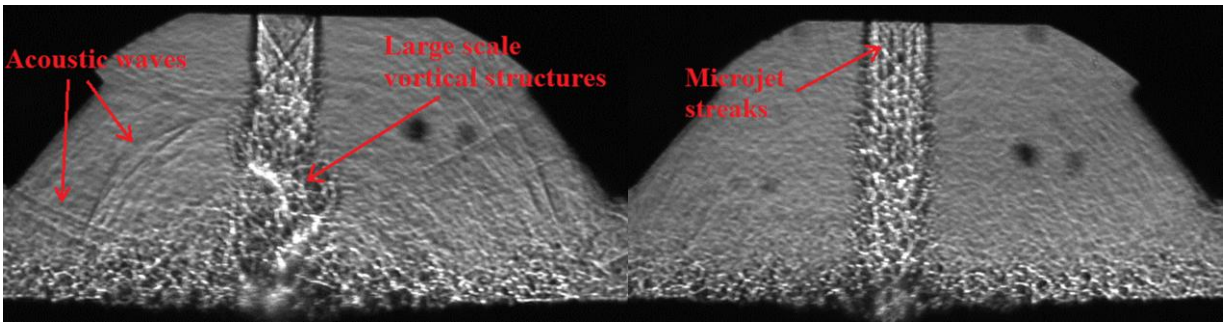

a) No control b) Control NPR_{mj}=7.8

Figure 19. Shadowgraph results for *NPR*=3.7, *h/d*=4.0 with and without REM control.

VII. Conclusion

Current research at the AAPL has shown that pulsed microjets can be effectively implemented as a control scheme for supersonic impinging jets and result in comparable or in some cases even better control than steady microjets. Benchtop results indicated that adjacent actuators at separation distances required for applications such as the one used in this study have little or no mutual interaction, shifting neither each other's phase nor their frequencies. Benchtop characterization also showed good agreement with characterization of the actuators after implementation indicating that REM actuators are robust enough to retain their characteristic pulsing behavior in less than ideal configurations. Furthermore, with the main jet flow in operation, the microjet actuators seemed to require slightly less supply pressure to achieve similar results to the no flow case, likely due to local reduction in ambient pressure.

When applied to the STOVL impinging jet flowfield, REM control is capable of up to 23 dB reduction in impinging tones when operated with high enough source pressure to produce distinct tones, and up to 26 dB reduction of impinging tones when operated with lower pressures producing only broadband noise spectra. Additionally, OASPL was reduced by 4 to 7 dB for tonal jets and up to 8 dB for non-tonal REM jets. These results indicate that these pulsed microjet actuators are generally slightly more effective for control when their cavity pressure oscillations are not periodic with distinct tones than when their pressure fluctuations are at distinct frequencies. This result is beneficial from an efficiency standpoint, as source pressure and mass flow requirements of these actuators serve as the effective "costs" of their operation, and improved control for lower supply pressures result in more efficient control. Shadowgraph results indicate that overall jet unsteadiness was reduced significantly by the REM control as well. In general, the data indicates that REM control is slightly more effective for reducing the impinging tones produced in the STOVL facility than steady jets, while showing comparable reduction in OASPL on the order of 5-8 dB.

This second generation implementation of REM actuators for control of the STOVL impinging jet flowfield shows greatly improved results over the first attempt with the redesigning of the STOVL lift plate to accommodate an evenly spaced microjet array. With the redistribution of the micronozzles, the secondary tones produced by the first generation implementation have been eliminated, and overall control has been significantly improved. This indicates that microjet separation is crucial to their effectiveness.

Further study is needed to optimize the REM control to maximize its effectiveness as well as to minimize the mass flow requirements. Continued research is also required to find what minimum supply pressures result in effective control with REM actuators as even the lowest pressures tested in this study showed significant results. Additionally, phase-based control should now be investigated in an effort to further optimize this already effective

control method. Having proven effective for controlling impinging jets, pulsed microjet control could also be further applied to other resonance-dominated flowfields requiring similar control methods. Due to the wide range of frequencies for which REM actuators can be designed, they have the potential to be adapted to a large variety of flows exhibiting a range of resonant frequencies.

Acknowledgements

This work was supported by the Florida Center for Advanced Aero-Propulsion (FCAAP) and the Air Force Office of Scientific Research (AFOSR). The authors would also like to thank Robert Avant and Adam Piotrowski, the machinists at the Advanced Aero Propulsion Lab (AAPL) at Florida State University (FSU). We also appreciate the help of Robby Freeborn-Scott and Phillip Kreth for their help in obtaining some of the data used in this study.

References

[1]Cattafesta, L. N., and Sheplak, M., "Actuators for Active Flow Control." *Annu. Rev. Fluid Mech.* 2011, 43:247-72

[2]Lou, H., Alvi, F. S., and Shih, C., "Active and Passive Control of Supersonic Impinging Jets," *AIAA Journal* Vol. 44, No. 1, January 2006.

[3]Powell, A., "The Sound-Producing Oscillations of Round Underexpanded Jets Impinging on Normal Plates." *Journal of the Acoustical Society of America,* Vol. 83, No. 2, February 1988.

[4]Krothapalli, A., Rajkuperan, E., Alvi, F., and Lourenco, L., "Flow Field and Noise Characteristics of a Supersonic Impinging Jet." *Journal of Fluid Mechanics*, Vol. 392, March 1999, pp. 155-181.

[5]Kweon, Y.-H., Miyazato, Y., Aoki, T., Kim, H.-D., and Setoguchi, T., "Control of Supersonic Jet Noise Using a Wire Device." *Journal of Sound and Vibration*, Vol. 297, 2006, pp. 167-182.

[6]Wiley, A., Kumar, and R., Alvi, F., "Noise and Flowfield Characteristics of a Supersonic Jet Impinging on a Porous Surface." AIAA Paper 2010-273.

[7]Samimy, M., Kim, J.-H., Kastner, J., Adamovich, I., and Utkin, Y., "Active Control of High-Speed and High-Reynolds-Number Jets Using Plasma Actuators." *Journal of Fluid Mechanics*, Vol. 578, 2007, pp. 305-330.

[8]Samimy, M., Kastner, J., and Debiasi, M., "Control of High-Speed Impinging Jets using Hartmann Tube Fluidic Actuators." AIAA Paper 2002-2822.

[9]Alvi, F. S., Shih, C., Elavarasan, R., Garg, G., and Krothapalli, A., "Control of Supersonic Impinging Jet Flows Using Supersonic Microjets," *AIAA Journal* Vol. 41, No. 7, July 2003.

[10]Alvi, F. S., Lou, H., Shih, C., and Kumar, R., "Experimental study of physical mechanisms in the control of supersonic impinging jets using microjets," *Journal of Fluid Mechanics*, Vol. 613, June 2008, pp. 55-83.

[11]Solomon, J. T., Kumar, R., and Alvi, F. S., "High Bandwidth Pulsed Microactuators for High-Speed Flow Control" *AIAA Journal*, Vol. 48, No. 10, October 2010.

[12]Ali, M. Y., Solomon, J. T., Gustavsson, J., Kumar, R., Alvi, F. S., "Control of Resonant Flow Inside a Supersonic Cavity Using High Bandwidth Pulsed Micro-actuators." AIAA Paper 2010-1198.

[13]Solomon, J. T., "High Bandwidth Unsteady Microactuators for Active Control of High Speed Flows," PhD Dissertation, Dept. of Mechanical Engineering, Florida State University, Tallahassee, FL, 2010.

[14]Solomon, J. T., Kumar, R., and Alvi, F. S., "High Bandwidth Micro-Actuators for Active Flow Control" AIAA Paper 2008-3042.

[15]Solomon, J. T., Hong, S., Wiley, A., Kumar, R., Annaswamy, A. M., and Alvi, F. S., "Control of Supersonic Resonant Flows Using High Bandwidth Micro-actuators," AIAA Paper 2009-3247.

[16]Wiley, A., "Effects of Unsteady Actuation on Resonance-Dominated Impinging Jets," Masters Thesis, Dept. of Mechanical Engineering, Florida State University, Tallahassee, FL, 2010.

[17]Solomon, J. T., Alvi, F. S., Kumar, and R., Gustavsson, J., "Principles of a High-Bandwidth Microactuator Producing Supersonic Pulsed Microjets," AIAA Paper 2010-1096.

[18]Foster, C. H., Solomon, J. T., and Alvi, F. S., "Visual Study of Resonance Dominated Microjet Flows Using Laser-Based Micro-Schlieren," AIAA Paper 2011-766.

15th AIAA/CEAS Aeroacoustics Conference (30th AIAA Aeroacoustics Conference)
11 - 13 May 2009, Miami, Florida

AIAA 2009-3247

Control of Supersonic Resonant Flows Using High Bandwidth Micro-actuators

J.T. Solomon[$1], S. Hong[#2], A. Wiley[$3], R. Kumar[$4], A. M. Annaswamy[#5] and F. S. Alvi[$6]

Florida Center for Advanced Aero-Propulsion (FCAAP)
Department of Mechanical Engineering
[$]Florida A & M University and Florida State University, Tallahassee, FL 32310
[#]Massachusetts Institute of Technology, Cambridge, MA 02139

Practical application of active flow control of high speed flows is dependent upon the development of simple and robust actuators that can produce high momentum and are reliable, low cost, and responsive and can be easily integrated. This paper presents an experimental investigation of the characterization and implementation of high bandwidth micro-actuators for the control of supersonic resonant flows. The striking feature of this micro-actuator is its high momentum mean flow along with high amplitude and a tunable frequency unsteady component. First generation micro-actuators are designed and their performance is tested in controlling the highly unsteady impinging jet flow field. The results show that the impinging tones are completely eliminated with the actuation of these micro-actuators, whereas, new peaks at a frequency different from the actuation frequency and its harmonics are observed in the spectra, the occurrence of which need to be further explored. A reduction of 3-4 dB in overall sound pressure levels (OASPL) is achieved over the range of test conditions.

I. Introduction

Active Control of shear and boundary layer flows have seen much attention by many researchers in recent years due to the potentially substantial benefits derived out of such control schemes. Unresolved flow control challenges persist in the diverging domain of aerodynamic applications that demand innovative strategies for more efficient operation of many high speed aerodynamic systems. The subsonic applications range from controlling flow separation and transition over various external aircraft components (including MAVs) to active control of flow over turbine and compressor blades/airfoils and active management of separation/flow distortion in engine inlets and S-ducts. In high-speed flows, control of flow oscillations in cavity flows, supersonic impinging jets and jet noise control are areas where various active control methods may lead to dramatic gains in performance. Effective control of flow and noise requires the use of efficient and robust actuators, which can be adapted for specific applications. Although various types of actuators have and are being explored, most designs have shown some limitations; either in terms of performance and range of operation in the lab or in the total 'cost' of performance – accounting for added weight and complexity, for eventual full-scale implementation. There is a clear need for actuators that produce *high-amplitude disturbances, over a broad range of frequencies.* Furthermore, the output of an ideal actuator should be 'tunable', both in terms of amplitude and frequency over a large dynamic range. Such actuators would

[1]Graduate Research Assistant, Student Member AIAA
[2]Graduate Research Assistant, Student Member AIAA
[3]Graduate Research Assistant, Student Member AIAA
[4]Research Scientist, Department of Mechanical Engineering, Member AIAA
[5]Senior Research Scientist, Department of Mechanical Engineering, Member AIAA
[6]Professor, Department of Mechanical Engineering, Associate Fellow AIAA

then be useful for subsonic and supersonic flow control applications where their properties can be adapted according to the specific applications and flight/operational regimes.

It is well known that cavity flows, such as those occurring in open cargo, landing gear and weapon bays, are governed by a flow-acoustic resonance. The turbulent structures in the shear layer grow as they propagate downstream towards the trailing edge. Upon impingement on the cavity trailing edge these structures generate very strong acoustic waves which propagate upstream – inside the cavity only for supersonic free stream and inside as well as outside for subsonic cases, and perturb the shear layer at the leading edge, thus completing the feedback which leads to resonance. At AAPL (Advanced Aero-propulsion Laboratories), we have been studying supersonic cavity flows both from a fundamental perspective and for developing means for controlling its undesirable aeroacoustic properties (Zhuang et al.[1]). Our prior studies have clearly established the dramatic effect of using *steady* microjet based actuation in reducing the flow unsteadiness and cavity noise in supersonic cavity flows (Zhuang et al.[1] and Zhuang[2]). It is anticipated that the effectiveness of microjet-based control will be significantly enhanced, producing greater reductions in flow unsteadiness and accompanying adverse effects, when *high amplitude pulsed actuator* designs are implemented in this test bed.

Another example, the impinging jet flow field, such as that occurring in STOVL aircraft during hover, is governed by a feedback-resonance phenomenon very similar in nature to that governing cavity flows. The instability waves in the jet that originate at the nozzle exit grow as they propagate downstream towards the impingement surface, and the acoustic waves that are produced upon impingement travel upstream and excite the nascent shear layer near the nozzle exit. The supersonic impinging jet, is another flow for which we have very extensive results both for the baseline, uncontrolled flow and with *steady* microjet control (Alvi et al.[3], Lou et al[4] and Kumar et al[5].). This configuration will also serve as the test bed for evaluating the unsteady micro-actuators that are designed and implemented for this study. Our hope is that the these high bandwidth actuators will more efficiently disrupt the feed back loop considered to be responsible for the highly unsteady flow field and the accompanying high levels of noise in impinging jet flows.

Flow control schemes are generally classified into active and passive methods based on the involvement of external energy in the activation process. Passive methods do not require external energy but make use of the energy associated with the primary flow for the purpose of control. Variations in nozzle geometry (rectangular, triangular, elliptic etc.), use of mechanical tabs of different shapes and the use of splitter plates are examples of various passive control methods adopted for the control of jet noise. On the other hand, in active flow control schemes, an external energy source is used for tailoring the natural instability behavior of a shear or a boundary layer flow according to the control objectives. The ability to efficiently adapt to changing flow conditions – the ultimate goal of active control schemes, makes them more attractive to passive methods.

Mechanical systems such as vibrating ribbons and cantilevered beams, electromechanical devices such as piezoelectric diaphragms, voice coils (speakers), etc. are used as external energy sources in various active flow control schemes. The vibration of a piezo material is used for generating low momentum air jet with zero net mass flux for the control of cavity flows (Cattafesta et al.[6]) and shear flows (Wiltse & Glezer[7]). Actuators based on synthetic jet have also been used for separation control over airfoils and cylinders (Amitay et al.[8]). Modified Hartmann tube has also been used as actuators by few researchers[9-11] with limited success. Although relatively successful at low speeds, many actuators are not very efficient when the primary flow velocities are high. Optimal manipulation of shear or boundary layer of high speed flows requires aero acoustic disturbances with high momentum or energy, whose steady and unsteady components can be manipulated. A simple and robust actuator, with high momentum and amplitude that can be easily integrated to practical high speed flow system is crucial for any active flow control schemes. The present studies are motivated and driven by this goal.

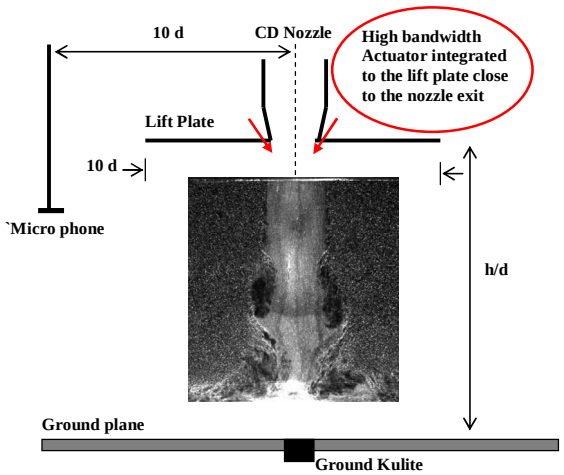

Figure 1 Schematic of the STOVL facility

II. Experimental Details

(a) Hardware and Model

The experiments were conducted in the Short Takeoff and Vertical Landing (STOVL) Facility, at the Advanced Aero Propulsion Laboratory (AAPL) of Florida State University.

A schematic of the experimental facility is shown in figure 1. The impinging flow field being controlled is generated by an ideally expanded jet issuing from a Mach 1.5 CD nozzle. Using an inline heater upstream of the plenum chamber, a temperature ratio of TR=1.0 (where TR = Stagnation temperature / Ambient temperature) was maintained for all cases tested. Simulation of the STOVL flow field at various operating conditions is generated by the automated movement of the impinging surface, a ground plane controlled by a hydraulic lift. The ground plate was equipped with a flush-mounted 100psia Kulite® transducer (Model XCE-062-100A) at centerline of the impinging jet (r/d = 0, where r is the radial distance from the centerline of the jet and d is the jet diameter at the throat of the nozzle).

A circular plate, referred to as the lift plate, with a diameter of the 10d was flush mounted with the nozzle exit plane to simulate the undersurface of an aircraft. The high-frequency, pulsed microjet actuators have been integrated in the lift plate. Figure 2 shows the actuator modules integrated in the lift plate where the exit of the microjets is flush with the main nozzle exit. Also seen in the picture is the radial slot in which a second Kulite® transducer (XCS-062-5D) is flush-mounted at r/d=2 to measure the unsteady pressure loads on the lift plate. To capture near field acoustics, a microphone was mounted at a radial distance 10d from the nozzle centerline, in the plane of the nozzle exit and lift plate. Additional details regarding model and facility can be found in Kumar et al.[5]

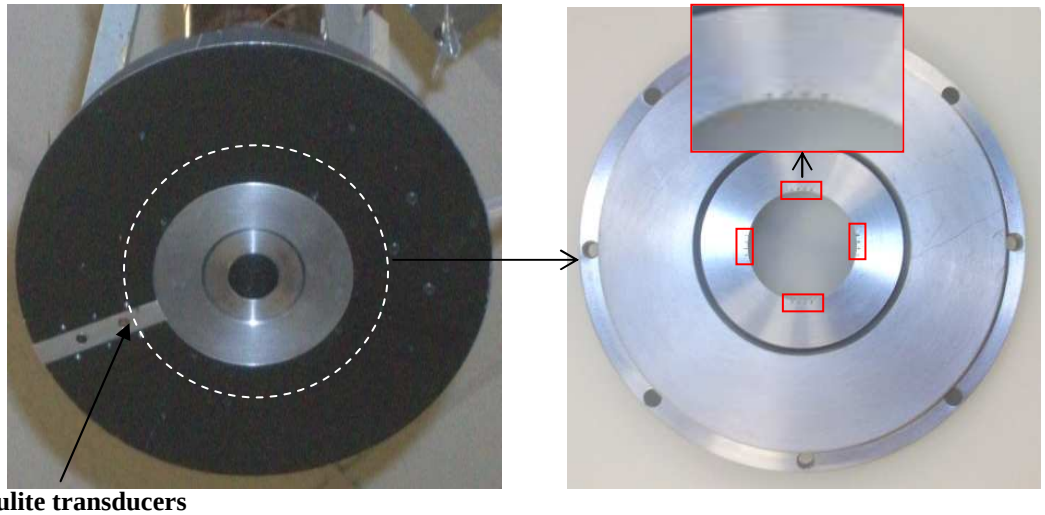

(a) Actuators integrated to lift plate (b) 4 actuator modules placed near nozzle exit

Figure 2 High bandwidth actuator modules integrated to the lift plate

The unsteady data from the Kulite sensors and the microphone were recorded using a National Instruments data acquisition card (PCI-6281) and LabVIEW® software. Data from each sensor was simultaneously recorded at a rate of 70 k samples/sec and low-pass filtered at 30 kHz. These datasets were post-processed using standard FFT-based statistical analytical schemes.

(b) Experimental Procedure

To confirm repeatability and to characterize the noise generated by the pulsed micro-actuators alone, acoustic measurements were obtained before each experiment using the near field microphone located at r/d=10. While keeping the main jet off, i.e. no flow, the actuator was operated at various conditions anticipated during the main jet on tests. The supply pressure to the actuator is varied from 85-120psig in 5psig intervals to cover the range of interest. Thereafter, the experiment flow is turned on for the impinging jet to bring it to Mach 1.5, ideally expanded conditions. Once the main flow conditions are established (NPR = 3.7, TR = 1.0 and a desired h/d), measurements were taken first without control. This data set was processed online to find the impinging tone of the base flow. Using the actuator characterization data (discussed in § III), the supply pressure to the pulsed actuator was adjusted to best match the actuator output frequency to that of the impinging tone. In addition, tests were also conducted with the actuator operating at a number of other pressures, above and below the optimal 'design' pressure.

Once the pressure sweep was complete, measurements were made once more without control to verify that conditions had not changed while the control was active. Finally, with the main jet off, near field acoustics of the actuator were again recorded not only at pre-run supply pressures, but also at the supply pressures actually used during the experiment. With this procedure one has the main jet's unsteady spectral properties (with and without actuator control), the actuator's output in-situ as well as a confirmation of repeatability.

III. Micro Actuator Design

(a) Summary of actuator design and performance

As discussed earlier, an actuator with high amplitude disturbance and whose frequency can be easily tuned over a large bandwidth is essential for optimal active and adaptive control of various high speed flow fields characterized by large unsteadiness. To realize this goal, we have designed and developed an actuator system that can produce *pulsed supersonic microjets* at any desired range of frequencies. This micro actuator produces high amplitude response by using a very simple geometric configuration that leverages the natural resonance behavior of various components of this micro-fluidic actuator system. The details of the 'early generations' of this micro actuator, including its performance and dependence upon the various geometric and flow parameters has been described in Solomon et al.[12, 13] Only a brief description, in the context of designing an actuator for the impinging jet flow field, is discussed here.

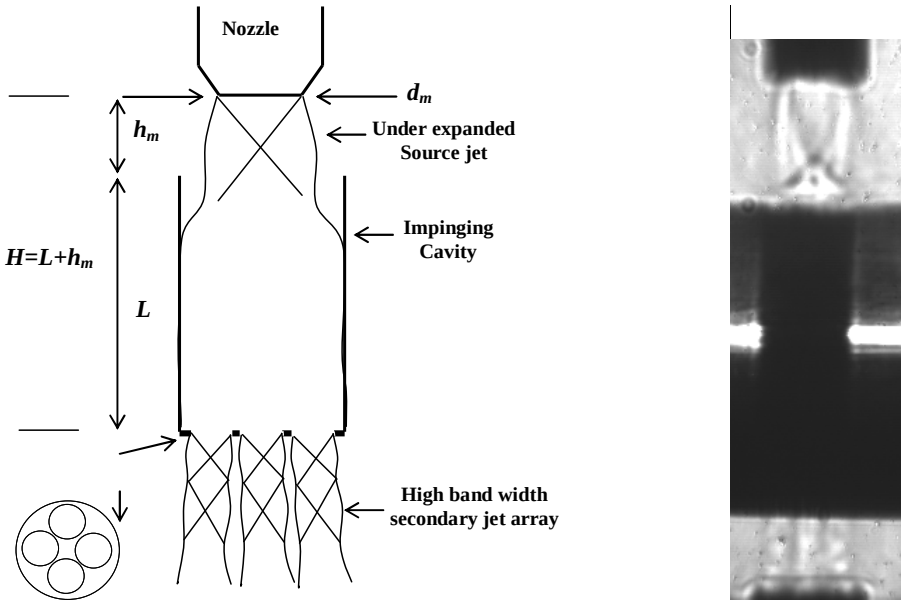

(a) Configuration (b) Micro schlieren image of the flow field

Figure 3 Schematic of micro actuator

A schematic of the actuator is shown in Figure 3a. As seen here, the micro-actuator consists of three main components: a) an under expanded source jet, which supplies the air into a cylindrical cavity, b) a cylindrical cavity upon which the source jet impinges, and c) multiple micro nozzles (i.e. microjet orifices) at the bottom of the cylindrical cavity, from which the high-momentum, unsteady microjets issue. Figure 3b shows a representative schlieren image of the flow field associated with the micro-actuator. This configuration allows one to exploit multiple flow-acoustic resonance phenomenon, including edge & hole tones, cavity resonance, Helmholtz resonance and other flow instabilities allowing us to efficiently amplify microjet (flow) unsteadiness. In the present design, the source jet was issued from a 1.0mm diameter (d_m) converging nozzle and the micronozzles array at the bottom of the cavity consists of four 400 μm holes in the pattern shown in Figure 3a.

The main parameters that govern the properties of the microjet array issuing from the actuator assembly are: a) the distance of cavity from the source jet $\boldsymbol{h_m}$, b) the length of the cylindrical cavity, $\boldsymbol{L}$ and c) the source jet pressure ratio,

($NPR)_m$. The two geometric parameters are indicated in Figure 3a. In the preliminary study, we examined the effect of these parameters on the flow issuing from the microjet actuator and to identify the optimal range and combination of these parameters that produce the desired micro-actuator flow. This has helped us to develop a preliminary design approach and scaling laws for such actuators.

Preliminary studies were conducted for different combinations of geometric and flow parameters such as L/d_m, $(h/d)_m$ and $(NPR)_m$. L/d_m is varied from 1-5, $(NPR)_m$ from 1.9 to 5.8 and $(h/d)_m$ from 1 to 2. Figure 4 shows the representative spectra corresponding to $L/d_m = 5$. For this case, experiments were carried out by varying $(h/d)_m$ for a fixed $(NPR)_m = 4.8$ and by varying $(NPR)_m$ keeping a fixed $(h/d)_m$ value.

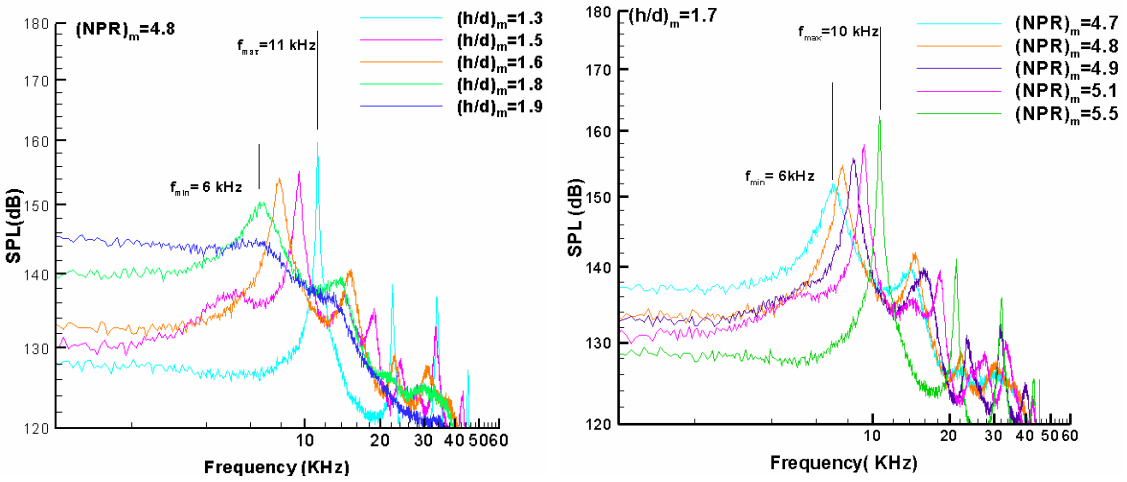

a) Variation in $(h/d)_m$ b) Variation in $(NPR)_m$

Figure 4 Representative spectra of actuator for L/d_m=5

The pressure spectra (Figure 4) clearly show the presence of high amplitude peaks indicating the presence of highly unsteady flow issuing from the actuators. Here we see that for $L/d_m = 5$, the control knobs, $(h/d)_m$ or $(NPR)_m$ variation produce high amplitude, unsteady microjets in the range of 6-11 kHz. Equally noteworthy is the trend of peak frequency variation, where a very small variation of h/d, by 600μm, leads to a significant shift in the peak frequency of 10 kHz. Consequently, there is significant potential for developing a compact, robust pulsed actuator with high mean and unsteady properties. This design approach allows for multiple 'control knobs' that can be used to modify the actuator properties in real time, as dictated by the application.

As shown in Figure 4, the data from the parametric study is classified into two sets, one is the data derived from the $(h/d)_m$ variation (Figure 4a) and the other set reflect the effect of $(NPR)_m$ variation (Figure 4b). This grouping can then be used for understanding the overall behavior in terms of these parameters and deriving a more general correlation that captures it; this is discussed in the following section.

(b) Actuator results from previous studies

Figure 5 (Solomon et al.[12]) summarizes the effect of $(NPR)_m$ and $(h/d)_m$ shown in Figure 4 but over a large range of cavity lengths, L/d_m. As seen here, for a given actuator design, i.e. fixed L/d_m, very small changes in the source jet distance and operating pressure allows one to sweep the output frequencies over a rather large range of $\Delta f_{actuator}$ = 10-20 kHz. However, this plot also shows a wide range of actuator frequencies can be produced for a given L/d_m, by varying $(h/d)_m$ or $(NPR)_m$. In order to better collapse the performance, in terms actuator dimensions, we define a new variable 'H' which is defined by 'H=h_m+L', where h_m is the distance of nozzle exit to the cavity entrance and L is the length of the cavity, as before. This parameter 'H' represents the length of the jet column from the micro-nozzle end to the impinging end of the cavity.

The actuator frequency is non dimensionalized using ideally expanded jet velocity of the primary under expanded source jet. Non dimensional frequency is given by

$$St_{ideal} = fd_m / U_{ideal} \qquad (1)$$

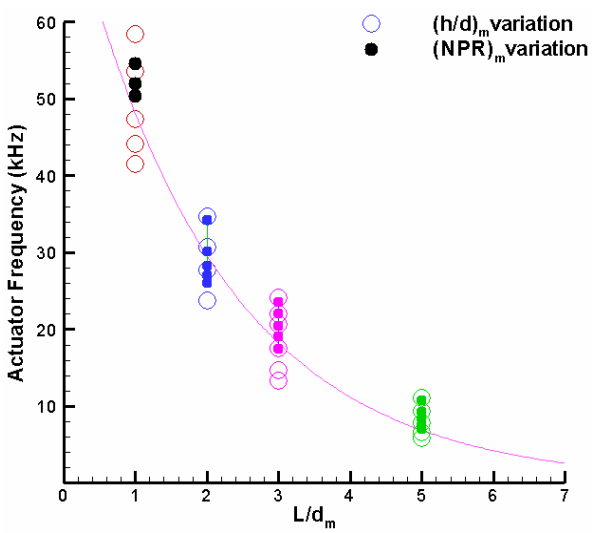

Figure 5 Summary of actuator data[12,13]

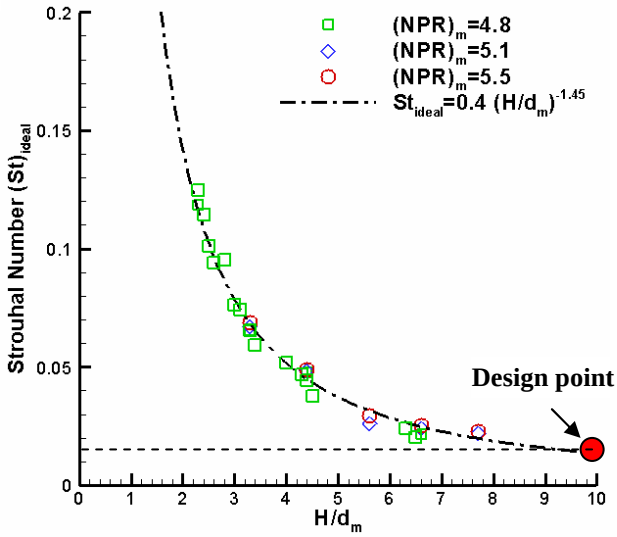

Figure 6 A correlation that predicts actuator dynamics

In equation (1) f is frequency of the actuator, d_m is source jet diameter and U_{ideal} is the ideally expanded jet velocity of the under expanded source jet. The new parameter H is plotted against the non dimensional frequency St_{ideal} as shown in figure 6. Interestingly these new variables collapsed into a single trend curve as seen in the figure. The collapsed curve is approximated as a general correlation, represented by the equation (2).

$$St_{ideal} = 0.4(H/d_m)^{-1.45} \qquad (2)$$

We used this correlation as a guide for designing the actuator for the present application. Recalling that the aim of this study is to examine the efficacy of this new pulsed micro-actuator system for the control of the supersonic impinging flow field created in our STOVL facility, the actuator output should closely match the impinging jet dynamics. Previous studies on supersonic impinging jets [3-5] show that this flow field produces high amplitude, nearly discrete frequency tones, in a range of 2-20 kHz where the maximum amplitude tones appear in the range of 4-6 kHz. Hence, the nominal design point for present condition was an actuator with maximum amplitude at ~ 6kHz. This frequency is indicated in figure 6 (corresponding to St_{ideal} ~0.012). More details of the actuator, designed for this application, will be described in the following section.

(c) Actuator requirements for the impinging jet flow field

Microjets have been used as actuators for the control of supersonic impinging jet flow by steady injection in a number of studies conducted in our laboratory[3-5]. It is anticipated that unsteady injection or actuation of those microjets, referred to as *pulsed microjets*, will be more advantageous in that it can induce more momentum than steady microjet injection for a given mass flow rate thus reducing mass flow requirements when operated at a given supply pressure. Choi[14] demonstrated that pulsed microjet injection suppresses impinging tones with less mass flow than steady injection, and that it produces larger reductions in OASPL (overall sound pressure level) at some operating conditions - such as lift plate-to-ground distance - where steady microjet injection was less effective. In addition, from a control-point of view, a control input modulated at the natural frequencies of the system would in principle be more desirable. This is because the control input at those frequency ranges has more of an impact on modulating the gain of the system at the natural frequency, thereby suppressing the impinging jet resonance. Since the actuator used by Choi[14] was operated at much lower frequencies (due to hardware limitations at the time) than the natural frequency of the base flow, it is important to develop an actuator that has a bandwidth comparable to the impinging tone frequencies. In the next section, the design of the actuator that has a high bandwidth of about 4 to 6 kHz is described.

(d) Design details for the impinging jet integrated actuator

In order to meet the actuator performance requirements described in the previous section, the present actuator was designed and fabricated with certain parameter values. As shown in Figure 7a, each actuator module is composed of one primary jet of 1mm-diameter and four microjets of 400μm-diameter. Each microjet has an inclination angle of

60º from the main jet nozzle axis as shown in Figure 7b, based on that prior studies using steady microjets have shown injection angles in this range to be most effective (Kumar et al.[5]). The distance from the source jet nozzle to the first cavity (h_m) is 1.65mm, and the length of first cavity (L) is 8mm. It should be noted that although the particular design parameters described in this section are based on the design correlation described in §III-(b), these represent only one possible combination of parameters that one can choose. The actuator designed herein represents the first step in our quest to develop a suitable actuator for active-adaptive control of this supersonic impinging jet flow. The optimal design, which involves choosing design parameters such as h_m, the number of microjets per one module, microjet-spacing, and so on, needs to be further investigated. In addition, in order to have microjets as uniformly distributed as possible at the periphery of the main nozzle exit, the circular design described in §III-(b) is modified to linear array design as shown in Figure 7a. Four of these modules are placed on the lift plate along the circumference of the main jet nozzle, thus forming total sixteen microjets (see Figure 7b). It should also be noted that the simple design of the module (as shown in Figure 7a) for the bench-top-tests had to be considerably modified for several reasons in order for the actuator modules to be incorporated with the lift plate. This was challenging both from a design and especially from a fabrication perspective. First, the microjets need to be inclined at 60º with respect to the jet axis and located at the periphery of the main jet nozzle exit. Second, since one module is composed of two blocks - one with primary jet, and another with the cavity and microjets - two blocks should be firmly put together and also assembled to the lift plate as well. Considering the actual size of the module is very small (order of 10^{-3}m), the fabrication process needs to be taken into account in the actuator design. Given these challenges from the fabrication-point of view, actuator modules were fabricated in such a way that the first set of blocks (which contain the actuator's primary or source jet) of four modules were machined in a circular plate insert, where the second set of blocks (which contain microjets) of four modules were machined in another circular plate. These two circular plates were combined together, thereafter incorporated with the lift plate (see Figure 2). In this paper, only the schematic of the actuator-lift plate-assembly is shown in Figure 7b.

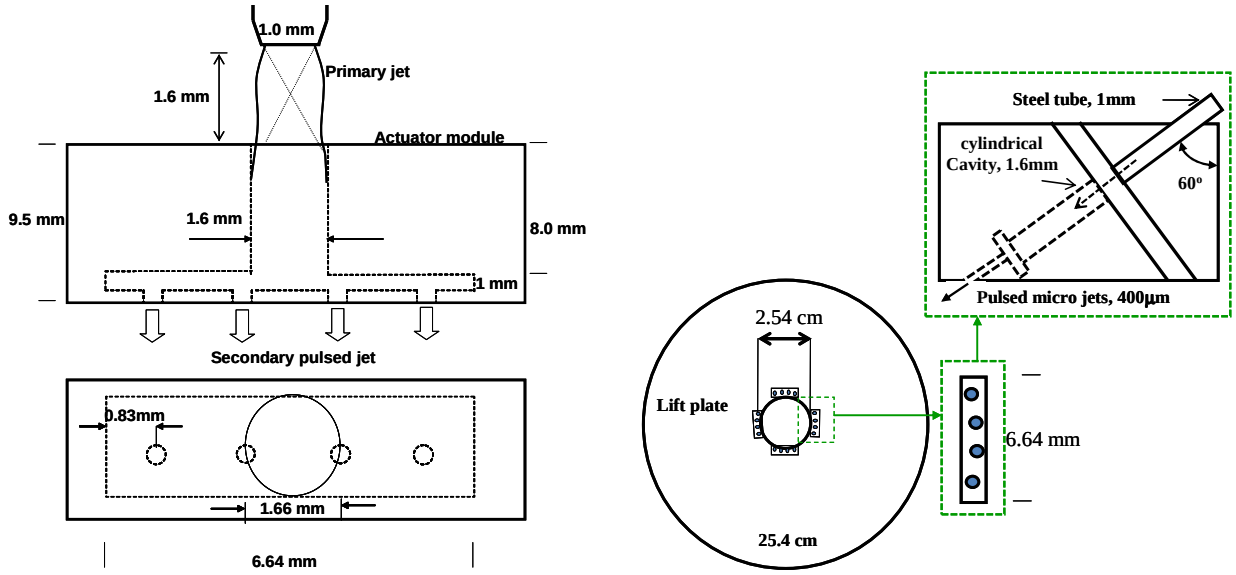

(a) Design details (b) Assembly details

Figure 7 High bandwidth Actuator used for the control of super sonic impinging flow

IV. Actuator performance and effect on impinging jet aeroacoustics

(a) Calibration and characterization of the actuator

The micro actuator fabricated as an integrated part of the lift plate is calibrated and characterized on the bench-top before being used for the actual tests. Figure 8a shows the performance spectra of the actuator from these bench top studies for a range of NPR. Three distinct regions of operations can be observed in the spectra, which are represented by 'steady', 'broadband', and 'high-amplitude discrete frequency' regions. As seen in Figure 8, for NPR roughly below 4.4, the pressure spectra of the secondary micro jets is low amplitude and broadband, corresponding to 'steady' response. Over a nominal range of 4.5<NPR<5.8, the actuator aero-acoustic properties evolve producing

microjets with significantly higher broadband energy without any distinct and discrete tones in the spectra. This region of operation is classified as the 'broadband' region. Finally, at higher NPR values (>5.8), distinct and high amplitude frequency components appear in the spectra –corresponding to the "high-amplitude discrete frequency" zone. As an example, at NPR=6.0 and 6.4, pulsed micro jets with a frequency of 4.5 and 5.2 kHz respectively were generated, close to the design expectation. Figure 8b represents characterization of actuator integrated to the lift plate using a near filed microphone. The actuator response is found very similar for both the cases.

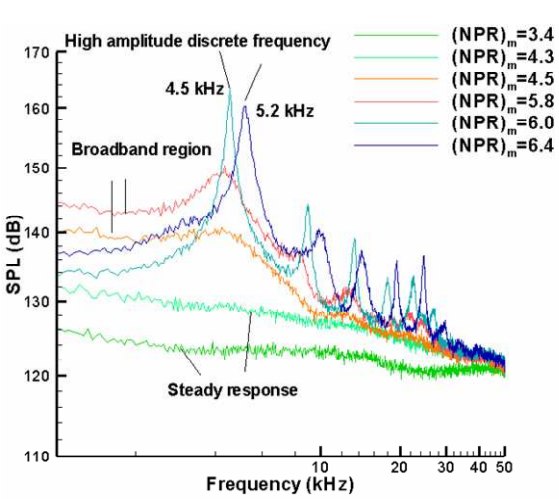

Figure 8a Bench top characterization of actuator (using Kulite probe)

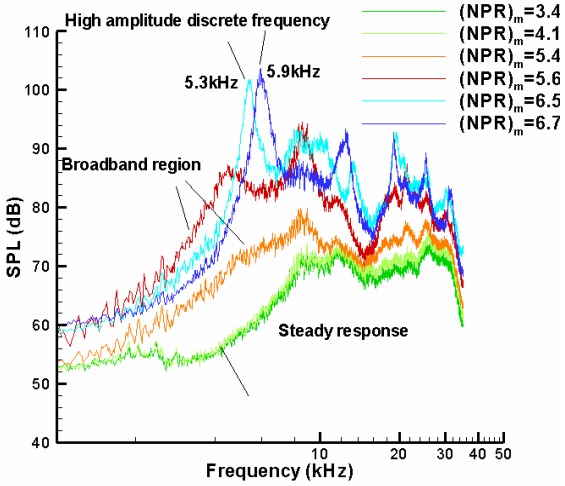

Figure 8b In-situ characterization of the actuator integrated into the 'lift plate' (using a near-field microphone)

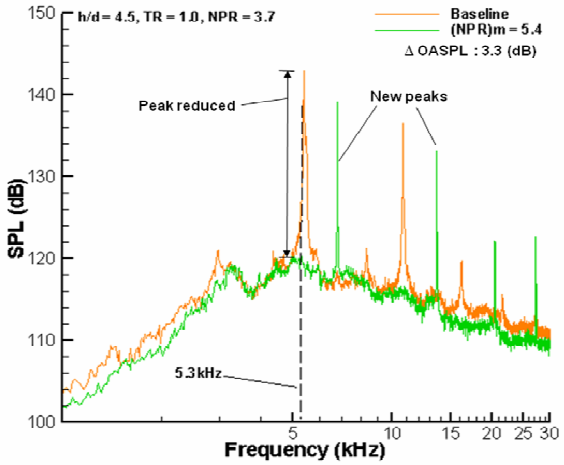

(a) Actuator operating at NPR=5.4

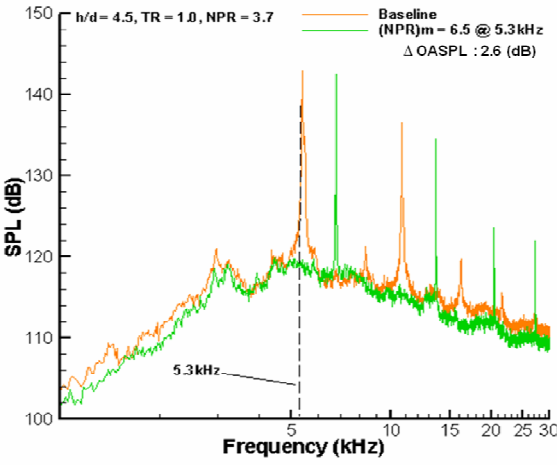

(b) Actuator operating at NPR=6.4 @ 5.3 kHz

Figure 9 Spectra of impinging jet with and without control at h/d=4.5

(b) Actuator performance in controlling the flow

The response of the impinging jet flow-field to the integration and use of the high bandwidth actuator is discussed next. Figures 9 and 10 show impinging flow field spectra with and without active control using this high bandwidth pulsed micro-actuator. Near-field noise spectra corresponding to the actuator operating in the 'broadband' and 'high-amplitude discrete frequency' regimes are shown. As seen in Figure 9a, when the actuator is in the broadband regime, the original impinging tones are completely eliminated, while a new peak and its harmonics are produced at different frequencies. It can be seen that even though the amplitude of new peak is almost the same as that of the

original impinging tone, the spectral density in sound pressure level of new peak is much less than that of the original impinging tone since it is much narrower than that of the original impinging tone. This result is also consistent with the fact that OASPL is reduced with microjet control, by 4 dB for this case, in spite of the new peaks cropping up. It should also be noted that neither the spectra of the baseline case nor that of the actuators (shown in Figure 8) has peaks at these new frequencies which appear in Figure 9. It is also worth noting that the same phenomenon occurred with this actuator at most of supply pressures in the broadband and tonal range of actuator operation.

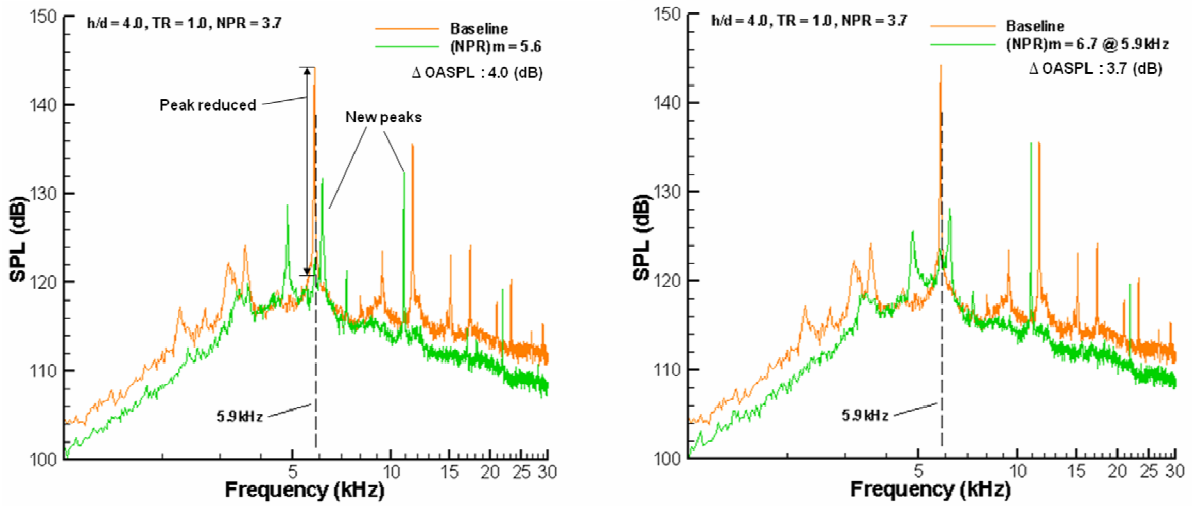

(a) Actuator operating at NPR=5.6 (b) Actuator operating at NPR =6.7 @ 5.9 kHz

Figure 10 Spectra of impinging jet with and without control at h/d=4.0, @ Microphone

The question that needs to be addressed is the reason for the occurrence of these new peaks. Such a phenomenon of secondary peaks has been observed in other flow control applications[15-17] such as combustion control and cavity control, where the corresponding frequencies do not correspond to the natural frequencies or those of the actuator. In some cases (Rowley et al.[16]), a single natural frequency is replaced by two frequencies on either side, thereby introducing a "peak-splitting." The reason for the occurrence of such secondary peaks is simply because of the gain and phase of the actuator over this range of frequencies, and the fact that the flow is capable of producing a range of frequencies depending on the nature of excitation of the instability waves. It was shown in Fleifil et al.[15] and Hathout et al.[17], for instance, that such secondary peaks occurred because of the control algorithm that was deployed and that when the gain and phase of the controller were modified using a systematic control methodology, these peaks were entirely removed. While in the combustion control example, the control algorithm was in a feedback loop that was explicitly designed, in the current problem, the feedback loop is implicitly present between the acoustics and instability waves, with the control action modifying the pressure distribution primarily at the nozzle. Our speculation is therefore that when the high bandwidth micro-actuator is deployed with a steady pressure, its gain and amplitude over a range of frequencies around the dominant impinging tone is such that the overall feedback loop produces the new peaks. We further speculate that with a different excitation, the precise nature of which is yet to be determined, its gain and amplitude can be suitably modified, similar to combustion control, thereby removing the secondary peaks while continuing to annihilate the dominant impinging tone. Further research needs to be carried out in order to determine these excitation methods. Detailed transfer-function models of the current actuator and of the system may need to be derived in order to identify the appropriate input into the actuator that will produce the necessary gain and phase over the suitable range of frequencies. Since NPR and the pulsing frequencies of microjets are not independent of each other due to the nature of the actuator, other inputs that can be independently varied may be needed so that one could generate the requisite degrees of freedom in the actuator response. Besides, if one could more accurately control the microjets using electronic methods, then it may be easier to implement a feedback control strategy using the current actuator for real-time control of supersonic impinging jet flow. These investigations are currently ongoing.

(c) Comparison of control efficacy with previous studies

In this section, the comparison between high bandwidth micro-actuator and the actuator used in Choi[14] using the rotating cap to produce pulsed microjets are described. First of all, the most obvious and simple difference lies in that the operating (pulsing) frequency ranges are different; the frequency range is at least one order higher in this study, where the number of microjets and their diameters are the same for both studies. Also, in this study, sixteen microjets are not uniformly distributed; rather, each module composed of four microjets is located in such a way that each module is apart from each other by 90º, which results in that only 30% of the main jet circumference is subjected to actuation, where all sixteen microjets are uniformly distributed in Choi[14]. The spatial extent of the microjet around the jet periphery is an important parameter, as the attenuation of the resonance loop generally dictates that it be disrupted over a significant spatial extent. It is anticipated that increasing microjet coverage to more than 30% will result in increased performance in terms of noise and flow control. The optimal actuator coverage is an area that warrants further study. It should be also noted that the microjet injection angle is 60º from the main nozzle axis in this study as in Kumar et al.[5] as described in §III-(d), where it is 30 º in Choi[14] since the injection angle could not be increased further due to the rotating cap. Furthermore, the mass flow used for the actuator in this study is smaller than the one in Alvi et al.[3] Four steel tubes are used for the primary jets in this study, where total sixteen of (the same diameter) steel tubes are used for microjets in Choi[14] . Moreover, the actual mass flow coming out of the microjet exit is only a fraction (maximum 64%) of the mass flow at the inlet of primary jet, thus the mass flow at given input pressure for high bandwidth micro-actuator is even less; 0.25×0.64 = 16%. Therefore, it should be taken into account when the effects of actuator are compared between two different configurations. One could expect that using high bandwidth micro-actuator with more mass flow usage (with more modules placed) could result in more effective control of the impinging jet.

A summary of the pulsed jet actuator performance and a comparison to previous 'steady microjet control' studies is shown in Table 1. Here we see that in terms of OASPL reduction, the current actuator has a comparable impact to steady and pulsed microjet used in Lou et al.[4] and Annaswamy et al.[18], respectively, even with less supply pressure $(NPR)_m$. On the other hand, as shown in Table 1, the largest OASPL reduction is achieved with low frequency pulsed actuator[18] by 5dB, where the micro-actuator in the present study reduced OASPL only by 4dB with the microjet pressure in the broadband regime. This may be because, as described in the previous paragraph, the mass flow used in the present study is much less than in Annaswamy et al.[18], and also the current actuator is placed only in 30% of the circumference of the main nozzle thus resulting in less impact. Furthermore, considering that the secondary peaks have been produced in near-field noise spectra with active control using the current actuator, it needs further study to eliminate these secondary peaks by means of suitably modifying the actuator output with appropriate gain and phase in those frequencies range, as described in §IV-(b), and thus achieving more OASPL reduction.

Table 1. Impact of active control using micro-actuator: comparison to previous studies

Main jet **NPR = 3.7** **TR = 1.0** **h/d = 4.5**	Steady microjet Control	Low frequency pulsed microjets	Pulsed Actuator Results from Present study		
	$(NPR)_m$~6.7 (Kumar et al.[5])	$(NPR)_m$~6.7) (Choi et al.[14])	**Steady regime $(NPR)_m$= 3.4**	**Broadband regime $(NPR)_m$ = 5.4**	**High amplitude tonal regime $(NPR)_m$ = 6.5**
OASPL reduction	3 dB	5dB	**3dB**	**4dB**	**3dB**
Tonal reduction	0 dB	12 dB	**22 dB**	**22 dB**	**23 dB**
Spectral features	No secondary peaks	No secondary peaks	**Secondary peaks produced**	**Secondary peaks produced**	**Secondary peaks produced**

Summary & Future Work

In the present study, a pulsed actuator that produces very high amplitude disturbance in the range of frequencies (4-6 kHz) matching the impinging jet flow field was designed. This actuator used the result of our work in this area (Solomon et al.[12-13]) and validated the design and scaling laws developed therein. The actuator performance results also demonstrated the flexibility in designing pulsed microjet arrays in various configurations, e.g. in a circular cluster and in a linear array as in earlier studies or along an arc as in the present work. Finally, the effect of implementing these pulsed microjet arrays on controlling the impinging jet flow field reveals the following:

- In the broadband and tonal range of operations, the pulsed microjets are much more effective than steady microjets (operating approximately at same pressures) in almost completely *annihilating the primary tones*.
- The cancellation of the primary tones, however, is accompanied by secondary peaks at other frequencies, which are significantly narrower and thus less energetic than the original peaks that are eliminated. It is speculated that the reason for the occurrence of these secondary peaks is due to the particular gain and phase of the current actuator design, which can be improved by suitably modifying the gain and phase of the actuator output over this range of frequencies, thereby eliminating both the impinging tone and the secondary peaks. In order to achieve appropriate gain and phase of the actuator, detailed transfer function model of the actuator may need to be derived, which are yet to be determined, and this further suggests that in future implementation, one may need some of hardware modification such that electronic control of microjets could make it easier to identify the transfer function of the actuator by means of giving the microjet actuator a temporal variation, thereby to generate a shaped input with appropriate gain and phase into the system. These investigations are currently underway.

Future work should entail the use of a second generation of actuators that take advantage of lessons learned from the present study. Some of the desired characteristics ideally include:

- Microjets to span a larger spatial extent, around the entire periphery of the main jet exit. This will enable a more direct comparison with past steady control approaches where impinging tones were typically reduced or even eliminated without any new tones appearing.
- Ability to modulate the frequency (and amplitude) with relatively minor changes in the minor changes in the microjet pressures. This would allow one to decouple the mean momentum, or steady $C\mu$, effect from the influence of the unsteady component.
- Testing of the steady microjets in a configuration in which the (steady) microjets are in locations similar to this study's actuator. This could give insight into whether the new tones observed are a result of the high frequency control itself or simply the design's configuration.

References

[1]Zhuang, N., Alvi. F.S., Alkislar. M. B., and Shih. C. "Supersonic cavity flows and their control" *AIAA Journal*, Vol. 44, No. 9, 2006, pp. 2118-2128.

[2]Zhuang, N., "Experimental Investigation of Supersonic Cavity Flow and Their Control", Ph. D. Dissertation, FAMU-FSU College of Engineering, 2007

[3]Alvi, F. S., Shih, C., Elavarasan, R., Garg, G. and Krothapalli, A., "Control of supersonic impinging jet flows using supersonic microjets," *AIAA Journal*, Vol. 41, No. 7, 2003, pp.1347-1355.

[4]Lou, H., Alvi, F. S. and Shih, C., "Active and adaptive control of supersonic impinging jets," *AIAA Journal*, Vol. 44, No. 1, 2006, pp.58-66.

[5]Kumar, R., Lazic, S., and Alvi, F. S., "Active control of high temperature supersonic impinging jets," AIAA-2008-360

[6]Cattafesta III, L. N., Garg, S., Choudhari, M. and Li, F. "Active Control of Flow-Induced Cavity Resonance," AIAA Paper 97-1804.

[7]Wiltse, J. M. and Glezer, A., "Manipulation of Free Shear Flows Using Piezoelectric Actuators," *J. Fluid Mech.*, Vol. 249, 1993, pp. 261-285.

[8]Amitay, M., Kibens, V., Parekh, D.E., and Glezer, A., "Flow reattachment dynamics over a thick airfoil controlled by synthetic jet actuators," AIAA Paper 99-1001.

[9]Raman, G. and Kibens, V., "Active flow control using integrated powered resonance tube actuators". AIAA Paper 2001-31330.

[10]Dziuba, M. and Rossmann, T., "Active control of a sonic transverse jet in a supersonic cross flow using a powered resonance tube", AIAA Paper 2005-897.

[11]Kastner, J and Samimy, M. "Development and characterization of Hartmann tube fluidic actuators for high-speed flow control", *AIAA Journal*, Vol. 40, No.10, 2002, pp.1926-1934.

[12]Solomon, T. J., Kumar, R. and Alvi, F. S. "High Bandwidth Micro-Actuators for Active flow control" AIAA paper 2008-3042.

[13]Solomon, T. J., Kumar, R. and Alvi, F. S. “Development and characterization of high bandwidth actuator” ASME paper, 2008-3042.

[14]Choi. J Active Noise Control in Supersonic Impinging Jets Using Pulsed Microjets: Actuator Design, Reduced-Order Modeling. PhD thesis, Massachusetts Institute of Technology, 2006.

[15]Fleifil. M., Hathout, J.P.,, Annaswamy, A.M., and Ghoniem. A.F., The origin of secondary peaks with active control of thermoacoustic instability. Combustion Science and Technology, 133:227 – 260, 1998

[16]Rowley, C. W., Williams, D.R., Colonius, T. Murray, R.M., and Macmynowski, D. G., Linear models for control of cavity flow oscillations. Journal of Fluid Mechanics, 547:317 – 330, 2006.

[17]J. P. Hathout, A. M. Annaswamy, M. Fleifil, and A. F. Ghoniem. A Model-Based Active Control Design for Thermoacoustic Instability, Combustion Science and Technology, 132:99-138, 1998.

[18]Annaswamy, A.M., Choi, J.J.,and Alvi, F.S.Pulsed microjet control of supersonic impinging jets via low-frequency excitation. Journal of Systems and Control Engineering, 222(5):279 – 296, 2008.

48th AIAA Aerospace Sciences Meeting Including the New Horizons Forum and Aerospace Exposition
4 - 7 January 2010, Orlando, Florida

AIAA 2010-1198

Control of Resonant Flow Inside a Supersonic Cavity Using High Bandwidth Pulsed Micro-actuators

M.Y.Ali *, J.T.Solomon †, J.Gustavsson ‡, R.Kumar §and F.S.Alvi ¶

Florida Center for Advanced Aero-Propulsion (FCAAP)

Department of Mechanical Engineering

Florida A & M Univeristy and Florida State University, Tallahassee, FL 32310

Active control of high speed flows has been dependent upon the development of simple yet robust actuators that are capable of producing high momentum and are reliable, responsive and have the capability of being integrated easily. This paper presents an experimental investigation of the characterization and implementation of high-bandwidth pulsed microjet-actuators for the control of supersonic resonant flows in a cavity. This pulsed microjet-actuator is capable of producing high momentum mean flow along with an unsteady component where frequency can be adapted. The results show that using this first generation design actuation of the pulsed microjets reduce the amplitude of the cavity tones by upto 7 dB and the overall sound pressure levels upto 5 dB. The effect of actuator pressure ratio was studied over a wide range. A comparison was made with the same actuator working in a steady mode of operation. The pulsed microjet injection alters the shear layer characteristics and significantly reduces the unsteadiness in the cavity as observed from the unsteady pressure measurements. Based on these results the actuator design is being modified to further improve its control authority. This is expected to lead to much improved control in future studies.

I. Introduction

Cavity flow has been the subject of research since the 1950's (Roshko[1]). Although geometrically simple, fluid dynamics in these flows is rather complicated. In practice these large fluctuating surface pressure loads are observed in cavities such as aircraft weapons, cargo and landing gear bays represent a serious concern. Mixing control and enhancement in supersonic combustion has also been a topic of research for many years. Active control of shear and boundary layer flows have attained wide attention in the recent years due to the potential and substantial benefits derived out of such control schemes. In high-speed flows, control of flow oscillations in cavity flows, supersonic impinging jets and jet noise control are areas where various active control methods may lead to dramatic gains in performance. Control schemes that have proved relatively successful in subsonic flow may not be ideal for the effective and efficient control of high speed flow. Effective control of flow and noise requires the use of robust actuators. Although various types of actuators have and are being explored, most designs have shown some limitations either due to their overall performance, range of operation, cost effectiveness and/or integrability into practical systems. There is a clear need for actuators that produce *high-amplitude excitation, over a broad range.* Furthermore, the output of an ideal actuator should be adjustable, both in terms of amplitude and frequency over a large dynamic range. Such actuators would then be useful for implementation in practical flows.

Cavity flows are governed by a flow-acoustic resonance. As the shear layer separates from the leading edge of the cavity, it starts to roll up into large-scale vortical structures. As these structures impinge on the

*Graduate Research Assistant, Student Member AIAA
†Graduate Research Assistant, Student Member AIAA
‡Research Scientist, Department of Mechanical Engineering, Senior Member AIAA
§Research Scientist, Department of Mechanical Engineering, Member AIAA
¶Professor, Department of Mechanical Engineering, Associate Fellow AIAA

trailing edge of the cavity, acoustic waves are generated. These waves propagate to the leading edge within the cavity and further excite the shear layer, completing the feedback loop. Under certain conditions, when the frequency and the phase of the acoustic waves match those of the shear layer instabilities, resonance is achieved producing significant unsteady acoustic loads on the nearby surfaces. The resonance can be so intense that it can lead to significant structural fatigue in open weapon bays and landing gears, in the context of cavity flows. Studies relating to supersonic cavity flow control have been carried out at the Advanced Aero-Propulsion Laboratory (AAPL). Steady microjets of Zhuang[2]and Zhuang et al.[3,4] have demonstrated the effectiveness of using microjet-based actuation in controlling flow unsteadiness. Ukeiley et al.[5,6] achieved significant reductions in the fluctuating surface pressures with modest amounts of mass flowing through the injectors. It is anticipated that the effectiveness of injection based control will be significantly enhanced when *high-amplitude pulsed actuator* designs are implemented.[14]

Flow control schemes can broadly be classified into active and passive methods. Passive methods do not require external energy but make use of the geometry variations for the purpose of control. Variations in nozzle geometry , use of mechanical tabs and the use of splitter plates are examples of various passive control methods adopted for the control of flow and jet noise. On the other hand, in active flow control schemes, an external energy source is used for tailoring the natural instability behavior of a shear or a boundary layer flow according to the control objectives. The ability to efficiently adapt to changing flow conditions - the ultimate goal of active control schemes, makes them more attractive to passive methods. Mechanical systems such as vibrating ribbons and cantilevered beams, electromechanical devices such as piezoelectric diaphragms, voice coils (speakers), synthetic jets etc. are used as external energy sources in various active flow control schemes. Cattafesta et al.[7] piezoelectric actuators for active control of flow-induced cavity resonance at low Mach numbers. Wiltse & Glezer[8] also used piezoelectric actuators for manipulation of free shear flows. Amitay et al.[9] used zero mass flux synthetic jets for dynamic control of flow reattachment and separation over a thick airfoil. Rowley & Williams[10] present an overview of recent advances in understanding, modeling, and controlling oscillations in the flow past a cavity. A review of active control of flow-induced cavity oscillations is presented by Cattafesta et al.[11] Although relatively successful at lower speeds, many actuators are not very efficient when the primary flow velocities are high. Optimal manipulation of shear or boundary layer of high speed flows requires high-energy aero-acoustic excitations, with controllable steady and unsteady components. A simple (no moving parts), durable and robust actuator, with high momentum and amplitude that can be easily integrated to practical high-speed flow systems is crucial for any active flow control scheme. The present study is motivated and driven by this goal.

II. Experimental Details

A. Facility Description

The experiments were conducted at the supersonic wind tunnel facility (Figure 1) at the Advanced Aero-Propulsion Laboratory (AAPL) of Florida State University. The tunnel is supplied with dry, pressurized air from a 10 m^3 air tank at 1600 psi.

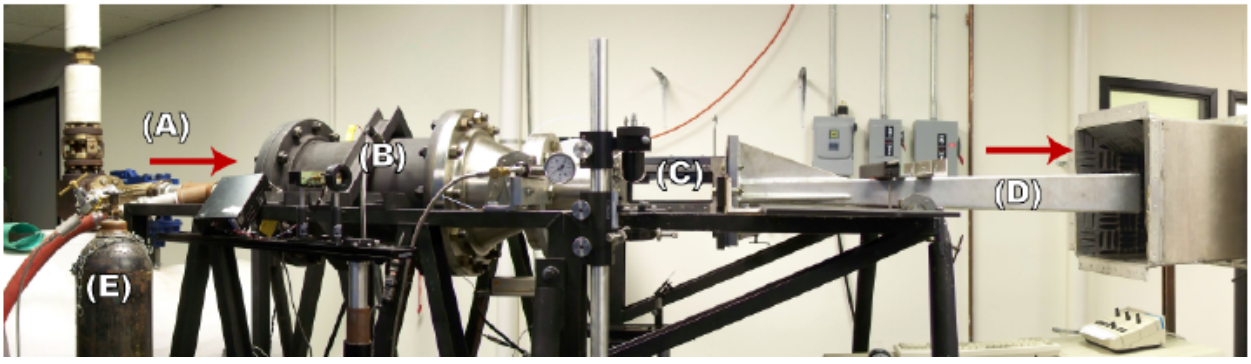

Figure 1. Layout of the supersonic wind tunnel. (A)Air from the supply, (B)Settling Chamber, (C)Test Section, (D)Diffuser, (E)Nitrogen for microjets

Control of air flow to the test section was maintained through the use of two inline valves, a Tescom^{TM}dome regulator and a Fisher^{TM}controls valve. The dome-loading regulator is used for the larger drop in pressure from the air tanks. An output pressure of 300 psi from the regulator is maintained. The Fisher controls valve was used for the fine control of the tunnel stagnation pressure and is operated from a PC based LabVIEW data acquisition program. Two inline heaters with a total power of 300kW, capable of heating the air to 700K are installed to raise the stagnation temperature of the incoming air and preventing condensation in the test section. The test section Mach number can be varied by use of interchangeable nozzle blocks. Current experiments were performed at a test section Mach number of 1.5. The run time of the tunnel at these conditions is 10-15 minutes. The test section is 305 mm long, 66 mm wide, and 44 mm high. The test section has optical access from the sides and bottom. The stagnation pressure and temperature were typically maintained at 35 psi and 130^{o}F, respectively. A LabVIEW based data acquisition program was used to measure and record the run conditions, control the wind tunnel and acquire unsteady surface pressure measurements. To supply pressure to the pulsed actuator nitrogen was used a supply gas. Pressurized gas from the nitrogen cylinder was routed to the actuator via a manifold. Needle valves were used for finer control of the pressure supplied to the actuator and a resolution to within 1 psi was realized and maintained.

B. Model and Actuator Details

A rectangular cavity with a L/D of 5.5 and L/W of 3 was used for the experiments where L is the length, W is the width and D is the depth of the rectangular cavity, respectively. The cavity was mounted with three unsteady pressure transducers labeled as CF1, CF2, CF3 at the cavity floor located at x/L of 0.89, 0.74 and 0.53, respectively, where x/L is measured from the leading edge of the cavity. A schematic and picture of the cavity are shown in Figure 2.

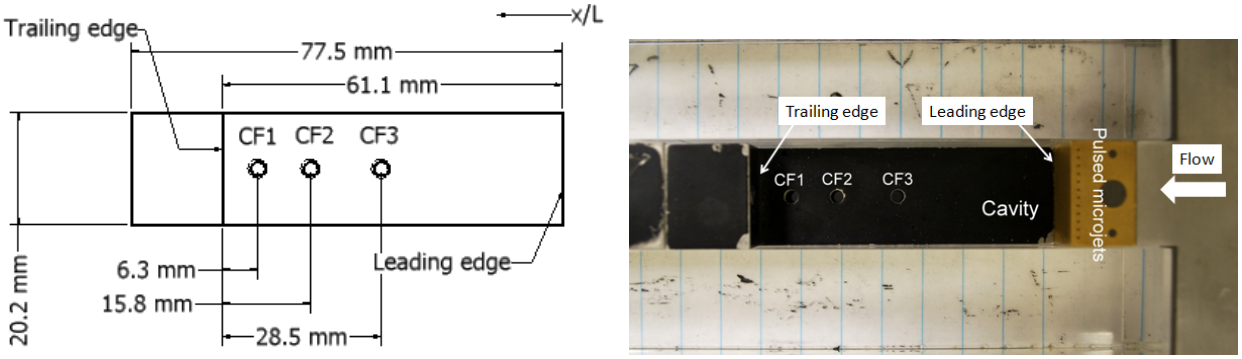

(a) Schematic of the rectangular cavity (top view)

(b) Location of the pulsed microjets and the sensors

Figure 2. Details of the Rectangular Cavity

The design details of the actuator are shown in Figure 3. The actuator consisted of two modules. Each module consists of one primary source jet of 1 mm diameter, a cylindrical cavity of 1.6 mm diameter, a spreader of 1 mm height and six orifices of 400μm diameter and 0.5 mm height. The distance between the primary jet and the cylindrical cavity was, $(h/d)_m = 1.6$. The vent area between the primary jet and cylindrical cavity is connected to atmosphere using a tube of 1.6 mm diameter and 40 mm in length. The isometric view of the pulsed actuator showing both the modules is shown in Figure 3a and the microjet orifices along with the spreader are shown in Figure 3b. As flow exits the primary jet it passes through a gap of height h_m=1.6 mm and enters the cylindrical cavity. The flow leaving the cylindrical cavity enters the spreader before finally exiting from the orifices. The spreader ensures that the flow issuing from the orifices is uniform. Another such module is placed along side the first one such that the orifices span the entire width of the cavity, W=20.2 mm. The spacing between the micro-orifices was uniform at 1.5 mm. The microjet orifices were located at a distance of 1.5 mm upstream from the leading edge of the cavity. The orientation of the orifices was kept normal to the flow direction. The pulsed actuator module integrated with the rectangular cavity on the test bed can also be seen in Figure 2b.

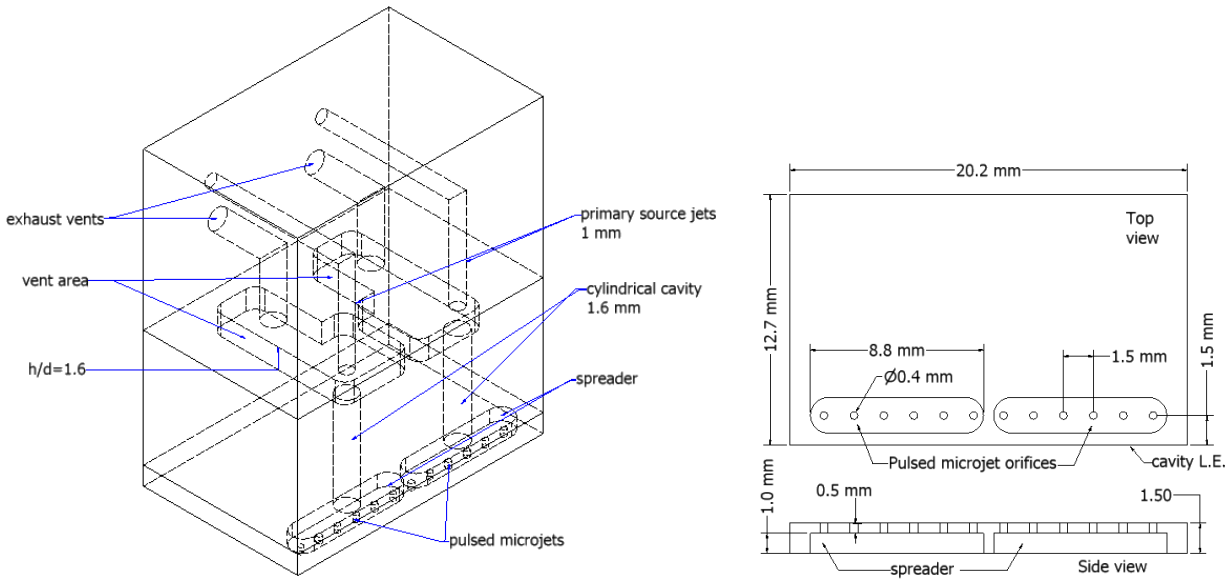

(a) Pulsed Actuator

(b) Spreader piece

Figure 3. Pulsed Actuator used for Supersonic Cavity Flow Control

C. Experimental Techniques

A conventional Z-type Toepler schlieren arrangement using a white-light source was used for flow visualization of the cavity. The light source is a pulsed, Xenon flash lamp, with a frequency up to 1000 Hz and a 5-10 μs pulse duration. A Kodak Megaplus ES1.0 (1008 x 1018 pixels) digital camera was used for image acquisition at a sampling rate of 100 Hz. The flow visualization was mostly used to ensure the tunnel startup.

Omega^{TM}pressure transducers were used to measure the steady pressures. The tunnel static pressure was monitored at a location upstream and downstream in the test section to establish the desired flow conditions. The tunnel upstream static pressure was measured at a distance of 1 inch upstream of the microjets. The tunnel stagnation pressure was monitored and the ratio of the tunnel static and stagnation conditions was used to establish the required Mach number. The microjet supply pressure was measured and used in the calculations of NPR, where $NPR = P_{o,MJ}/P_s$($P_{o,MJ}$ is the microjet supply pressure and P_s is the tunnel static pressure). Steady pressure data was sampled at a rate of 1 kHz and was acquired using National Instruments PCI- MIO-16E-1, 12 bit data acquisition card.

Kulite^{TM}pressure transducers were used to obtain unsteady pressure measurements within the cavity model. Model XCE-062-5D Kulites were used for the three cavity floor locations. The sensors were powered by a DC power supply, and the signal was passed through an amplifier and a low pass filter. Data was acquired using National Instruments PCI-6120, 16 bit data acquisition card with four simultaneous channels. The signals from the Kulite transducers were simultaneously sampled at a rate of 131 kHz and then passed through a Stanford Research Systems, INC. model SR640 low-pass filter with a cutoff frequency of 50 kHz. The spectra used a FFT size of 4096, giving 128 averages and a frequency resolution of 32 Hz.

III. Pulsed Micro-Actuator Design

A. Brief summary of original actuator design

Active and adaptive flow control of supersonic flows which are characterized by high unsteadiness requires actuators which have a high amplitude and is tunable over a frequency range. The details of the design and performance of such a pulsed micro-actuator which produces a high-amplitude response by using a very simple geometry can be found in Solomon et al.[12,13] A brief discussion about the design methodology of the actuator for supersonic cavity flows is presented here. A schematic of the actuator is shown in Figure 4. The

micro-actuator consists of three main components: a) an under-expanded source jet, b) a cylindrical cavity upon which the source jet impinges, and c) multiple micro-nozzles at the bottom of the cylindrical cavity, from which the high-momentum, unsteady microjets issue. Figure 4 also shows a schlieren image of the flow field associated with the micro-actuator. This configuration allows one to exploit multiple flow-acoustic resonance phenomena, including edge and hole tones, cavity resonance, Helmholtz resonance and other flow instabilities, allowing us to efficiently amplify microjet unsteadiness. (See Solomon et. al[12,13] for details)

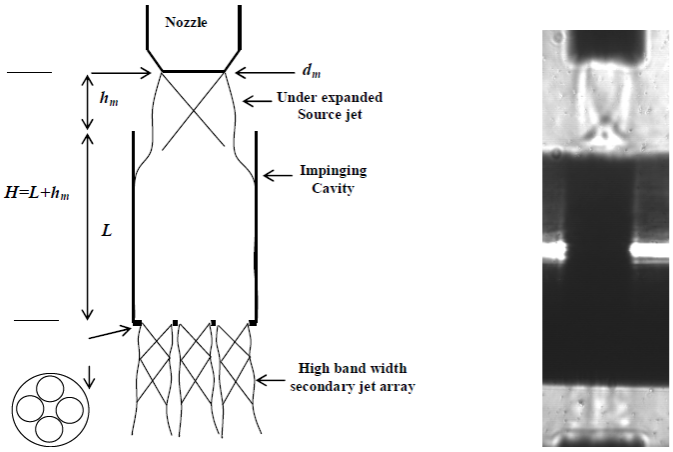

Figure 4. Schematic and configuration of the micro actuator

The governing parameters of the microjet array issuing from the actuator assembly are:[12] a) the distance of cavity from the source jet h_m, b) the length of the cylindrical cavity, L and c) the source jet pressure ratio $(NPR)_m$. The geometric parameters are indicated in Figure 4.

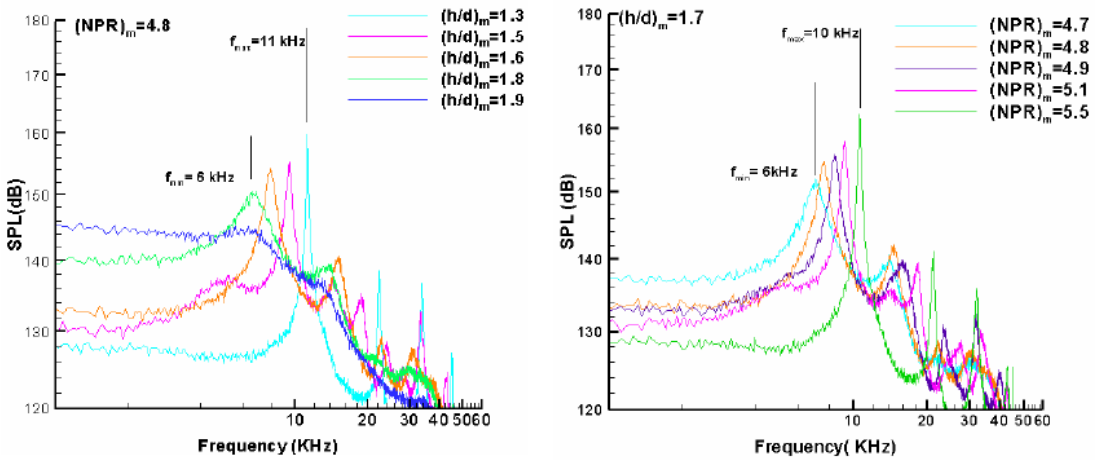

(a) Variation in $(h/d)_m$

(b) Variation in $(NPR)_m$

Figure 5. Spectra[14] for a $(L/d)_m$=5

Preliminary studies of these parameters has led to the identification of the optimal range and combination of these parameters that produce the desired flow from the actuator. Representative results obtained from these preliminary studies are presented below in Figure 5. The presence of high amplitude peaks which indicate the presence of highly unsteady flow can be clearly seen on the spectra. It can also be seen that for fixed $(L/d)_m = 5$, the frequency can be tuned either by varying $(h/d)_m$ or $(NPR)_m$ within a range of 6-11 kHz. These results led to the development of simple yet a robust pulsed actuator with a high mean momentum and a high unsteady component.

B. Actuator results from previous studies

The summary of the effect of $(NPR)_m$ and $(h/d)_m$ on actuator frequency over a range of cavity lengths is presented in Figure 6 (Solomon et. al[12,13]).The sweep in frequency can be obtained by varying the distance of the source jet and/or the operating pressure.

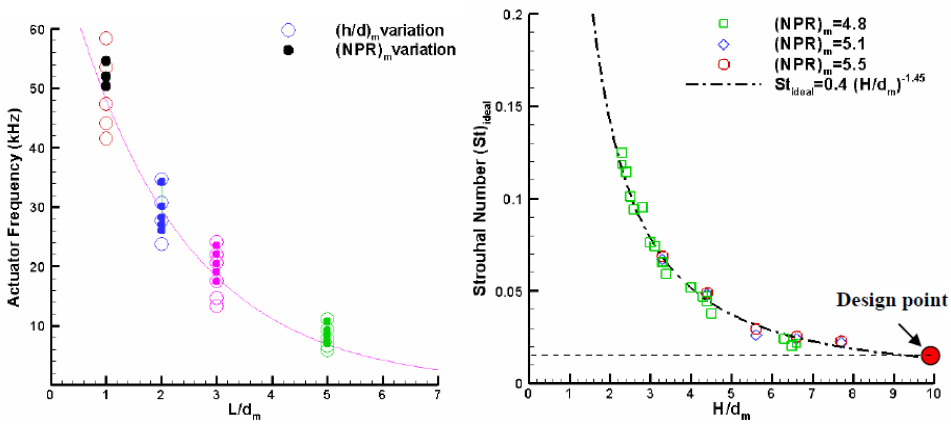

(a) Design curve for actuator[12,13] (b) Correlation predicting actuator dynamics

Figure 6. Summary of Actuator Data

The above figures clearly show the wide range of frequencies that can be obtained for a given L/d_m by varying $(h/d)_m$ or $(NPR)_m$. The total length represented as $H = l + h$, of the jet column from the micro nozzle end to the impinging end of the cavity.

The non-dimensional frequency as given by the Strouhal number

$$St_{ideal} = f d_m / U_{ideal} \tag{1}$$

where f is the frequency of the actuator, d_m is the source jet diameter and U_{ideal} is the ideally- expanded source jet velocity. Using these relations,the data can be collapsed on a single curve given by Eq.(2)

$$St_{ideal} = 0.4(H/d_m)^{-1.45} \tag{2}$$

We used this correlation as a guide for designing the actuator for the present application. Recalling that the aim of this study is to examine the efficacy of this new pulsed micro-actuator system for the control of the supersonic cavity flow, the actuator output should closely match the cavity tones. Earlier studies on supersonic cavity flows[2,5] show that this flow field produces high amplitude, nearly discrete frequency tones, in a range of 2-20 kHz where the maximum amplitude tones appear in the range of 4-6 kHz. *Hence, the nominal design point for present condition was an actuator with maximum amplitude at 5 kHz.* This frequency is indicated in Figure 6 (corresponding to St_{ideal}=0.012). More details of the actuator, designed for this application, will be described in the following section.

C. Actuator requirements for supersonic cavity flow field

After the successful implementation of the design methodology to the impinging jet flow field (Solomon et al.[14]), an actuator design for cavity flow field is attempted. Steady microjets have been used successfully for the control of supersonic cavity flows.[2,3,5,6] A representative result from Zhuang et al.[2] for the same rectangular cavity at $M = 2$, tunnel stagnation pressure of 32 psi and a steady microjet actuator operating at $NPR = 11$ is shown in Figure 7. The figure shows a dramatic reduction in the flow unsteadiness with control for a sensor located near the leading edge of the cavity. The dominant cavity tone is suppressed by nearly 23 dB, whereas the secondary tones were reduced by approximately 5 dB which translates to a 9 dB reduction in the aggregate unsteady pressure levels.

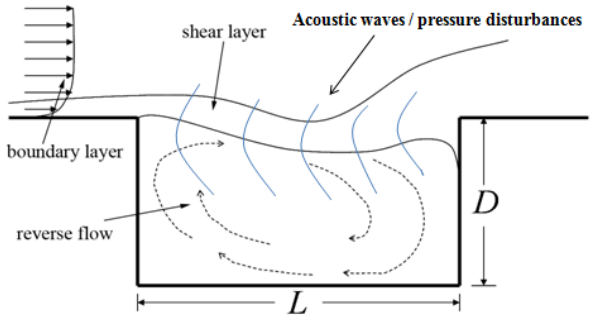

(a) Control scheme for a rectangular cavity in a supersonic flow

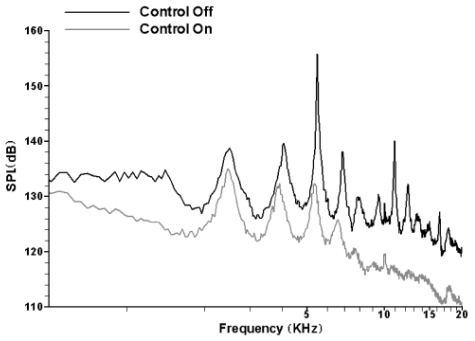

(b) Spectra comparison between baseline and controlled cases for M=2.0 cavity flow field[2]

Figure 7. Schematic and spectra for cavity flow control

This reduction tonal amplitude was accompanied by a reduction in the broadband noise level. It is anticipated that unsteady injection using pulsed microjets, will be more effective due to their higher time averaged momentum for the same mass flow rate.

IV. Actuator Performance and Effect on Cavity Flow Field

A. Characterization of the Actuator

The actuator was integrated with the cavity setup and was characterized inside the test section of the wind tunnel using a 100 psia Kulite^{TM}pressure sensor probe. The probe was aligned such that flow coming out of the microjets is normal to the probe. Figure 8 shows the performance spectra of the actuator for a range of $(NPR)_m$ which is defined as the ratio of microjet supply pressure to the tunnel static pressure. The spectra can be broadly be classified into two regions, broadband or high-amplitude discrete frequency regions. In the broadband region, the response of the actuator was nearly flat at lower frequencies till about 4 kHz and starts to roll-off at about 3 dB/octave at higher frequencies of about 7 kHz. Although not shown here, it was observed that for $(NPR)_m \leq 4.5$ the pressure spectrum of the pulsed microjets has low amplitude and is mostly broadband corresponding to the broadband region of operation. As $(NPR)_m$ is increased, a high-amplitude discrete tone starts to appear corresponding to the high- amplitude discrete frequency region of operation. It can be seen that at NPR values of 5.8, 6.5, 7.2 and 7.9 discrete frequency tones of the pulsed microjets are visible at 4.4, 5.1, 5.2 and 5.6 kHz, respectively. Recall from §III B, that the actuator was designed to produce high-amplitude excitations between 4 to 6 kHz; this is confirmed through these tests.

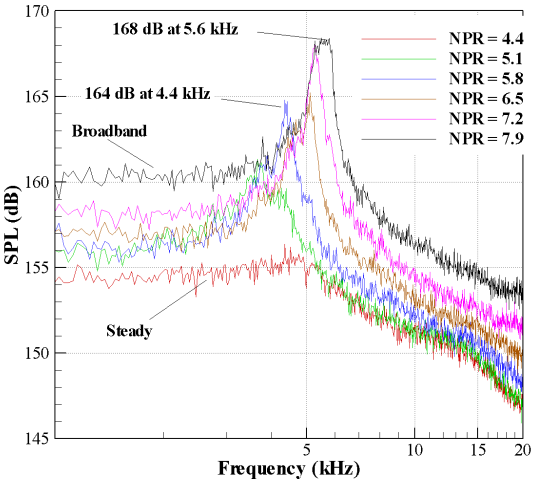

Figure 8. Spectra of actuator characterization integrated into the cavity

B. Cavity Flow Response to Control

1. Baseline flow

The presence of waves and the feedback mechanism lead to a highly unsteady flow inside the cavity. The spectra of the fluctuating pressures measured by using flush-mounted Kulites on the cavity floor confirm this. The pulsed actuator is equipped with exhaust vents to operate in the pulsing mode as discussed earlier.

Entrainment of flow through the exhaust vents into the main flow may alter the characteristics of the baseline flow, hence the baseline flow over the cavity was obtained with the exhaust vents closed. The frequency spectra of the baseline flow over the rectangular cavity at three different cavity floor locations, namely $x/L = 0.53$, 0.74 and 0.89, are shown in Figure 9. The presence of high-amplitude peaks that correspond to the cavity tones can be seen in the frequency spectra. The cavity tones occur at the same frequency independent of the transducer location along the length of the cavity but their relative strengths vary between locations. The transducer CF3 (x/L=0.53), which is nearer to the leading edge shows the strongest peaks whereas transducer CF1 (x/L=0.89), which is farther downstream, shows peaks that are significantly lower but has higher broadband levels. This change in the spectral content is expected along the cavity length due to the changes in the cavity mixing layer characteristics and the propagation of the acoustic disturbances due to the feedback loop and has been documented in previous studies by Zhuang et al.[3] and Ukeiley et al.[6]

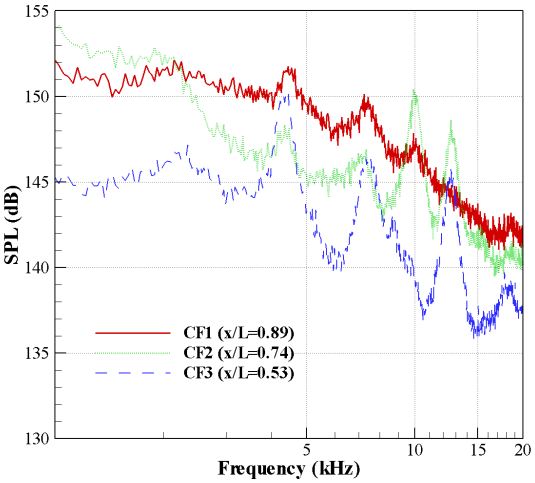

Figure 9. Spectra of the baseline flow over the rectangular cavity at three cavity floor locations

2. Pulsed microjet control

An array of 12 pulsed microjets located near the leading edge of the cavity were used as actuators to control the resonance in the cavity. The microjet supply pressure was varied such that $0 \leq NPR \leq 13$ was achieved. The entire range of NPR is not shown in the results discussed here to avoid clutter. The effect of flow control at three different axial locations, $x/L = 0.89$, 0.74 and 0.53, is shown in Figure 10 at two select values of NPR. It was observed that as the value of NPR is increased the reduction in the dominant tone and the overall sound pressure level also increases, i.e. the control is more effective. The spectra for values of $NPR \leq 5$ evolves gradually having little effect on the suppression of the dominant tone although a clear reduction in the OASPL was seen. A similar trend was observed for higher values of $NPR(\geq 10)$, where the suppression of the dominant tone and OASPL leveled off. The reduction in the flow unsteadiness can be clearly seen in Figure 10. A reduction in the overall broadband level is seen in Figure 10 (a) for the transducer CF1 (x/L=0.89) and was found to be nearly 4 to 6 dB below the baseline for lower and higher NPR, respectively. The spectra of the transducer CF2(x/L=0.74) is shown in Figure 10 (b), where a reduction in the peaks at frequencies ranging from 4.4 to 12.6 kHz is accompanied by a broadband reduction similar to that of transducer CF1. The most dramatic peak reduction occurs at transducer CF3 (x/L=0.53), which is nearest to the leading edge of the cavity, is seen in Figure 10(c), the peak at 4.4 kHz is reduced by approximately 7 dB. A reduction of 6 and 8 dB in the second and third peaks, at 7.5 kHz and 12.6 kHz respectively, was also observed at this location. The reduction in the broadband levels at CF3 (x/L=0.53) was found to be nearly 4 dB. It was also observed that, as one moves downstream along the cavity, the energy contained in the spectrum shifts towards the lower frequencies and the tonal content of the energy is reduced. As a result, when control is applied the reduction in the overall broadband levels is higher than the reduction in the tonal region near the trailing edge.

The effect of the pulsed microjets on the overall sound pressure level (OASPL), which is a parameter that is often used as a measure of efficacy of the flow control, is summarized in Figure 11. A significant drop in the OASPL can be seen as NPR is increased from no injection to around 10. The curve tends to flatten out for values of $NPR \geq 10$. Although a clear saturation value of the OASPL as a function of NPR was not found, it was observed that it is approximately 171 dB for transducers CF1 and CF2 and 168 dB for transducer CF3 at a NPR of 13. The reduction in the dominant cavity tone at 4.4 kHz and the change in OASPL for the transducer located at x/L=0.53 are also shown in Figure 12. Figure 12 shows that the reduction in tonal amplitude is similar to OASPL reduction. Furthermore it also confirms the fact that the actuator is more effective in suppressing the dominant tone at 4.4 kHz than the broadband noise, producing twice the reduction in the dominant tone compared to the OASPL.

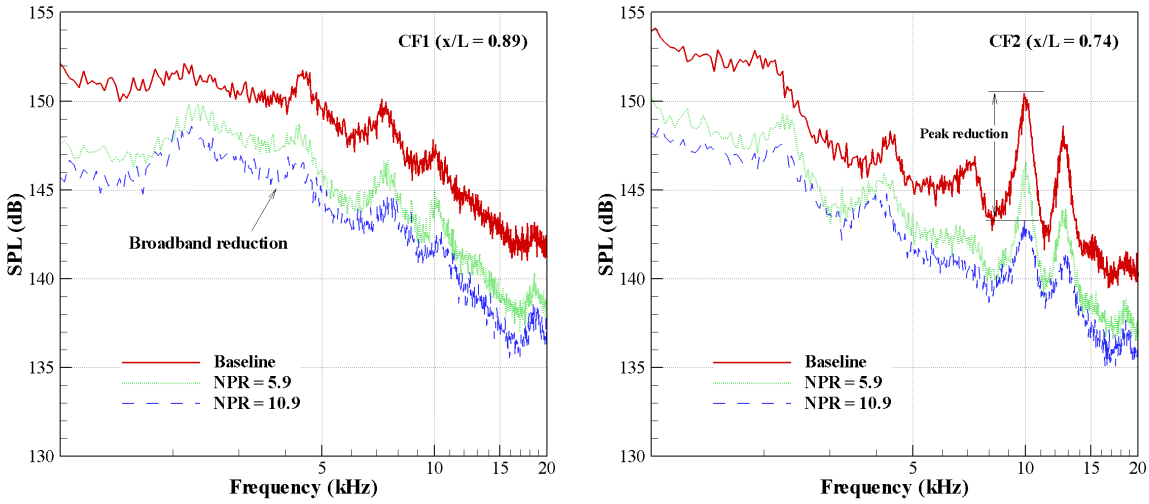

(a) (b)

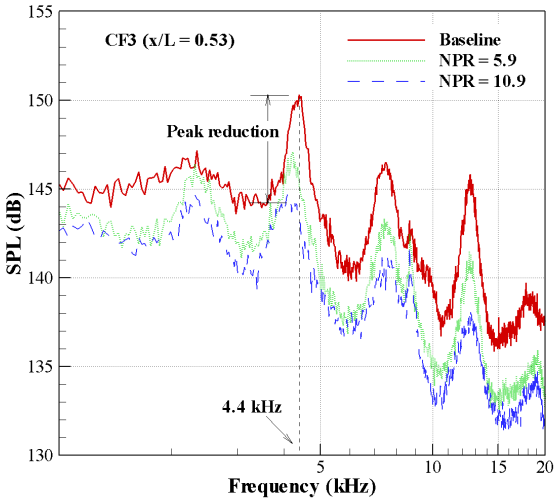

(c)

Figure 10. Comparison of spectra with and without pulsed control

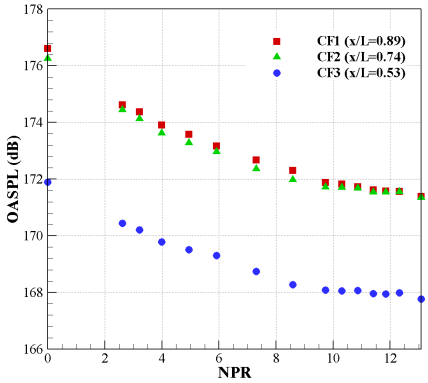

Figure 11. Variation of OASPL with pulsed microjet pressure, NPR

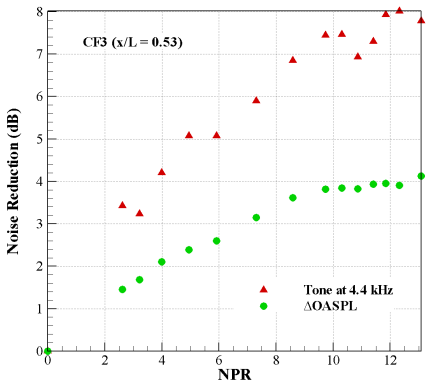

Figure 12. Noise reduction for transducer CF3 with control

3. *Steady microjet control*

The pulsed microjets used as actuators for flow control were operated in steady mode by closing the exhaust vents of the actuator. Experiments were conducted to obtain the baseline and control cases for the steady mode to allow direct comparison with pulsed actuation under the same flow conditions. As expected, the pulsed actuator when operated in *steady mode* show different characteristics than when operated in *pulsed mode*. Figure 13 shows the frequency spectra in the steady mode of operation for no control and at two microjet pressures. It can be seen from the figure that NPR=7 produces broadband reduction of 3 dB. Increasing the NPR to 10 has little effect on the broadband. The steady mode microjets produce reductions of 4 and 8 dB for the peaks at 7.5 and 12.6 kHz, respectively, at NPR=10. It is interesting to note, however, that the dominant tone at 4.4 kHz is less suppressed and in fact amplified by 2 dB at NPR=7.

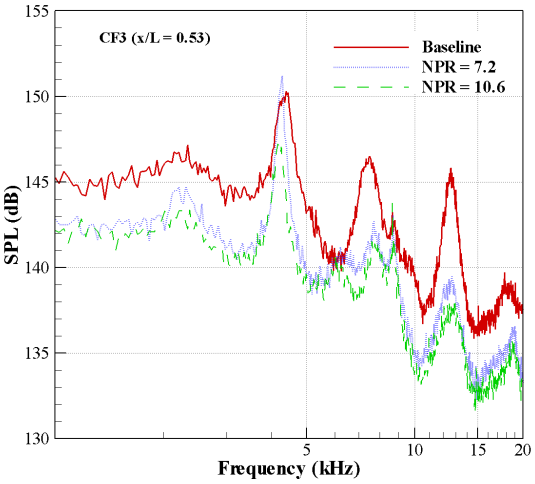

Figure 13. Spectra for steady mode of operation

V. Discussions and Comparison with Previous Studies

A comparison of the actuator working in *pulsed* and *steady* modes at NPR of 10.6 is shown in Figure 14(a) and (b) for CF1(x/L=0.89) and CF3(x/L=0.53), respectively. The spectra for CF2(x/L=0.74) shows similar trends with the spectra at CF1(x/L=0.89) and hence is not shown here. It can be seen from the spectra that the suppression of the dominant cavity tone at 4.4 kHz is better for the pulsed actuation relative to the steady actuation, although the second and third tones are equally suppressed in both cases. This is most evident from the spectra of transducer CF3(x/L=0.53) where the cavity tone at 4.4 kHz is suppressed by 7dB for pulsed actuation compared to a 4 dB suppression for steady actuation. It is interesting to note that, although the spectra is nearly identical for the two modes of operations apart from the suppression of the dominant tone at 4.4 kHz, a striking feature is the stronger suppression near 6 kHz for the pulsed actuation. This additional suppression near 6 kHz can be attributed to the design of the pulsed actuator to produce high-amplitude excitations in the range of 4-6 kHz as shown earlier in Figure 8 and demonstrates the tuning capability of the pulsed actuator in the design frequency range.

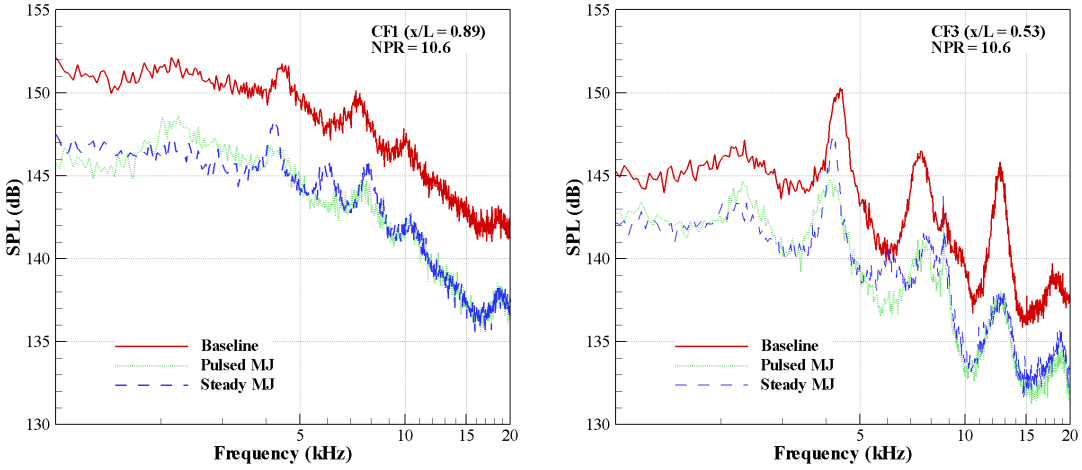

(a) (b)

Figure 14. Effect of pulsed and steady microjet control on cavity flow

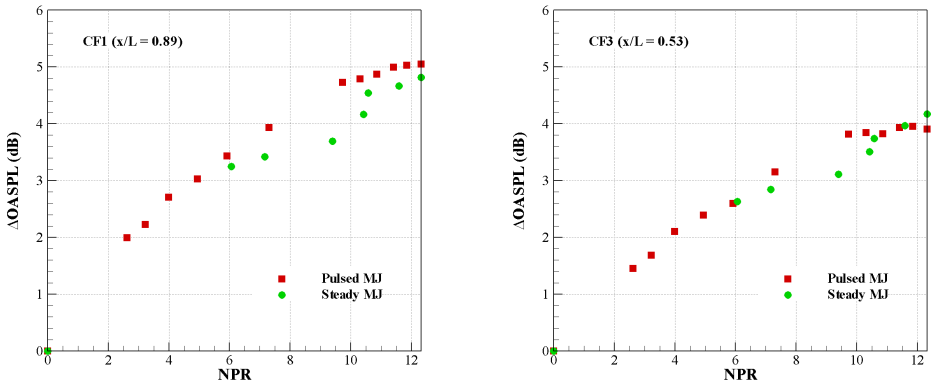

(a) (b)

Figure 15. Noise reduction for pulsed and steady microjets

A similar trend and magnitude was seen in the overall sound pressure levels for the two modes of operation as shown in Figure 15. The reduction in the noise levels for the pulsed actuation is nearly 1 dB higher for pulsed actuation compared to steady actuation for values of NPR ranging from 7-10 at transducer location CF1(x/L=0.89). It was observed that at both transducer locations, larger noise reduction was achieved for lower values of NPR for both the cases. For higher NPR, the noise reduction for the pulsed case nearly flattens out. Based on the current results appears that the pulse mode of operation is indeed more efficient than the steady mode of operation for the same actuator.

In the impinging jet studies,[14] the dominant tones were suppressed by the use of a pulsed actuator, but newer tones at higher frequencies than the dominant tone were observed which had lower energy and amplitude. The reasons for the appearance of newer tones is currently being investigated. The pulsed actuators designed so far by Solomon et al.[14] operated at conditions where the primary jet enters into the cylindrical cavity without any constraints provided by the existence of a wall around the vent area (Figure 3) unlike the present design. The bench top characterization of the pulsed actuator module as shown in Figure 5(b) shows that for NPR=5.5, the peak was nearly 30 dB above the baseline, whereas the characterization of the pulsed actuator integrated into the cavity model yields a peak of 10 dB above the baseline for NPR=5.8 as shown in Figure 8. The location of the peaks were also different being at 10 kHz for the bench top results and 4.4 kHz for the cavity integrated tests, respectively. This difference can be attributed to insufficient venting of the pulsed actuator when integrated into the cavity setup. It is speculated that the presence of solid wall around the vent area as in the present case changes the aeroacoustic properties of the primary jet entering the cylindrical cavity and thus alters the overall performance of the pulsed actuators. Proper design for the exhausts appears to be a critical parameter as it directly influences the NPR. Investigations on how to provide a more efficient way of venting are currently underway.

Finally, in order to compare the present result to the earlier steady microjet control studies in our facility a comparison with the steady microjets of Sheehan[15] at M=1.5, stagnation pressure of 26 psi using the same rectangular cavity as in the present study, is shown in Figure 16. Substantial suppres-

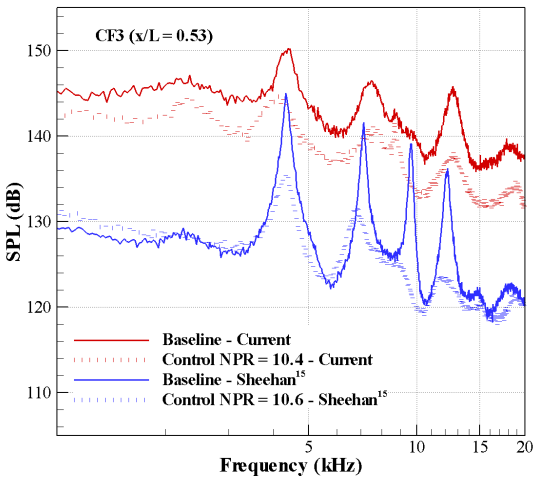

Figure 16. Spectra comparison with pulsed and steady[15] microjets

sion of the dominant cavity tone at as achieved by the steady microjets of Sheehan[15] was not observed in the present study. One of the possible reasons is that the dominant peak at 4.4 kHz in the baseline flow spectra for the above author was at 15 dB above the noise floor which is higher than the present study. It is speculated that the modifications made to the current test section has altered the boundary layer characteristics of the flow making it noisier than before and thus a baseline flow spectra similar to the one obtained by the above author was not achieved. The above discussion about the baseline being different is evident from the the figure. The location of the cavity tones is the same but the amplitude of the tones in the current experiments relative to the broadband is much lower. It can also be seen that the broadband reduction is higher for the pulsed actuation case than the steady microjets.

VI. Summary and Future Work

In the present study, a pulsed microjet actuator that is capable of producing high-amplitude excitations in the frequency range of 4-6 kHz was designed and integrated into the supersonic flow over a rectangular cavity. The actuator design was a result of the previous work done by Solomon et al.[12,13] This study shows the flexibility and integration capability of the pulsed actuator to be implemented in practical flow fields.

It was found that the actuator was capable of suppressing the dominant cavity tone (4.4 kHz) by nearly 7 dB along with an overall reduction in the broadband levels (4-6 dB). It was also observed that the actuator performed better when operating in the pulsed mode rather than the steady mode of operation. Although the design of the present pulsed actuator was not the most optimum in terms of the exhaust venting (a parameter that directly governs NPR_m) due to the constraints of the current model, it was learned that exhaust venting is a critical parameter for optimum performance and it is expected that better exhausts for the pulsed actuators will yield significantly better performance and results at lower values of NPR. Given that the current study represents the use of the first generation pulsed actuators, it is expected that control efficiency will be notably improved in the future studies using improved pulsed actuator design.

Work is currently underway to design a second generation of pulsed actuators keeping in mind the lessons learned from the current study, by providing them with better exhaust vents thus producing higher amplitude excitations and are thus tunable over a larger range of frequencies. A measure of the required mass flow for the pulsed actuator will be a parameter that will also be measured to compare the efficacy of the pulsed actuators to the steady actuators.

Acknowledgments

This work was supported by Florida Center for Advanced Aero-Propulsion (FCAAP). The authors would like to thank Robert Avant, the master machinist at the Advanced Aero Propulsion Laboratory at Florida State University.

References

[1] Roshko, A., "Some Measurements of Flow in a Rectangular Cutout," NACA, Technical Note 3488, 1955.

[2] Zhuang, N., Alvi, F. S., Alkislar, B. and Shih, C.. "Supersonic Cavity Flows and Their Control," AIAA Journal Vol.44, No. 9, 2006, pp. 2118-2128.

[3] Zhuang, N., Alvi, F. S. and Shih, C.. "Another Look at Supersonic Cavity Flows and Their Control," AIAA Paper 2005-2803.

[4] Zhuang, N., "Supersonic Open Cavity Flows and their Control," Florida State University, PhD. Dissertation, 2007.

[5] Ukeiley, L., Sheehan, M., Coiffet, F., Alvi, F., Arunajatesan, S., and Jansen, " Control of Pressure Loads in Complex Cavity Configurations," AIAA Paper 2007-1238, 2007.

[6] Ukeiley, L. Sheehan, M., Coiffet, F., Alvi, F. S., Arunajatesan, S. and Jansen, B.,"Control of Pressure Loads in Geometrically Complex Cavities," Journal of Aircraft, 45, No. 3., 2008, 1014-1024.

[7] Cattafesta III, L. N., Garg, S., Choudhari, M. and Li, F. "Active Control of Flow-Induced Cavity Resonance," AIAA Paper 97-1804.

[8] Wiltse, J. M. and Glezer, A., "Manipulation of Free Shear Flows Using Piezoelectric Actuators," J. Fluid Mech., Vol. 249, 1993, pp. 261-285.

[9] Amitay, M., Kibens, V., Parekh, D.E., and Glezer, A., "Flow reattachment dynamics over a thick airfoil controlled by synthetic jet actuators," AIAA Paper 99-1001.

[10]Rowley, C., and Williams, D., "Dynamics and Control of High-Reynolds Number Flow over Open Cavities," Annual Review of Fluid Mechanics, Vol. 38, Jan. 2006, pp. 251276.

[11]Cattafesta, L. N., Williams, D., Rowley, C. and Alvi, F. S., "Review of Active Control of Flow-Induced Cavity Oscillations," Progress in Aerospace Sciences, 44, 2008, 479502.

[12]Solomon, T. J., Kumar, R. and Alvi, F. S.,"High Bandwidth Micro-Actuators for Active flow control," AIAA paper 2008-3042.

[13]Solomon, T. J., Kumar, R. and Alvi, F. S.,"Development and Characterization of High Bandwidth Actuator," ASME paper, 2008-3042.

[14]Solomon, T. J.,Hong, S.,Wiley, A.,Kumar, R., Annaswamy, A. M., Alvi, F. S.,"Control of Supersonic Resonant Flows using High Bandwidth Micro-actuators,"AIAA paper 2009-3247.

[15]Sheehan, M.V., "Supersonic Flow and its Control in Highly Three-Dimensional Cavities," Florida State University, Masters Thesis, 2007.